CONTRACTION DYSSYNCHRONY AND LEFT VENTRICULAR MECHANO-ENERGETIC FUNCTION

by

Lauren Johnson

B.S.E., Mechanical Engineering, Geneva College, 2004

Submitted to the Graduate Faculty of

Swanson School of Engineering in partial fulfillment

of the requirements for the degree of

Doctor of Philosophy

University of Pittsburgh

2008

UNIVERSITY OF PITTSBURGH

SWANSON SCHOOL OF ENGINEERING

This dissertation was presented

by

Lauren Johnson

It was defended on

September 26, 2008

and approved by

Harvey S. Borovetz, Ph.D.
Professor, Departments of Bioengineering, Chemical, and Petroleum Engineering; Robert L. Hardesty Professor, Department of Surgery

John Gorcsan III, M.D.
Professor, Department of Medicine

Michael R. Pinsky, M.D.
Professor, Departments of Critical Care Medicine, Bioengineering, and Anesthesiology

George Stetten, Ph.D.
Professor, Department of Bioengineering

Dissertation Director: Sanjeev G. Shroff, Ph.D.
Professor and Gerald McGinnis Chair, Department of Bioengineering

CONTRACTION DYSSYNCHRONY AND LEFT VENTRICULAR MECHANO-ENERGETIC FUNCTION

Lauren Johnson, Ph.D.

University of Pittsburgh, 2008

Left ventricular (LV) contraction dyssynchrony is common among patients with heart failure and is often associated with significantly greater cardiac risks. Cardiac resynchronization therapy (CRT) is clinically used to treat dyssynchrony by simultaneously activating the ventricles using a cardiac pacemaker. Although a promising therapy, ~30% of patients fail to respond to CRT, possibly due to the following issues: limited knowledge regarding mechanisms underlying the detrimental mechano-energetic effects of dyssynchrony, lack of robust algorithms for quantifying dyssynchrony, and inadequate patient selection criteria. The goal of the present research was to address some of these issues.

In an isolated heart model, dyssynchrony resulted in depressed LV mechanical function and increased myocardial oxygen consumption. This adverse mechano-energetic effect of dyssynchrony can be reconciled by the hypothesis that the observed mechanical activity at the global level underestimated internal cellular work, which is likely to be the true determinant of myocardial oxygen consumption.

Using data from canine models, cross-correlation analysis was developed to quantify dyssynchrony, both at the integrated and segmental levels. This fully automated, robust tool took into account the entire systolic portion of the cardiac cycle. As a result, this methodology was associated with less intra-group variability compared to current methods that focus on

manually chosen time points, which are subject to user interpretability. The segmental cross-correlation analysis provided insight into the integrated LV contraction pattern.

Changes in radial synchrony did not always predict changes in global LV function. For example, in some instances, global LV depression was associated with longitudinal dyssynchrony and preserved radial synchrony, indicating that multi-faceted dyssynchrony analysis is necessary for comprehensive evaluation of contraction.

In a chronic canine model, dyssynchrony and its adverse functional effects were exaggerated as heart failure progressed. In contrast, resynchronization using LV free-wall pacing was equally efficacious regardless of the degree of heart failure.

Preliminary clinical studies indicated that dyssynchrony was better characterized using cross-correlation analysis compared to standard indices. Although these results are promising, additional studies with a larger patient cohort is necessary to translate cross-correlation analysis into the clinical realm as a standard tool to quantify dyssynchrony and identify patients for CRT.

TABLE OF CONTENTS

LIST OF TABLES

LIST OF FIGURES

LIST OF ABBREVIATIONS

AVO_2: arteriovenous oxygen content difference

BiVf: biventricular free-wall

$CCSI_{int}$: integrated cross-correlation synchrony index

$CCSI_{seg}$: segmental cross-correlation synchrony index

CRT: cardiac resynchronization therapy

CRTa: cardiac resynchronization therapy at LV apex

CRTf: cardiac resynchronization therapy at LV free-wall

EDP: end-diastolic pressure

EDPVR: end-diastolic pressure-volume relationship

EDV: end-diastolic volume

ESP: end-systolic pressure

ESPVR: end-systolic pressure-volume relationship

ESV: end-systolic volume

LBBB: left bundle branch block

LV: left ventricle

MVO_2: myocardial oxygen consumption

P-V: pressure-volume

PVA: pressure-volume area

Q_{cor}: coronary flow

RA: right atrial

RVa: right ventricular apex

RVOT: right ventricular outflow tract

TDI: tissue Doppler imaging

ACKNOWLEDGEMENTS

I would like to thank my advisor, Sanjeev Shroff, for his support and guidance over the years. You have had the greatest impact on my academic career and I appreciate all the opportunities that you have provided for me so that I could learn and grow as a scientist. I would also like to thank my co-advisor, Michael Pinsky, for the opportunity to be involved in his studies. Your expertise lead to a well-rounded research project and I greatly appreciate your guidance through the years. I would also like to deeply extend my gratitude to the rest of my committee,, Harvey Borovetz, John Gorcsan, and George Stetten, for their invaluable time and advice. Special thanks go to David Schwartzman for generously offering his knowledge and advice, and especially for the opportunity to include the human data in my dissertation.

Sincere appreciation is expressed to those of you who spent the last few years with me in the Cardiovascular Systems Laboratory: Caroline, Dan, Jonathan, Steve, Yong, and Jamie. Special thanks go to Caroline for supporting me daily, both on scientific and friendship bases. You were instrumental in recruiting me into this lab and I am forever grateful as it was the best decision I have ever made. You are a wonderful person and I will dearly miss your company. I also would like to thank Marc Simon for his help with the isolated heart project. I will always remember the struggles we had with the isolated rabbit heart preparation for three years; but ultimately, it was a success. And of course, Yong, for generously rearranging his schedule to accommodate my availability and for his input on the rabbit project.

I would like to extend my thanks to the fellows in the Pinsky laboratory (Drs. Kim, Tanabe, Lamia, and Tanaka) who were instrumental in providing me with the canine data. Special thanks go to Lisa Gordon, Judy Thoma, and Dave Fischer for their technical expertise and help with the canine experiments. I am thankful to various individuals from the laboratories of Drs. Kameneva, Wagner, and Apodaca for their help with the isolated rabbit heart studies. Finally, the collaboration with Chris Kaufmann from St. Paul Heart Clinic and Dan Kaiser from Medtronic on the human studies was an invaluable opportunity.

I would also like to thank Steve Winowich and Robert Kormos for the opportunity to join the Artificial Heart Program so early in my academic career. It was an honor to be part of the program and the impact that several patients had on me will always have a special place in my heart. Working for this program lead me to where I am today and I will always be grateful for it.

I would like to acknowledge the funding sources that allowed me to pursue my research and complete my degree. The animal studies were supported by a grant from the National Institutes of Health and McGinnis Chair Endowment funds, and the human study was funded by Medtronic.

Finally, I would like to express my deepest gratitude to my family. Dad, thank you for instilling your work ethic in me, pushing me to succeed, and always reinforcing your love. Mom, thank you for your constant support. More importantly, thank you for understanding the person that I am and for your unwavering love. Mandy, for being by my side for the past 26 years and always supporting me. Finally, Brandon, for being my companion and for your patience through the ups and downs. Thank you for taking care of me, the animals, and the house so that I can concentrate on my studies. I appreciate every little thing that you do for me. Your love means everything to me and I look forward to continuing our lives together.

1.0 INTRODUCTION

1.1 CLINICAL RELEVANCE

Effective myocardial contraction requires the synchronization of individual elements in the ventricular wall. Disruption in normal contraction synchrony of the left ventricular (LV) wall can result from electrical and/or structural abnormalities. Regardless of the underlying etiology, disruption of normal electrical conduction introduces mechanical disturbances in the intrinsic contraction pattern of the LV. Clinically coined LV contraction dyssynchrony, this condition is common among patients with systolic heart failure and is often associated with significantly greater cardiac risks by exacerbating cardiac depression [1]. With dyssynchrony, individual regions of the LV reach their maximum shortening at different times, resulting in depression of global LV performance (e.g., decreased ejection fraction). Furthermore, dyssynchrony adversely affects global LV energetic function, presumably by increasing oxygen consumption through the competing regions. For the past decade, cardiac resynchronization therapy (CRT) has been clinically used to treat contraction dyssynchrony by simultaneously activating the left and right ventricles using a pacemaker device (i.e., biventricular pacing; **Figure 1-1**) [2]. Clinical indications for CRT include NYHA functional class III or IV heart failure, LV ejection fraction (EF) ≤ 35%, and QRS duration greater than 120 ms [2]. The goal of CRT is to improve global LV performance and energetic function by resynchronizing the ventricles.

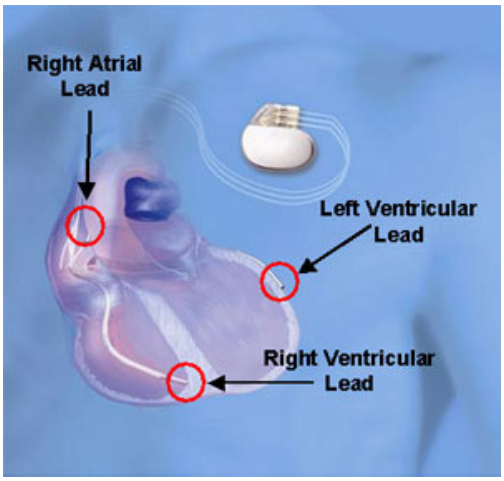

Figure 1-1. Biventricular pacing device for cardiac resynchronization therapy.

CRT provides atrial-synchronized, biventricular pacing using standard pacing technology. Following a sensed atrial contraction or atrial-paced event, both ventricles are stimulated to synchronize their contraction [3].

1.2 SPECIFIC AIMS

Although CRT has shown to improve functional status and survival [4-11], about 30% of patients still do not respond to this therapy [12]. The following factors may contribute to this variability in benefit: (1) limited knowledge regarding the mechanisms underlying the detrimental mechano-energetic effects of dyssynchrony and the beneficial effects of CRT; (2) lack of robust algorithms for quantifying dyssynchrony and identifying the optimal pacing site(s) that improve synchrony and LV function; (3) improper criteria for patient selection; (4) inconsistencies in the identification of improvement or response; and (5) limited choices of pacing sites available in the clinical setting. The goal of the current thesis is to address some of these issues. Specifically, are aims are as follows:

Aim 1. Assess the impact of LV dyssynchrony on global left ventricular mechano-energetic function in a Langendorff isolated rabbit heart preparation. This study is expected to provide insight into the mechanism behind increased myocardial oxygen consumption with dyssynchronous contraction.

Aim 2. Develop an efficient, robust clinical tool to quantify dyssynchrony and identify responders for CRT. Current methods use only a single point in the cardiac cycle; however, our newly developed tool (cross-correlation analysis) will use a novel algorithm that assesses the entire systolic period for a more vigorous approach to quantify dyssynchrony.

Aim 3. Investigate the link between regional and global LV function under different contraction patterns induced by ventricular pacing at various sites. Establishment of this link may help to identify responders for CRT.

Aim 4. Apply cross-correlation analysis to a multi-plane dataset to quantify synchrony for a comprehensive characterization of regional LV function. In addition, we plan to construct a color-coded "bull's eye" representation of synchrony indices to facilitate physician interpretation in quantifying dyssynchrony and optimizing pacing sites for CRT.

Aim 5. Assess global LV function and synchrony patterns in a tachycardia pacing-induced model of heart failure. Compared to a healthy heart, we anticipate unique changes in regional and global LV function with a failing heart.

Aim 6. Extend our analyses into the clinical realm by assessing the efficacy of cross-correlation analysis in a select cohort of human patients.

2.0 BACKGROUND

2.1 THE INTRINSIC CONDUCTION PATHWAY AND NORMAL CONTRACTION PATTERNS

The myocardium has a specialized excitatory and conductive system that activates and controls cardiac contraction. Normal electrical conduction begins in the right atria where autorhythmic cells of the sinoatrial (SA) node create spontaneous impulses (**Figure 2-1**). Inherent leaky sodium-calcium ion channels cause the SA node to self-excite and therefore serve as the natural pacemaker of the heart [13]. Rhythmic impulses of the SA node immediately spread and activate the atrial tissue through internodal pathways (**Figure 2-1**). Concordant with atrial contraction, the action potentials from the SA node spread to the atrioventricular (AV) node. A delay in electrical conduction is then caused by a decrease in gap junctions between successive cells at the AV node. This delay is necessary to allow sufficient time for the atria to eject all blood into the ventricles. Following the AV delay, the electrical impulse rapidly splits into the right and left bundle branches of the His-Purkinje system located in the subendocardium of the ventricular septum (**Figure 2-1**). The right and left bundle branches spread distally to the apex then turn towards the free-wall of the respective ventricle about one-third from the ventricular apex. Importantly, the conduction velocity of the specialized Purkinje system is significantly faster than that of myocardial muscle to ensure rapid and concordant activation of the left and right

ventricles for synchronous contraction [13]. Once the electrical impulse exits the Purkinje system, the impulse is transmitted through gap junctions in the myocardial muscle. The impulse is transmitted from the apex to the base as well as from the subendocardium to the epicardium of the ventricles.

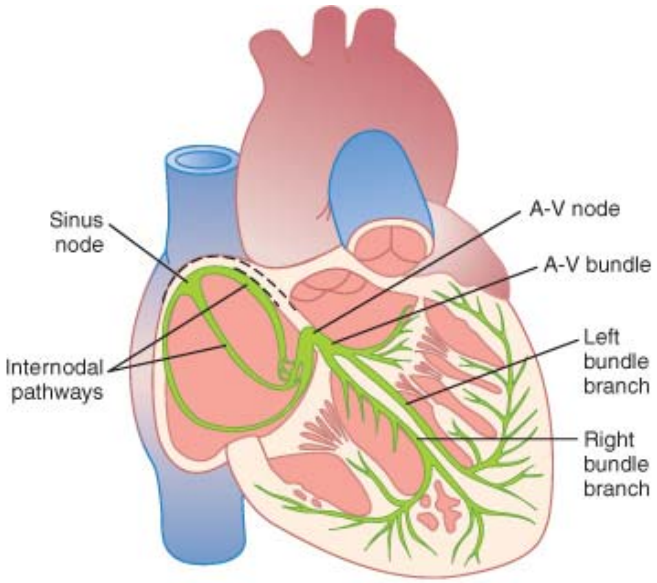

Figure 2-1. Intrinsic conduction pathway of the myocardium.

Intrinsic conduction initiates at the sinus node and travels through the internodal pathways to the atrio-ventricular (A-V) node. After a delay at the A-V node, conduction travels through the A-V bundle where it is split at the left and right bundle branches [13].

The inherent contraction pattern of the left ventricle follows that of the electrical activation sequence (i.e., from apex to base). If the electrical activation is uninterrupted, the ventricle contracts, moving blood from the apex towards the base where it is ejected out of the ventricle into the arterial circulation. Contraction involves shortening in the radial, circumferential, and longitudinal directions along the helical course of the myocardial fibers. For example, the apex has mostly circumferentially oriented fibers from the endocardium to the epicardium, whereas fibers near the base are arranged obliquely on the epicardium, circumferentially in the middle layer, and longitudinally in the endocardium [14]. It is essential

that the ventricle maintains this pattern of contraction to efficiently eject blood into the arterial circulation to deliver vital nutrients to itself and the body. Any disturbance in this inherent contraction pattern may lead to inefficient ejection and decreased ventricular performance.

2.2 THE DISEASE: DISTURBANCES IN ELECTRICAL PROPAGATION LEAD TO MECHANICAL DYSSYNCHRONY

A disturbance in the rapid conduction system (i.e., His-Purkinje system) causes abnormal impulse propagation and subsequently dyssynchronous activation of the left ventricle. Alterations in the His-Purkinje system include left bundle branch block (LBBB) and other intra-ventricular conduction defects, manifested as widening of the QRS complex [15]. A disturbance in conduction can also be caused by structural abnormalities including functional changes of the myocardium induced by dilated cardiomyopathy and ischemic disease [16, 17]. Importantly, the conduction through the LV is up to four times slower than the rapid His-Purkinje system[18], resulting in heterogeneous mechanical activation of the LV. When the electrical wavefront cannot propagate through the His-Purkinje system, it is forced to travel through the slow conducting myocardium. For example, with LBBB, the right ventricle is activated before the LV. The imbalance of mechanical activation begins with pre-systolic septal contraction, followed by late LV contraction with paradoxical movement of the septum toward the RV, and a final septal motion towards the LV now against a higher load [19, 20]. Instead of producing an efficient output, this dyssynchronous wall motion causes substantial volume shifts within the LV cavity, resulting in a decrease in cardiac performance. Even with an intact His-Purkinje system, electrical propagation can be inhibited by scar tissue and therefore must find an alternate

pathway, which also leads to heterogeneous activation patterns. Regardless of the cause, an electrical disturbance results in abnormal conduction and subsequent mechanical dyssynchrony, where blood is no longer efficiently moved out of the left ventricle, compromising global LV function.

2.3 TREATMENT FOR LEFT VENTRICULAR DYSSYNCHRONY IN THE SETTING OF HEART FAILURE

Cardiac resynchronization therapy is suggested for a subset of heart failure patients with cardiac dyssynchrony defined as prolonged QRS duration [2]. CRT is implemented via atrial-synchronized biventricular (right and left ventricular) electrical stimulation using a pacemaker device (**Figure 1-1**). Standard transvenous leads are position in the right atrial (RA) appendage and right ventricular (RV) apex, but implantation of the LV lead is more complicated. The LV lead is inserted into a cardiac vein via the coronary sinus, with the goal of placing the lead tip on the LV free-wall at a mid-cardiac position with adequate physical and electrical separation from the RV lead [8, 21, 22]. However, due to considerable variability in the coronary venous anatomy [23], optimal lead position may not be feasible. In this case, a surgical epicardial approach through a limited thoracotomy may be more appropriate. Once the leads are positioned and attached to a specialized pacemaker device and all parameters are optimized, CRT can be implemented to resynchronize contraction of the ventricles and improve cardiac function.

Large randomized clinical trials have demonstrated the beneficial effects on LV systolic function and heart failure symptoms [4, 5, 7-9, 11]. The inclusion criteria for these trials were: (1) NYHA functional class III or IV heart failure; (2) depressed systolic function with ejection

fraction ≤ 35%; and (3) QRS complex >120 ms. Despite promising results from large randomized clinical trials, a large percentage of patients (~30%) do not benefit from this therapy. Importantly, this variability in benefit may be a result of the poor dyssynchrony selection criterion: electrical dyssynchrony manifested as a wide QRS.

2.4 ELECTRICAL VS. MECHANICAL DYSSYNCHRONY

Currently, cardiac dyssynchrony is defined as an interventricular electrical delay between the left and right ventricles [2]. However, increasing evidence has shown that a poor correlation exists between immediate response to CRT and either basal QRS duration [24] or a decrease in QRS duration after CRT [25]. Therefore, electrical dyssynchrony is not a robust criterion to identify patients likely to benefit from CRT.

Contraction dyssynchrony can be thought of as a "disconnect" between electrical activation and mechanical response where inhibition of conduction (e.g., LBBB) results in dyssynchronous mechanical response. Likewise, disparities can also exist in the electrical pathway which lead to dyssynchronous mechanical activation. Regardless, the deleterious effect of dyssynchrony is mainly caused by disparities in the LV contraction pattern. Since CRT should theoretically improve or restore contraction, it is reasonable to postulate that a mechanical marker of dyssynchrony may be a more accurate criterion for this therapy. Surprisingly, in early clinical trials, only one study used a mechanical marker of LV dyssynchrony as an inclusion criteria for CRT [12]. More recently, increasing evidence has shown that mechanical dyssynchrony better predicts short-term [24] and long-term [26-29] response to CRT. Although

the paradigm has now shifted to using mechanical instead of electrical markers to assess dyssynchrony, a robust method to quantify dyssynchrony still does not exist.

2.5 QUANTIFYING DYSSYNCHRONY: A REGIONAL PERSPECTIVE

Disturbances in mechanical synchrony can be assessed by different imaging techniques. Myocardial tagging with cardiac magnetic resonance imaging (MRI) can accurately track regional myocardial mechanics [30, 31]. However, MRI does not have widespread clinical availability and bedside use. Therefore, the majority of studies investigating dyssynchrony and the response to CRT use echocardiographic techniques to assess LV mechanics. These techniques include M-mode assessment, two-dimensional tissue Doppler imaging (TDI), and two- and three-dimensional echocardiography.

2.5.1 Echocardiographic Techniques to Assess LV Wall Motion

M-mode echocardiography is the simplest echocardiographic technique. This technique often assesses wall motion via the parasternal short-axis view, therefore only providing a one-dimensional view of the heart. TDI in contrast allows for two-dimensional characterization of wall motion. This is one of the most widely studied techniques for the assessment of LV dyssynchrony [12]. Based on the Doppler effect, TDI quantifies velocity at specific locations within the myocardium, indicating the rate at which a myocardial segment moves toward or away from the transducer. Short-axis or long-axis images can be obtained to quantify radial/circumferential or longitudinal velocity, respectively. Tissue Doppler-derived velocity can

be measured using pulsed-wave or color-coded TDI. A major disadvantage of pulsed-wave TDI is that only one segment can be assessed at a time, which makes this method very time consuming and less accurate. Accordingly, there is limited evidence showing the benefits of pulsed-wave TDI to assess dyssynchrony and predict response to CRT [12]. In contrast, 2-D color-coded TDI acquires tissue velocity tracings from the entire sector (i.e., short- or long-axis view) allowing assessment from multiple sites simultaneously [32]. A disadvantage for this method is that derivation and assessment of theses tracings from images must be performed offline. Regardless, color-coded TDI allows for an extensive evaluation of wall motion by integrating velocity tracings over time to obtain tissue displacement. Furthermore, myocardial strain can be derived from TDI to quantify tissue deformation of individual segments throughout the cardiac cycle. In summary, regional function can be assessed using myocardial velocity, displacement or strain derived from a variety of techniques.

2.5.2 Current Approaches to Quantify Dyssynchrony

Mechanical dyssynchrony has been defined by an array of different metrics. The simplest index of dyssynchrony quantifies the time delay between septal and posterior LV wall motion (SPWMD) using one-dimensional M-mode echocardiography at a mid-LV, short-axis view [33-35]. Although some studies have shown that SPWMD predicted response to CRT [34, 35], another study reported that this measure was insufficient to predict LV reverse remodeling [33]. The main disadvantage of this index is that it assesses dyssynchrony in one-dimension using only the septum and LV free-wall. If systolic motion is not clear due to akinesis of these regions, assessment of dyssynchrony using this index is not feasible. A more accurate measure of dyssynchrony can be obtained from two-dimensional tissue Doppler imaging technique.

Dyssynchrony is commonly quantified using color-coded TDI to derive indices using information from time to peak systolic longitudinal velocity [26, 28, 29, 36-40]. From myocardial velocity tracings (i.e., velocity *vs.* time waveforms), time to peak systolic velocity can be identified for individual segments in the myocardium. One study showed that a delay of ≥60 ms between septal and lateral time to peak velocities was predictive of acute response to CRT [40]. An extension of this index is a four-segment model that included the septal, lateral, inferior, and anterior LV walls at the base [26]; this study reported that a delay of ≥65 ms predicted response to CRT. However, the most extensive models using time to peak velocity have been developed by Yu et al. [29, 38, 39]. Using a 12-segment model, they showed that a standard deviation of ≥31 ms of the time to peak longitudinal velocities predicted response to CRT with a sensitivity of 96% and specificity of 78% [39]. Although prediction of response to CRT based on time to peak longitudinal systolic velocities appears promising, difficulties may exist with TD angle dependence, signal noise, translational effects of scar, and variations in heart rate [38, 39, 41], which can affect the outcome and predictability of this approach.

Mechanical dyssynchrony can also be described using tissue strain data based on the extent and timing of myocardial deformation. Furthermore, the rate of myocardial deformation (i.e., strain rate) can also be assessed. Importantly, tissue strain echocardiography has the advantage over TD velocity with respect to differentiating active contraction from passive motion or tethering, which are important confounding variables in patients with ischemic heart disease [42]. Although initial studies reported relatively low predictive values for response to CRT using longitudinal strain rate to quantify dyssynchrony [39], radial strain has recently been shown to predict both acute and chronic clinical response to CRT using the maximal strain time delay [43, 44].

The majority of these mechanical markers of dyssynchrony use information derived from time-to-peak amplitude of velocity or strain information. As explained above, the native contraction pattern of the LV is extremely complex and becomes increasingly complicated with dyssynchronous deformation. Therefore, indices that focus on a single point during contraction may not completely characterize the complex deformations. *We plan to address this issue through **Specific Aims 2 and 4** by developing a more robust tool to assess contraction patterns and quantify dyssynchrony.*

2.6 CONSEQUENCES OF DYSSYNCHRONY: A GLOBAL PERSPECTIVE

Disparities in normal contraction patterns are known to adversely affect global LV performance by a variety of mechanisms, including having regional segments reach maximal shortening at different times and dyssynchronous papillary muscle contraction leading to mitral valve dysfunction and inefficient ejection. Importantly, this dysfunction further exacerbates systolic heart failure, placing patients at significantly greater cardiac risk [1]. Several animal studies have mimicked contraction dyssynchrony using a LBBB pattern of contraction [45-47]. LBBB can be achieved either by cardiac ablation of the left bundle branch or right ventricular outflow pacing. Both techniques lead to a similar dyssynchronous contraction pattern [48]: early septal activation inducing pre-stretch of the LV wall followed by late activation of the LV free-wall with post-systolic shortening of the earlier activated septum [49]. This contraction pattern has deleterious effects on measures of global LV performance. Studies have shown that compared to control, the maximum and minimum rate of pressure change (i.e., dP/dt_{max} and dP/dt_{min}, respectively), stroke volume, and stroke work are all significantly depressed following induction

of dyssynchrony [45-47]. Furthermore, global LV mechanical function (i.e., contractility) is also depressed with dyssynchrony [50-52] and this depression appears to be proportional to the degree of contraction dyssynchrony [51]. In addition, a decrease in energetic efficiency concomitant with the depression in function has been reported with dyssynchrony [53, 54]. Therefore, alterations in regional contraction patterns adversely affects all aspects of global LV function: (1) global LV performance (e.g., cardiac output, stroke work, dP/dt_{max}) (2) global LV mechanics (i.e., contractility); and (3) global LV energetics (i.e., myocardial oxygen consumption).

2.6.1 Evaluation of Global LV Performance and Mechanics

Global LV performance and mechanics can be quantified by evaluating LV pressure-volume (P-V) data. The volume of the LV cavity can be determined using a conductance catheter; LV volume is calculated by converting intracavitary electrical conductance to volume after calibration factors are applied [55]. Conductance catheters also have a micromanometer pressure transducer to measure LV pressure. From this technique, pressure and volume information can be plotted individually over time (**Figure 2-2A, B**) or pressure can be plotted against volume to derive P-V loops (**Figure 2-2C**). These loops provide useful information describing volume and pressure changes throughout the cardiac cycle. For example, the upper left hand corner of the P-V loop indicates end-systole and the bottom right hand corner marks end-diastole. In addition, stroke volume can be calculated as the change in volume between end-diastole and end-systole, and stroke work (amount of work performed by the ventricle) can be derived as the area inside of the P-V loop.

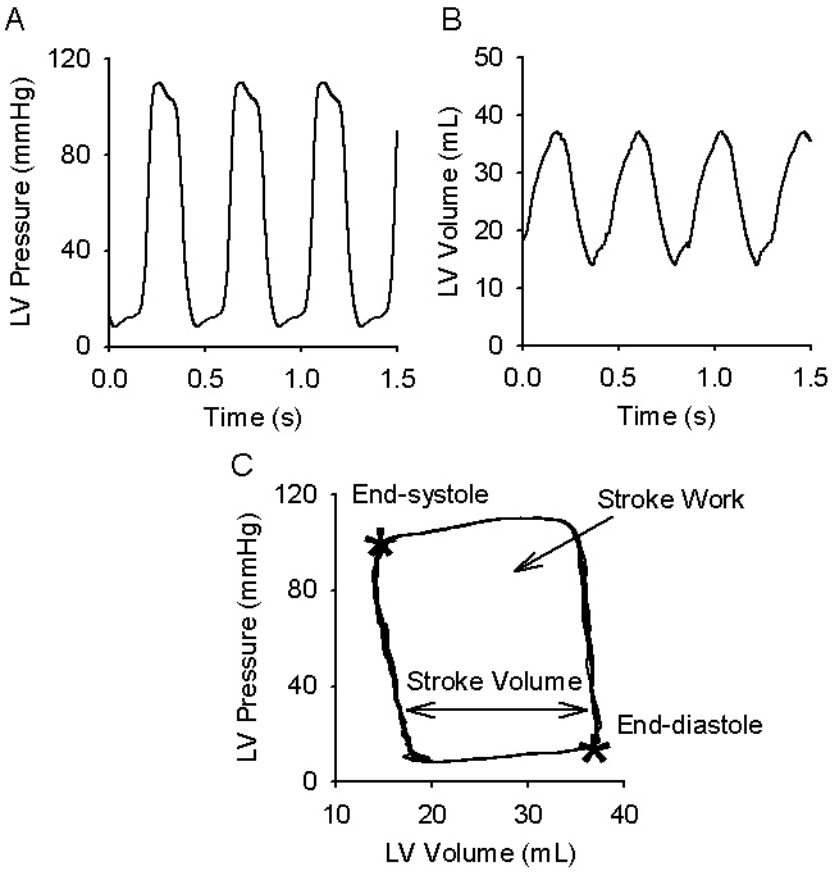

Figure 2-2. Hemodynamic data used to derive pressure-volume loops.

Left ventricular **(A)** pressure and **(B)** volume over time. **(C)** Left ventricular pressure plotted against LV volume constructing a P-V loop. The lower left and upper right hand corners of the loop marks end-diastole and end-systole, respectively. The width of the loop quantifies LV stoke volume and the area within the loop is proportional to LV stroke work.

Left ventricular pressure-volume loops are an important tool in quantifying mechanical properties of the LV. By varying preload or afterload, a series of P-V loops can be constructed. For example, during inferior vena-caval (IVC) occlusion experiments, preload is altered by banding the IVC, and P-V loops change according to the Frank-Starling Law (i.e., decreased force development due to less preload). In their initial pioneering studies, Suga and Sagawa conducted experiments that defined left ventricular mechanics using these series of P-V loops [56]. They showed that global LV intrinsic active and passive mechanical properties can be defined using the end-systolic pressure (ESP)-volume (ESV) relationship (ESPVR) and end-

diastolic pressure (EDP)-volume (EDV) relationship (EDPVR), respectively (**Figure 2-3**). The top left point of each P-V loop defines end-systole, and the ESPVR is defined by the time-varying elastance model:

$$ESP = E_{es} \cdot [ESV - V_d] \quad \textbf{(2-1)}$$

where E_{es} and V_d are parameters to be estimated from experimental measurements or extrapolation. Suga and Sagawa showed that E_{es} and V_d were not altered with changes in filling or ejection characteristics and therefore represented the global systolic intrinsic mechanical properties of the LV [56]. Also, they found that the slope of the ESPVR, called the end-systolic elastance (E_{es}), increased with inotropic stimulation and coined E_{es} as a preload independent index of the innate contractility of the heart [56]. Glower et al. showed that the relationship between stroke work and end-diastolic volume was preload independent, insensitive to changes in afterload, and responsive to changes in inotropic state [57]. Therefore, the intrinsic systolic properties of the LV can also be quantified using the preload recruitable stroke work (PRSW) relationship:

$$SW = M_w \cdot [EDV - V_w] \quad \textbf{(2-2)}$$

where M_w and V_w are parameters [57]. The linearity of the PRSW relationship allows for quantification of cardiac performance by a simple slope and x-axis intercept with the concept of determining the work performed (stroke work) by the input (end-diastolic volume) of the system. The end-diastolic pressure-volume relationship is typically defined by a nonlinear monoexponential equation:

$$EDP = \alpha \cdot [e^{\beta \cdot (EDV - V_o)} - 1] \quad \textbf{(2-3)}$$

where α, β, and V_o are parameters [58]. From this relationship, the passive intrinsic mechanical properties of the LV can be deduced. Specifically, V_o defines the passive unstressed volume of

the LV (i.e., volume at zero EDP). Also, chamber stiffness is linearly related to EDP, and the slope of this relationship defines the modulus of chamber stiffness. Importantly, these relationships were derived under ideal, rigorously controlled conditions. *We plan to investigate the utility of these tools in quantifying global LV mechanical properties during dyssynchronous contraction and their relationship with regional function in* ***Specific Aim 3.***

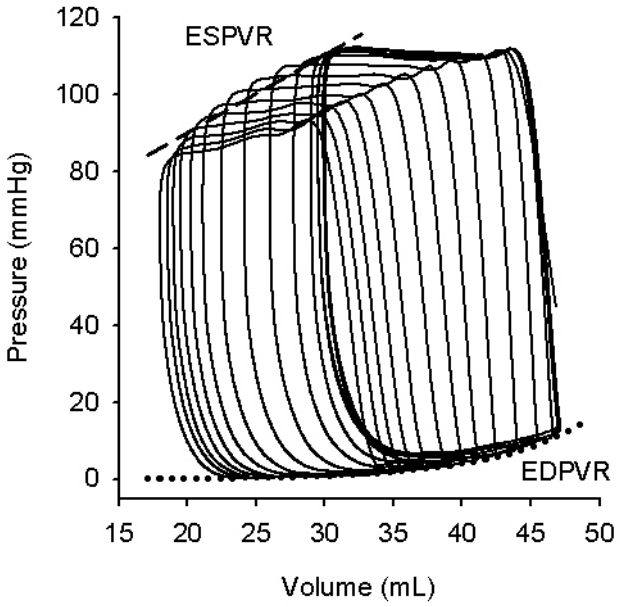

Figure 2-3. Pressure-volume loops during inferior vena caval occlusion.

Series of pressure-volume loops collected during altered preload from inferior vena caval occlusion. As the vena cava is occluded, LV pressure and volume decrease, and loops become smaller and shift to the left. The end-diastolic points for each loop (lower right hand corner) can be fit to a monoexponential equation to derive the end-diastolic pressure-volume relationship (EDPVR) and quantify passive global LV mechanical properties. Similarly, the upper left hand points for each loop (end-systolic points) can be fit to a linear equation to derive end-systolic pressure-volume relationship (ESPVR) and quantify active global LV mechanical properties.

2.6.2 Evaluation of Global LV Mechano-Energetic Function

Suga and Sagawa extended their initial pioneering studies by showing that the addition of the graphic area inside the LV pressure-volume loop (stroke work, SW, **Figure 2-4A**) and the ESPVR defined left-sided triangle (potential energy, PE, **Figure 2-4A**) is a mechanical

determinant of myocardial energetics [59, 60]. More specifically, they called this the pressure-volume loop area (PVA, **Figure 2-4B**). They showed that myocardial oxygen consumption (MVO_2) varied linearly with PVA (**Figure 2-4C**) and can be represented by:

$$PVA = a \cdot MVO_2 + b \qquad \textbf{(2-4)}$$

where the slope (i.e., a) represents the energy cost of the PVA and its inverse indicates the contractile efficiency from oxygen consumption to PVA, and the intercept (i.e., b) represents the MVO_2 of basal metabolism and excitation-contraction coupling. This relationship is important because it offers information about the underlying processes of the left ventricle simply by obtaining global mechanic and energetic measurements. *Importantly, there is limited knowledge regarding the mechanisms underlying the detrimental mechano-energetic effects of dyssynchrony. We plan to assess this issue through* ***Specific Aim 1****.*

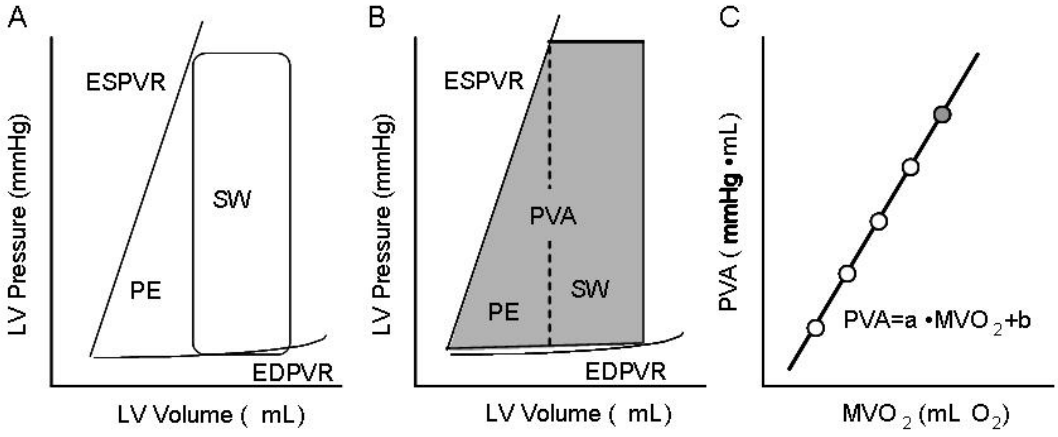

Figure 2-4. Global left ventricular mechano-energetic function.

(A) Potential energy (PE) is enclosed by the ESPVR, EDPVR, and left-hand side of pressure volume loop. Area enclosing the pressure-volume loop is stroke work (SW). **(B)** The addition of PE and SW is pressure-volume area (PVA). **(C)** Each PVA calculated linearly correlates with the measured myocardial oxygen consumption (MVO_2) during that contraction. Grey circle corresponds to the PVA calculated from **(B)**.

2.7 THE LINK BETWEEN REGIONAL AND GLOBAL LV FUNCTION

One would expect that the degree of global LV functional improvement with CRT would be proportional to the improvements in contraction synchrony. However, establishment of the link between global LV function and contraction synchrony is confounded by the lack of standard and comprehensive indices for synchrony and criteria for defining CRT responders. This link is important because it may help to identify those likely to benefit from this therapy. Response to CRT is commonly assessed by clinical status, echocardiographic parameters, or both. Clinical status can be established by the 6-minute walk test, NYHA functional class, and quality of life score [12]. The majority of studies demonstrate improvement in clinical status with CRT, however, many clinical parameters are subjective and a substantial placebo effect may be present in a large percentage of patients [4]. A more objective definition of response may involve echocardiographic-derived parameters. However, again, multiple parameters could be derived from echocardiographic evaluation to determine response such as ejection fraction, end-systolic volume, end-diastolic volume, or mitral regurgitation. Although the degree of improvement in EF with CRT has varied in different studies [4, 8, 61], changes in LV volumes seem to more consistently define response to CRT [4, 8, 9, 61]. A reduction of ≥10% in ESV following CRT, called reverse remodeling, has become a very commonly used marker to indicate response to CRT [62]. However, a universally accepted index of dyssynchrony still remains to be established. Results of the Predictors of Response to CRT (PROSPECT) trial suggested that mechanical dyssynchrony defined as a variety of echocardiographic-derived measures such as time delay between earliest and latest peak systolic velocity could not predict response to CRT defined as either reverse remodeling or clinical status [63].

Another relevant factor that will affect response to CRT is the identification of optimal pacing site(s) for individual patients. The standard pacing modality for CRT is biventricular pacing with RV apical and LV free wall pacing sites. However, single-site LV free-wall pacing may be more beneficial to some patients rather than biventricular pacing. In addition, LV apical pacing may be superior to LV free-wall pacing in other patients. Therefore, the current body of work was aimed to understand the mechanisms underlying the detrimental mechano-energetic effects of dyssynchrony and to investigate the link between regional and global LV function under varying contraction patterns induced by ventricular pacing at different sites.

3.0 STUDY 1: INSIGHTS INTO THE EFFECTS OF CONTRACTION DYSSYNCHRONY ON GLOBAL LEFT VENTRICULAR MECHANO-ENERGETIC FUNCTION

Specific Aim 1. To assess the direct impact of LV dyssynchrony on *global left ventricular mechano-energetic function* in a Langendorff isolated rabbit heart preparation.

3.1 INTRODUCTION

The effects of contraction dyssynchrony on global LV mechanical function has been well documented, however its effect on LV energetic function has received less attention. Furthermore, results from few studies examining this issue have not been consistent. The blood-perfused isolated heart preparation offers a rigorously controlled environment to evaluate intrinsic LV mechano-energetic function. Here the heart is devoid of external neurohumoral stimuli, loading conditions can be independently controlled [64], and global LV mechano-energetic function can be quantified in terms of the myocardial oxygen consumption (MVO_2)-pressure-volume area (PVA) relationship [65, 66].

The primary goal of this study was to assess the effects of contraction dyssynchrony on global LV mechano-energetic function in an isolated rabbit heart preparation. We used a right ventricular outflow tract (RVOT) pacing-induced model of LBBB-like contraction

dyssynchrony. It should be noted that RVOT pacing was used to create dyssynchrony; it was not meant to correspond to a clinically used pacing site (e.g., right ventricular apex).

3.2 METHODS

3.2.1 Langendorff Isolated Rabbit Heart Preparation

The isolated heart preparation is ideally suited for studying global LV mechano-energetics. This preparation consists of an isolated heart, a perfusion medium, and a loading system. Oscar Langendorff devised this method to study the mechanical activity of the isolated mammalian heart [67]. The basic principle behind the Langendorff heart (or isolated heart) preparation is retrograde perfusion of the coronary circulation. When the aorta is cannulated and ligated, the perfusion medium closes the aortic valve and is forced through the coronary ostia where it enters the coronary vasculature providing vital nutrients to the myocardium. Although the ventricles remain essentially empty, after traveling through the coronary vasculature, the perfusate travels to the right atrium and right ventricle where it then exits the heart through the pulmonary artery.

3.2.2 Biological Preparation

This investigation conforms with the *Guide for the Care and Use of Laboratory Animals* published by the US National Institutes of Health (NIH Publication No. 85-23, revised 1996). Eleven New Zealand rabbits weighing 2.60 ± 0.04 kg were used in an isolated perfused Langendorff preparation to study LV mechano-energetic function. Animals were anesthetized

with an intramuscular injection of ketamine [45 mg•kg^{-1}] and xylazine [5 mg•kg^{-1}] and thereafter an intravenous catheter was inserted into the ear vein to provide a continuous infusion of ketamine [1.38 mg•min^{-1}•kg^{-1}]. The rabbits were artificially ventilated with room air via a tracheotomy. After median sternotomy, the heart was removed and a metal cannula was inserted into the aorta to begin retrograde perfusion of the coronary arteries at constant perfusion pressure (80 mmHg) and temperature (37 °C). Hearts were perfused with oxygenated (95% O_2/5% CO_2 mixture) crystalloid perfusate (modified Krebs-Hanseleit (KH) solution) containing washed erythrocytes (see **Appendix A.1**). Previous studies have shown that perfusion with washed erythrocytes is superior to crystalloid in that the performance of the heart is stable over a longer period of time and the metabolic measurements are more reliable [68, 69]. Oxygenation was accomplished using a hollow fiber membrane contactor (Membrana, Charlotte, NC) and a 95% O_2/5% CO_2 mixture. The perfusate was not recirculated and the coronary perfusion pressure was held constant using a servo-controlled roller pump. To prevent microaggregates from entering the heart, an in-line 40 μm filter was used. A thin latex balloon, secured at the end of an automated volume-injection device, was positioned in the LV via the mitral orifice. The balloon did not generate any intrinsic pressure at its maximum volume; therefore the measured pressure represented that of the LV only. A suture around excess left-atrial tissue secured the heart to the volume-injection device. Epicardial pacemaker leads were placed on the right atrium (RA) and right ventricular (RV) free-wall near the anterior infundibulum, also known as the RV outflow tract. After all protocols were completed, the atria and RV were removed and the LV was weighed (3.45 ± 0.13 g).

3.2.3 Perfusion Medium

The isolated hearts were perfused with washed bovine erythrocytes suspended in a modified KH solution [70]. Whole bovine blood was collected from a local slaughterhouse and anticoagulation was maintained with heparin [10 $U \bullet mL^{-1}$]. Gentomyosin [250 $mg \bullet L^{-1}$] was added to retard bacterial growth, and blood was filtered through a 40 μm filter to remove gross particles. Red blood cells (RBCs) were isolated by washing the whole blood in KH solution (without calcium) using a cell-saver machine (Haemonetics Corp., Braintree, MA) (see **Appendix A.1**). Isolated RBCs were then diluted with KH solution to obtain a hematocrit of 32 ± 0.6%. Calcium chloride [1.8 mM] was added after another heparin bolus [10 $U \bullet mL^{-1}$]. Albumin [0.3%] was used to maintain osmolarity, and a pH of 7.46 ± 0.02 was obtained with the addition of sodium bicarbonate [3%] to the final suspension.

3.2.4 Experimental Measurements

Instantaneous left ventricular pressure was measured by a catheter-tip pressure transducer (Millar Instruments Inc., Houston, TX) positioned in the LV via a side port in the volume-injection system. Left ventricular end-diastolic volume was controlled using an infusion pump (Harvard Apparatus, Holliston, MA). Instantaneous pressure was digitized on–line at a sampling rate of 1000 Hz. Total coronary flow (Q_{cor}) was measured by an ultrasonic, in-line, transit-time flow probe (2N158, Transonic) in series with the aortic perfusion cannula. Arterio-venous oxygen content difference (AVO_2) was measured by a continuous oxygen difference analyzer (A-VOX Systems, San Antonio, TX). The use of this device for accurate measurement of AVO_2 has been verified [71, 72]. Arterial blood was collected from a side port in the aortic perfusion cannula

directly above the flow probe and venous blood was directed to the AVO_2 analyzer via a 12 Fr. Foley catheter inserted into the right ventricle through the pulmonary artery. Myocardial oxygen consumption (MVO_2) was calculated as the product of Q_{cor} and AVO_2. Since the right ventricle was kept collapsed with the Foley catheter, the measured MVO_2 was taken to represent oxygen consumption of the LV only.

3.2.5 Calculation of Pressure-Volume Area

Instantaneous LV pressure data were recorded during steady-state isovolumic contractions at four to six LV EDVs within the end–diastolic pressure range of 5-30 mmHg (Frank-Starling protocol, **Figure 3-1A**). After each volume step, we waited approximately 2 minutes to allow for equilibrium of the metabolic state before collecting data. The functional state of the heart was quantified in terms of peak active and passive P-V relationships (**Figure 3-1B**) [56]. The ESPVR was derived by fitting peak active pressure points to a linear elastance model (**Equation 2-1**) and end-diastolic P-V points were fit to a monoexponential equation (**Equation 2-2**) to derive the EDPVR. ESPVR and EDPVR were calculated from raw data using a custom-written software program (The MathWorks Inc., Natick, MA) (see **Appendix A.2**). Using the same custom-written software, PVA was calculated as the area enclosed by ESPVR, EDPVR, and the pressure-volume trajectory for each EDV (**Figure 3-1B**). MVO_2 was linearly correlated to PVA using **Equation 2-4** (**Figure 3-1C**).

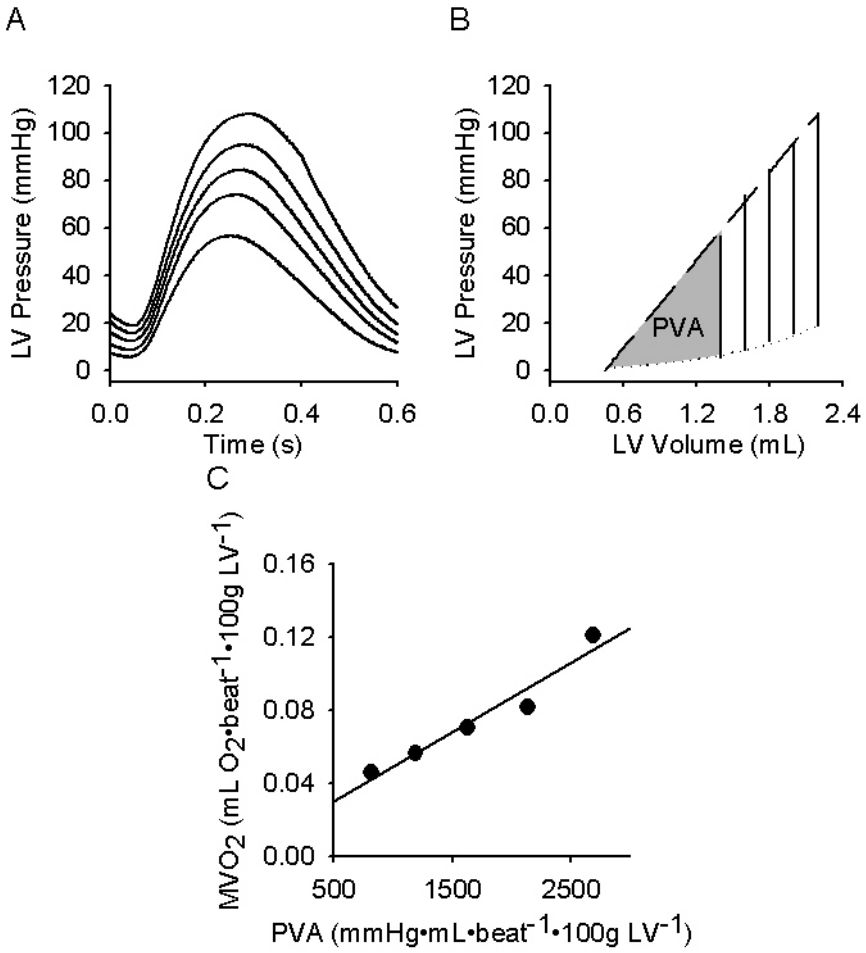

Figure 3-1. Pressure-volume area concept.

(A) LV pressure was collected for incremental volumes during isovolumic contraction. **(B)** ESPVR and EDPVR were then fitted through peak end-systolic and end-diastolic points (dashed and dotted lines, respectively). PVA was calculated as the area enclosed by the ESPVR, EDPVR, and pressure-volume trajectory for that volume increment (e.g., gray area is the PVA for the first volume increment). **(C)** MVO_2 was linearly correlated to PVA at its corresponding volume step. Abbreviations: ESPVR = end-systolic pressure-volume relationship; EDPVR = end-diastolic pressure-volume relationship; LV = left ventricular; MVO_2 = myocardial oxygen consumption; PVA = pressure-volume area.

3.2.6 Pacing Protocols

Mechanical (LV pressure and volume) and energetics (Q_{cor} and AVO_2) data were first collected under right-atrial (RA) pacing, which served as the heart rate control condition. Hearts were paced at 111 ± 7 beats•min^{-1}. After mechano-energetic data were collected under RA pacing,

contraction dyssynchrony was induced by simultaneous RA-RVOT pacing, referred to as RVOT pacing. Approximately 3 minutes after the induction of contraction dyssynchrony, mechano-energetic data were collected again. The total experimental duration was 73±5 minutes.

3.2.7 Statistical Analysis

Data are presented as mean ± SEM. The statistical analysis consisted of comparing relationships (e.g., ESPVR and MVO_2-PVA) between two conditions: control (RA pacing) and dyssynchronous (RVOT pacing) contractions. Because these relationships were obtained for both conditions from each heart, a repeated measures ANCOVA structure exists. Importantly, multi-linear regression analysis with dummy variables allows for only fixed effects (i.e., it does not allow for variability between animals and assumes independence across measurements within animals). However, a mixed model approach assumes dependence across repeated measurements within an animal therefore allowing for random effects in addition to fixed effects [73]. Therefore, statistical analysis was performed using a mixed linear model to account for random (i.e., between hearts within a condition) and fixed (i.e., between conditions) effects via SAS statistical software package (SAS Institute Inc., Cary, NC) (see **Appendix A.3**). Significance was determined as $P<0.05$.

3.3 RESULTS

3.3.1 Effects of Contraction Dyssynchrony on Global LV Mechanical Function

RVOT pacing-induced contraction dyssynchrony resulted in a small change in global LV mechanical function compared to RA pacing (**Figure 3-2**, "Mechanics" panels). The ESPVR decreased in five of eight experiments with RVOT pacing and was unchanged in three experiments. The depression in global LV function was also apparent when comparing pressures at each end-diastolic volume during the Frank-Starling protocol (**Table 3-1**). For example, the maximum peak active systolic pressure generated was 92 ± 5 mmHg after the induction of dyssynchrony, which was approximately a 10% decrease from the RA pacing value (101± 6 mm Hg). Statistical analysis of all data using a mixed model approach showed that the ESPVR during RVOT pacing was significantly different from that of RA pacing. The slope of the ESPVR (i.e., E_{es}) was not altered with RVOT pacing (**Figure 3-3A**, RA pacing: 56.1 ± 5.1, RVOT pacing: 58.5 ± 5.0 mmHg•mL^{-1}, P=NS). However, the ESPVR volume intercept (V_d) increased from 0.58 ± 0.10 mL with RA pacing to 0.67 ± 0.10 mL with RVOT pacing (P<0.05, **Figure 3-3B**). Therefore, the depression in global LV mechanical function with dyssynchrony manifested as a small, but statistically significant rightward shift of the ESPVR.

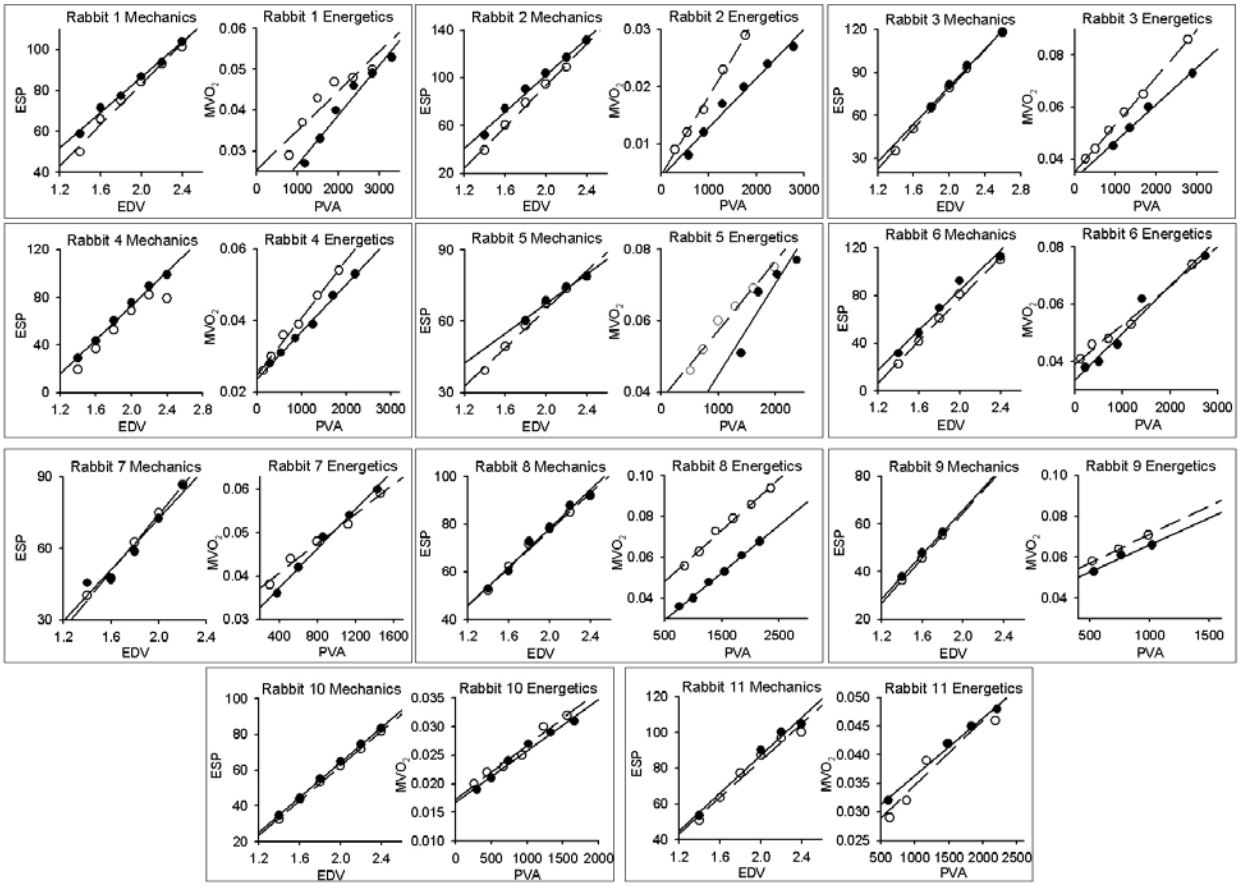

Figure 3-2. Raw data for isolated rabbit heart preparations (n=11).

Left panels are global LV mechanical data expressed as ESPVR, and right panels are global LV energetic data expressed as MVO_2-PVA relationships. Closed and open circles represent values under RA and RVOT pacing, respectively. Solid and dashed lines are relationships for RA and RVOT pacing, respectively. Note that for all experiments, the ESPVR decreased slightly and the MVO_2-PVA relationship increased with RVOT pacing. Abbreviations: ESP = end-systolic pressure (mmHg); EDV = end-diastolic volume (mL); PVA = pressure-volume area (mmHg•mL•beat^{-1}•100g LV^{-1}); MVO_2 = myocardial oxygen consumption (mL O_2•beat^{-1}•100g LV^{-1}); RA = right atrial; RVOT = right ventricular outflow tract; other abbreviations as in **Figure 3-1**.

Table 3-1. Global LV mechanical and energetic variables during isovolumic contractions.

Pacing	LV EDV	LV ESP	PVA	AVO_2	Q_{cor}	MVO_2	*n*
RA Pacing	*1.4*	44 ± 4	540 ± 100	1.7 ± 0.4	9.3 ± 1.4	3.08e-2 ± 0.42e-2	9
	1.6	55 ± 4	795 ± 126	1.6 ± 0.4	10.1 ± 1.4	3.50e-2 ± 0.52e-2	8
	1.8	67 ± 4	1123 ± 114	1.8 ± 0.3	10.2 ± 1.3	4.21e-2 ± 0.44e-2	10
	2.0	82 ± 4	1502 ± 121	2.1 ± 0.3	10.0 ± 1.3	4.63e-2 ± 0.47e-2	10
	2.2	91 ± 4	1896 ± 150	2.4 ± 0.4	9.5 ± 1.3	4.98e-2 ± 0.53e-2	9
	2.4	101 ± 6	2431 ± 178	2.5 ± 0.5	10.5 ± 1.5	5.43e-2 ± 0.68e-2	8
RVOT Pacing	*1.4*	38 ± 3	426 ± 76	1.9 ± 0.4	9.2 ± 1.3	3.56e-2 ± 0.45e-2	11
	1.6	52 ± 3	662 ± 84	2.0 ± 0.4	9.4 ± 1.2	4.05e-2 ± 0.49e-2	11
	1.8	65 ± 3	956 ± 88	2.2 ± 0.4	9.5 ± 1.2	4.62e-2 ± 0.54e-2	11
	2.0	78 ± 3	1308 ± 98	2.2 ± 0.3	9.7 ± 1.2	4.82e-2 ± 0.54e-2	10
	2.2	88 ± 4	1702 ± 116	2.6 ± 0.4	9.1 ± 1.2	5.31e-2 ± 0.62e-2	9
	2.4	92 ± 5	2174 ± 162	2.9 ± 0.4	9.2 ± 1.4	6.07e-2 ± 0.80e-2	7

Data: mean ± SEM for each isovolumic volume during the Frank-Starling protocol; n, number of experiments with data at each end-diastolic volume. AVO_2 = arterial-venous oxygen content difference (mL O_2•100 mL^{-1}); EDV = end-diastolic volume (mL); ESP = end-systolic pressure (mmHg); LV = left ventricular; MVO_2 = myocardial oxygen consumption (mL O_2•$beat^{-1}$•100g LV^{-1}•10^{-2}); PVA = pressure-volume area (mmHg•mL•100gLV^{-1}); Q_{cor} = coronary blood flow (mL•min^{-1}); RA = right atrial; RVOT = right ventricular outflow tract.

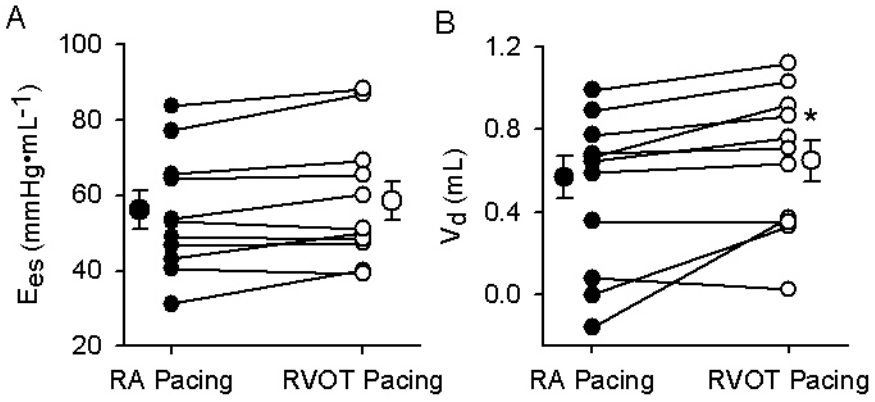

Figure 3-3. Global LV mechanical function quantified by the ESPVR.

(A) Compared to RA pacing, the slope (E_{es}) of the ESPVR was not different compared to RVOT pacing. **(B)** However, RVOT pacing increased the volume-axis intercept (V_d) of the ESPVR. Data: *n*=11; **P*<0.05 vs. RA pacing as analyzed using all data in a mixed statistical model. Abbreviations: E_{es} = end-systolic elastance; V_d = dead volume or volume-axis intercept of ESPVR. Other abbreviations as in **Figures 3-1 and 3-2**.

3.3.2 Effects of Contraction Dyssynchrony on Global LV Mechano-Energetic Function

Dyssynchronous contraction with RVOT pacing had an adverse effect on LV energetic function. In spite of lower PVA, dyssynchronous contraction for any given end-diastolic volume was associated with greater AVO_2 and little change in Q_{cor} (**Table 3-1**). Thus, although global LV mechanical function was depressed, MVO_2 was elevated during dyssynchronous contraction compared to RA pacing (**Figure 3-2**, "Energetics" panels). The increase in MVO_2 was primarily due to an increase in AVO_2.

Statistical analysis of all data using the mixed model approach showed that a trend towards a significantly lower MVO_2-PVA relationship slope was observed with RVOT pacing (**Figure 3-4A**; RA pacing: $1.49x10^{-5} \pm 0.17x10^{-5}$, RVOT pacing: $1.68\ x10^{-5} \pm 0.17\ x10^{-5}$ mL $O_2 \bullet mmHg^{-1} \bullet ml^{-1}$, P=0.055). However, compared to RA pacing, the MVO_2-PVA relationship intercept markedly increased with dyssynchronous contraction (**Figure 3-4B**; RA pacing: 0.025 ± 0.003, RVOT pacing: 0.029 ± 0.003 mL $O_2 \bullet beat^{-1} \bullet 100gLV^{-1}$, $P<0.05$).

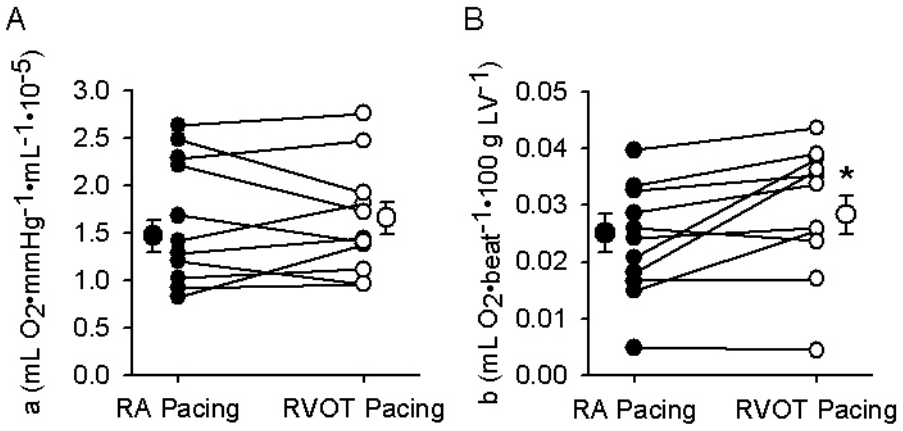

Figure 3-4. Global LV energetic function quantified by the MVO_2-PVA relationship.

(A) Compared to RA pacing, RVOT pacing did not alter the slope (i.e., a) of the MVO_2-PVA relationship. **(B)** However, RVOT pacing increased the intercept (i.e., b) of the MVO_2-PVA relationship. Data: n=11; *$P<0.05$ vs. RA pacing as analyzed using all data in a mixed statistical model. Abbreviations as in **Figures 3-1 and 3-2**.

The responses of mechano-energetic function between RA and RVOT pacing can be better appreciated by the presentation of the data in **Figure 3-5**. Mean (±SEM) data points at each end-diastolic volume during isovolumic contraction are plotted for the ESPVR and MVO_2-PVA relationship. Decreased global LV mechanical function with dyssynchrony was apparent by the marked rightward shift of ESPVR (i.e., increase in V_d) compared to RA pacing. Dyssynchronous contraction resulted in significantly greater oxygen consumption, as illustrated by the upward shift of the MVO_2-PVA relationship. Thus, significantly greater energy (i.e., MVO_2) was required with dyssynchrony to achieve the same mechanical output (i.e., PVA).

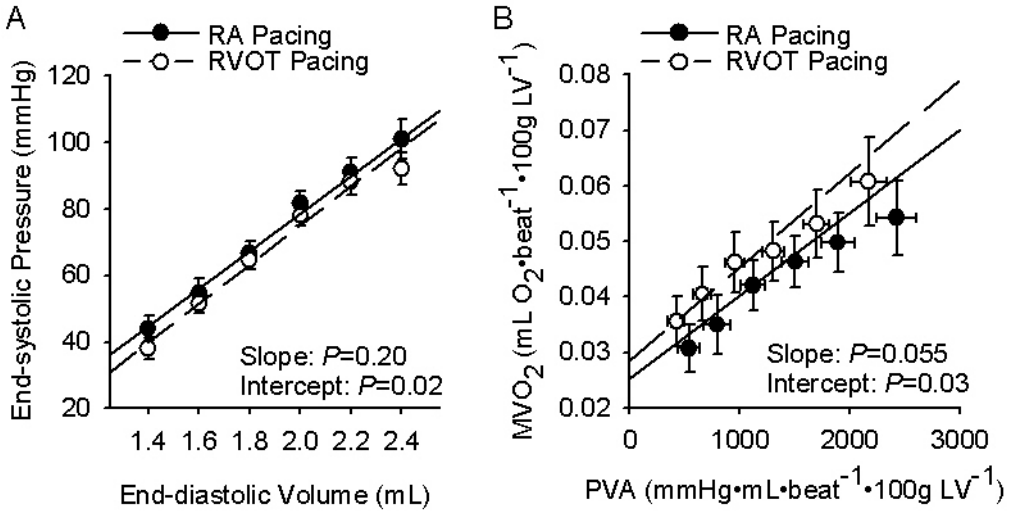

Figure 3-5. Mean (±SEM) data points for global LV mechanical and energetic function.

(A) Compared to RA pacing, the ESPVR was depressed with RVOT pacing indicated by a rightward shift of the ESPVR volume intercept. **(B)** Despite the depression in mechanics, RVOT pacing adversely affected global LV energetics manifested as an increase in the MVO_2-PVA intercept. Data: n=11; RA vs. RVOT pacing as analyzed using all data in a mixed statistical model. Abbreviations as in **Figures 3-1 and 3-2**.

In the presence of contraction dyssynchrony, we hypothesized that there is a disconnect between the mechanical activity occurring at the regional level and the mechanical activity that is observable at the global level. We believe that the summation of all regional mechanical activity represents an internal PVA (say PVA′) that is greater than the PVA observable at the global level. Although only a portion of PVA′ is observed at the global level, this internal PVA

ultimately determines the measured MVO_2 during contraction dyssynchrony. Assuming that the MVO_2-PVA′ relationship with RVOT pacing is the same as the MVO_2-PVA relationship with RA pacing [$MVO_{2\ RA} = a_{RA} \bullet PVA_{RA} + b_{RA}$], we calculated PVA′ (i.e., internal PVA) for each MVO_2 measured under RVOT pacing by: $PVA' = (MVO_{2\ RVOT} - b_{RA})/a_{RA}$ (**Figure 3-6**). Thus, the lost PVA, which is the difference of *calculated* PVA′ and *measured* PVA with RVOT pacing (i.e., $\Delta PVA = PVA' - PVA_{RVOT}$), represents the mechanical energy that is not observable at the global level. Accordingly, excess oxygen consumption that was wasted during global mechanical energy loss is defined as the difference between *measured* MVO_2 with RVOT pacing and *measured* MVO_2 with RA pacing (i.e., $\Delta MVO_2 = MVO_{2\ RVOT} - MVO_{2\ RA}$).

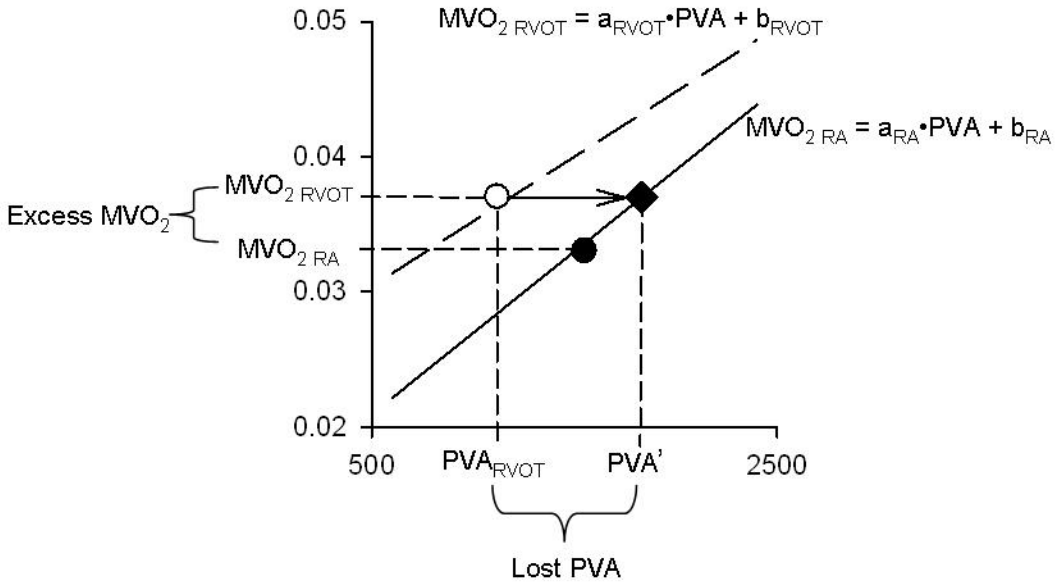

Figure 3-6. Demonstration of PVA′ calculation and concept of lost PVA and excess MVO_2.

Opened and closed circles represent *measured* MVO_2-PVA data points for RA and RVOT pacing, respectively, during one isovolumic contraction. Using the MVO_2 measured under RVOT pacing, PVA′ (diamond) is *calculated* according to the MVO_2-PVA relationship under RA pacing [i.e., $PVA' = (MVO_{2\ RVOT} - b_{RA})/a_{RA}$]. Lost PVA is calculated by the difference between PVA′ and PVA_{RVOT}. Excess MVO_2 (i.e., ΔMVO_2) is calculated by the difference between $MVO_{2\ RVOT}$ and $MVO_{2\ RA}$. Abbreviations: RA = right atrial; RVOT = right ventricular outflow tract. **Other abbreviations as in Figure 3-1**.

For our dataset, a significant correlation (R^2=0.54 P<0.001, **Figure 3-7**) existed between excess MVO_2 (i.e., $MVO_{2\ RVOT} - MVO_{2\ RA}$) and excess PVA (PVA′ – PVA_{RVOT}). It should be noted that this message reiterates the parallel shift (i.e., increased MVO_2 for a given PVA) observed with the MVO_2-PVA relationship as shown in **Figure 3-5**. However, this presentation clearly shows how the excess MVO_2 observed with RVOT pacing can be explained by the mechanical energy loss at the global level.

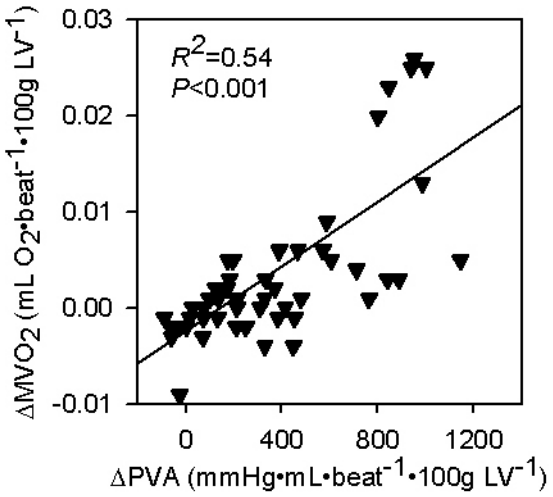

Figure 3-7. Proposed mechanism explaining increased MVO_2 with RVOT pacing.

Correlation between excess MVO_2 ($\Delta MVO_2 = MVO_{2\ RVOT} - MVO_{2\ RA}$) and excess PVA ($\Delta PVA$ = PVA′ – PVA_{RVOT}) calculated for each end-diastolic volume in all experiments. See text for details. Abbreviations as in **Figures 3-1 and 3-2**.

3.4 DISCUSSION

The current study reports two primary findings. First, a small, but significant depression in global LV mechanical function was observed with RVOT pacing. We suspect that dyssynchronous contraction induced by RVOT pacing is responsible for the depression in global LV mechanics. Second, despite the depression in LV mechanical function, LV contraction

dyssynchrony was associated with greater oxygen consumption. Because RVOT pacing consumed more oxygen at a given PVA, dyssynchronous contraction results in decreased myocardial mechanical conversion efficiency (i.e., PVA/MVO_2). In addition, we showed that the increase in oxygen consumption with dyssynchrony significantly correlated with the mechanical energy loss at the global level (i.e., the energy that did not contribute to efficient mechanical output). Certain methodological issues are considered first, before we discuss these findings in detail.

3.4.1 Methodological Considerations

3.4.1.1 Dyssynchrony Model

In the current study, we used RVOT pacing to induce LV contraction dyssynchrony. Pacing at the RVOT is known to prematurely excite the septum and consequently produce delayed LV free-wall contraction causing a LBBB-like contraction pattern [42]. However, echocardiographic evaluation of septal to free-wall dyssynchrony with RVOT pacing has not been confirmed in the isolated rabbit heart preparation. We attempted to quantify septal to free-wall motion in the isolated rabbit heart by echocardiography, but were unable to obtain reliable images for evaluation of contraction dyssynchrony. In addition, we recognize that RV apical pacing, which has been implicated in dyssynchrony and heart failure exacerbation, is more relevant in the human setting than RVOT pacing. However, we previously have shown in canines that RVOT pacing induces marked dyssynchrony similar to a LBBB-contraction pattern and is also associated with depression of global LV function [42, 74]. Therefore, we decided to

use RVOT pacing as a reliable model of dyssynchronous contraction and depression of global LV function.

3.4.1.2 Stability of Isolated Heart Preparation

Although the isolated perfused heart preparation has been extensively used to study various aspects of mechano-energetic function [59, 60, 66, 69, 75], there is always the potentially confounding effects of time. Therefore, we conducted two experiments with RA pacing alone and collected data at the same time intervals as the original protocol. We observed that although global LV mechanical function slightly decreased with time (Figure 3-8, RA1 vs. RA2), MVO_2-PVA relationships were shifted downwards. These changes in MVO_2-PVA relationships are in the opposite direction to those observed with RVOT pacing-induced dyssynchrony (Figure 3-2, "Energetics" panels). However, they are consistent with downward shifts in MVO_2-PVA relationships observed with acute depression in LV contractile state (e.g., reduced extracellular calcium, infusion of β-receptor antagonists) [59, 76]. Therefore, time-dependent preparation deterioration is not a confounder for the observed adverse effect of contraction dyssynchrony on global LV mechano-energetic function.

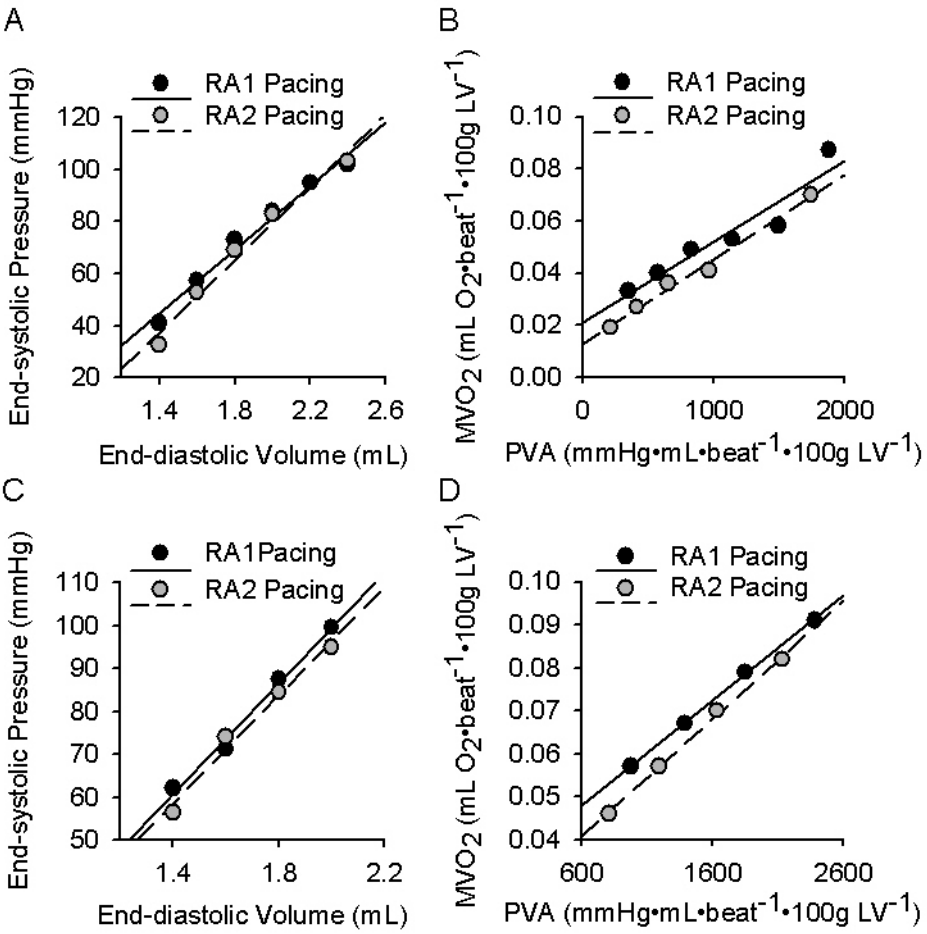

Figure 3-8. Validation of isolated rabbit heart preparation stability.

Global LV mechanical and energetic function for two rabbits (**A-B:** rabbit #1; **C-D:** rabbit #2) under RA pacing conditions only. Although a slight decrease in ESPVR was observed in both experiments for the two pacing protocols (i.e., RA1 and RA2 in **A** and **C**), mechano-energetic coupling was not adversely affected with time, as indicated by a decrease in the MVO_2-PVA relationship **(B, D)**. Abbreviations as in **Figures 3-1 and 3-2**.

3.4.1.3 Isovolumic Contractions

Because all data were collected with hearts contracting under isovolumic conditions (i.e., with a fixed LV volume throughout the cardiac cycle), the relevance of our observations to ejecting contractions may be questioned. However, previous studies have shown that for a fixed contractile state, MVO2-PVA relationship is independent of loading conditions (preload and/or

afterload) such that isovolumic or ejecting contractions yield the same relationship [66, 77]. Therefore, the observations reported here should be equally valid for ejecting contractions.

3.4.2 Interpretation of the Changes in MVO_2-PVA Relationship with LV Dyssynchrony

In the present study, LV contraction dyssynchrony resulted in increased MVO_2 for a given PVA. Specifically, MVO_2–PVA intercept significantly increased (P=0.03) with RVOT pacing-induced dyssynchrony. Although MVO_2–PVA slope tended to increase, it did not reach statistical significance (P=0.055). Based on the scatter in our data with control RA pacing (**Figure 3-4**), it is likely that an increase in the number of experiments will yield a statistically significant increase in the slope value as well. It should be noted, however, that an increase in slope further strengthens our main observation of increased MVO_2 for a given PVA in the presence of LV contraction dyssynchrony.

A potential mechanism explaining the increase of MVO_2 with RVOT pacing is as follows: the observed PVA in the setting of contraction dyssynchrony may underestimate the mechanical activity at the cellular level (termed "internal" PVA) that determines the measured MVO_2. In other words, in the presence of contraction dyssynchrony, there is a disconnect between mechanical activity occurring at the regional level and the mechanical activity observable at the global level such that the "summation" of all regional mechanical activity (i.e., PVA′) is greater than the experimentally measured (global) PVA. This is not a completely theoretical conjecture; there is experimental evidence for it. Early activated regions with ventricular pacing are associated with pre-systolic shortening (or shortening against minimal load) and therefore, perform minimal regional work and contribute little to pressure generation [18, 78]. In contrast, the late-activated regions are typically stretched due to the shortening of

the early activated regions [18, 78] and they contract against higher load, resulting in greater regional work. The temporal discordance of contraction results in a loss of mechanical energy (i.e., energy that does not contribute to pressure generation or volume displacement at the global level). This is primarily due to contraction of one region that stretches the other region over the systolic period (i.e., in early systole: stretching of late activated region by contraction of early activated region; in late systole: stretching of early activated region by contraction of late activated region). In addition to differential deformation patterns in early and late activated regions, it has been shown that myocardial blood flow is significantly higher in late activated regions than at earlier activated regions [78]. Specifically, Prinzen et al. [78] have shown that compared to control RA pacing, RVOT pacing resulted in 87% lower fiber strain and 19% less blood flow in early activated regions. In contrast, fiber strain and blood flow increased by 268% and 142% for the late activated regions. It is interesting to note that the increments for the late activated regions are significantly more than the decrements for the early activated regions, which supports the notion that the mechanical activity summated over all regions could be greater under RVOT pacing.

Although we were unable to measure regional mechanical activity at various locations within the LV to obtain a direct measure of PVA′, we had the knowledge of the system mechano-energetic behavior (MVO_2-PVA relationship) under synchronous contraction (i.e., control RA pacing). The luxury of having this extra piece of information allowed us to calculate PVA′ (i.e., PVA that was consistent with measured MVO_2 under RVOT pacing). Our dataset revealed a significant correlation between excess MVO_2 (i.e., $MVO_{2\ RVOT} - MVO_{2\ RA}$) and the PVA that was not converted into an efficient mechanical output (i.e., the portion of PVA′ not observable at the global level). We readily accept that the excess MVO_2-lost PVA relationship in **Figure 3-7**,

which requires invoking the concept of PVA′ and associated calculations as described above, conveys exactly the same information as the MVO_2-PVA relationships in **Figure 3-5B**. However, the format of data presentation in **Figure 3-7** makes it easy to appreciate the relationship between the lost PVA (i.e., PVA not seen at the global level) and excess MVO_2 associated with RVOT pacing-induced dyssynchrony.

3.4.3 LV Dyssynchrony and Mechano-energetics: Comparison with Previous Studies

Similar to the current study, Burkhoff et al. [79] investigated the influence of ventricular pacing on mechano-energetic function using the MVO_2-PVA relationship. In an isolated canine heart preparation, they observed a concomitant decrease in global LV mechanics and energetics following RV free-wall pacing such that the MVO_2-PVA relationship was not affected. This is inconsistent with our observation of an upward shift in the MVO_2-PVA relationship following dyssynchrony induced by RVOT pacing. The difference in the pacing site (RVOT in the current study vs. RV free-wall in the Burkhoff study) may explain this discrepancy. Contraction patterns are known to depend on ventricular pacing sites. We hypothesize that RV free-wall pacing (Burkhoff study) produced larger early activated regions as compared to RVOT pacing (current study), primarily because RVOT pacing provides a more direct route to the His Purkinje system. This differential contraction pattern may explain the apparent discrepancy in MVO_2: the greater amount of early activated regions in the Burkhoff study resulted in reduced total regional work and consequently, MVO_2 and the opposite was true for the current study. This conjecture is consistent with the potential mechanism proposed above to explain changes in the MVO_2-PVA relationship with contraction dyssynchrony (i.e., the observed PVA may underestimate the internal PVA at the cellular level that determines the measured MVO_2). The discrepancy

between our results and those of Burkhoff et al. underscores the notion that all dyssynchronous contractions are not created equal; the mechano-energetic consequences are dependent on the specific pattern of dyssynchrony. Further studies are required to investigate the mechanism of changes in global LV mechano-energetics under different contraction patterns.

3.4.4 Clinical Implications

It is important to note that we observed an increase in myocardial oxygen consumption with dyssynchrony (RVOT pacing), even though the mechanical function was depressed. Interestingly, data from the DAVID Trial indicated that right ventricular stimulation was associated with deleterious effects, leading to progressive decline of global LV function and higher risk of congestive heart failure due to ventricular desynchronization [80]. Although there is a difference in RV pacing site (RVOT vs. RV apical), the increased energetic demand associated with ventricular dyssynchrony as observed in the current study may be a contributing factor to the progressive decline in global LV function observed in the DAVID Trial. It is reasonable to speculate that worsening of myocardial mechanical conversion efficiency with dyssynchrony may contribute to the exacerbation of heart failure. In addition, Nelson et al. [22] reported that patients with LBBB and dilated cardiomyopathy benefited from left ventricular pacing as indicated by improved systolic function and decreased myocardial energy demands. We can interpret these findings in the context of our results: cardiac resynchronization therapy (CRT) corrects dyssynchronous contraction, eliminating the difference between internal and external (measured) PVA and excess MVO_2. This supports our proposed mechanism that the dyssynchronous myocardial elements are responsible for increased myocardial oxygen demands. Although CRT-induced improvement in mechanical function is well established, our results

reveal how this therapy may reverse the adverse effects of dyssynchrony on global LV energetic function.

3.5 CONCLUSIONS

Following RVOT pacing-induced contraction dyssynchrony, global LV mechano-energetic function was adversely affected. Although a small, but significant depression in global LV mechanical function was observed with RVOT pacing, this contraction pattern was associated with an increase in MVO_2 for a given PVA, resulting in decreased myocardial mechanical conversion efficiency (i.e., PVA/MVO_2). A possible mechanism explaining the observed increase in MVO_2 with dyssynchrony is that the observed PVA at the global level underestimates the internal PVA at the cellular level, which is likely to be the true determinant of MVO_2. Irrespective of the mechanism of action, our data clearly demonstrate that dyssynchronous contraction not only depresses global LV mechanical function, but also places an energetic burden on the myocardium. Combined results of the present and previous studies underscore the notion that all dyssynchronous contractions are not created equal; mechano-energetic consequences are dependent on the specific pattern of dyssynchrony induced by different pacing sites.

4.0 STUDY 2: DIFFERENTIAL EFFECTS OF LEFT VENTRICULAR PACING SITES IN AN ACUTE CANINE MODEL OF CONTRACTION DYSSYNCHRONY

Specific Aim 2. To develop an efficient, robust clinical tool to *quantify dyssynchrony* and identify responders for CRT.

Specific Aim 3. To investigate the *link between regional and global LV function* under different contraction patterns induced by ventricular pacing at various sites.

4.1 INTRODUCTION

The clinical efficacy of CRT is generally quantified in terms of its effects on LV systolic function and other hemodynamic indices, such as LV ejection fraction, stroke volume, stroke work, maximum rate of LV pressure increase (dP/dt_{max}), and aortic pulse pressure [41, 46, 47, 81, 82]. As previously mentioned, several clinical trials have documented that CRT improves functional status and survival [4-11], but 20-30% of patients do not benefit from this therapy [12]. Two potential factors that may contribute to this variability in CRT benefit include limited knowledge regarding the mechanisms underlying the beneficial effects of CRT and lack of robust algorithms for identifying the optimal pacing site(s). Accordingly, although several studies have focused on deriving an algorithm to assess contraction dyssynchrony [39, 42, 44,

83], an ideal standard is yet to be developed, particularly from the perspective of robustness and ease-of-use.

The primary goal of the present study was to assess the effects of LV pacing site (apex *vs*. free-wall) on restoration of radial contraction synchrony and global LV performance in a canine model of contraction dyssynchrony. We also report a new robust algorithm to quantify radial synchrony. Portions of this work have been previously published elsewhere [74].

4.2 METHODS

4.2.1 Preparation

The protocol was approved by the Institutional Animal Care and Use Committee and conformed to the position of the American Physiological Society on research animal use. Seven mongrel dogs, weighing 21.0 ± 1.5 kg were studied after an overnight fast. All dogs were anesthetized with sodium pentobarbital (30 $mg \cdot kg^{-1}$ induction; 1.0 $mg \cdot kg^{-1} \cdot h^{-1}$ with intermittent boluses, as needed), their tracheas intubated (8 Fr. Portex endotracheal tube) and mechanically ventilated (Harvard dual-phase animal ventilator) with a 10 $mg \cdot kg^{-1}$ tidal volume. Frequency was adjusted to maintain an arterial pCO_2 between 35-40 mm Hg. A 6 Fr. 11 pole multi-electrode conductance catheter (Webster Laboratories, Irvine, CA) and an LV micromanometer catheter (MPC-500, Millar, Houston, TX) were placed for LV pressure-volume analysis via the right internal carotid artery and the left common carotid artery, respectively, as previously described by us [84]. These devices allowed for the continuous measurement of LV pressure and volume allowing calculation of LV stroke volume and stroke work. The pericardium was opened and

epicardial pacemaker leads were placed on the right atrium (RA), right ventricular (RV) free-wall near the anterior infundibulum (i.e., RV outflow tract), LV mid-free-wall near the mid-posterior-lateral wall, and LV apex for multi-site stimulation. The pericardium was re-opposed with multiple interrupted sutures and positive end-expiratory pressure (PEEP) applied to re-expand the lungs. Afterward, 5 cm H_2O PEEP was applied to maintain end-expiratory lung volume for the remainder of the experiment. Fluid resuscitation was performed prior to starting the protocol to restore apneic LV end-diastolic volume to values similar to where they were prior to sternotomy.

4.2.2 Protocol

All measurements were made with respirations suspended at end-expiration of 5 cm H_2O PEEP to control for the effects of cardiopulmonary interactions. The protocol consisted of pacing and then creating a stable apneic steady state for data acquisition. To avoid retrograde conduction for all pacing steps of the protocol, RA pacing was performed at frequencies 5-10 min^{-1} above the intrinsic rhythm. Right atrial pacing is defined as normal ventricular contraction for subsequent comparisons. All succeeding ventricular pacing studies were then done with sequential pacing at an A-V delay of 30 ms. This pacing delay prevented ventricular fusion beats from contaminating the ventricular pacing effects of CRT. Contraction dyssynchrony was created by simultaneous RA and high RV free-wall pacing, which induced a LBBB-like contraction pattern. We then compared the impact of counter-pacing at two different LV sites on the RV pacing induced dyssynchronous contraction pattern. We chose to simultaneously pace at either the LV apex or posterior-lateral LV free-wall at the mid-ventricular level below the left circumflex artery to mimic CRT, referred to as CRTa and CRTf, respectively. The order of apical and free-wall

pacing was alternated among sequential animals to eliminate any sequencing effects. Pacing was sustained for > 30 seconds before measurements were made for each step so that hemodynamic equilibrium could be established. In practice, hemodynamic stability usually took < 15 seconds to occur. Between each ventricular paced rhythm interval, the animals were returned to RA pacing and all hemodynamic variables were stabilized to baseline levels before the next step in the protocol was initiated.

4.2.3 Echocardiographic Tissue Doppler and Tissue Strain Imaging

An echocardiographic system with tissue Doppler (TD) imaging capabilities was used (Aplio SSA-770A, Toshiba Medical Systems Corporation, Tokyo, Japan) with a 3.0 MHz transducer. Digitized routine and color-coded TD images were acquired from mid-LV short-axis levels using epicardial imaging and a transducer stand. TD system frame rates were a minimum of 49 frames·sec^{-1} with a pulse repetition frequency of 4.5 kHz. Velocity ranges were from ± 17.0 to ± 13.0 cm·sec^{-1} to select the lowest possible range to maximize the sensitivity of low velocity values while aliasing did not occur. Color TD video data were analyzed off-line using custom software (TDI-Q, Toshiba Medical Systems Corporation, Tokyo, Japan) as described by us for this canine preparation [42]. Briefly, the myocardial vector (V) of motion toward a manually placed point of contraction center was calculated as: $V_{motion} = V_{beam}/\text{cosine}(\theta)$, where θ is the angle of incidence of the ultrasound beam. Sectors were masked where the angle of incidence approached 90º and Doppler calculations were not possible. The mid-LV short-axis image was segmented into six sectors: mid-septum (MS), antero-septum (AS), antero-lateral (AL), postero-lateral (PL), posterior (P) and inferior (I), manually drawn as linear polygons placed in the inner third of the wall (**Figure 4-1**, left panel). This subendocardial region was selected to represent

the major component of transmural thickening and to minimize translational or right ventricular effects on regional LV wall dynamics. A tracking algorithm was employed with manual adjustment of the size and shape of the regions of interest to maintain its subendocardial location throughout the cardiac cycle. Strain was calculated as time integral of velocity gradient that was calculated along radii of a distance (Δr) toward the contractile center. Angle corrected, color-coded Lagrangian strain was calculated as percent wall thickening toward the contraction center and displayed on a continuous scale from dark red to bright orange-yellow as positive strain corresponding to wall thickening. Radial strain waveforms were derived for each myocardial segment (**Figure 4-1**, right panel) and stored for off-line analysis.

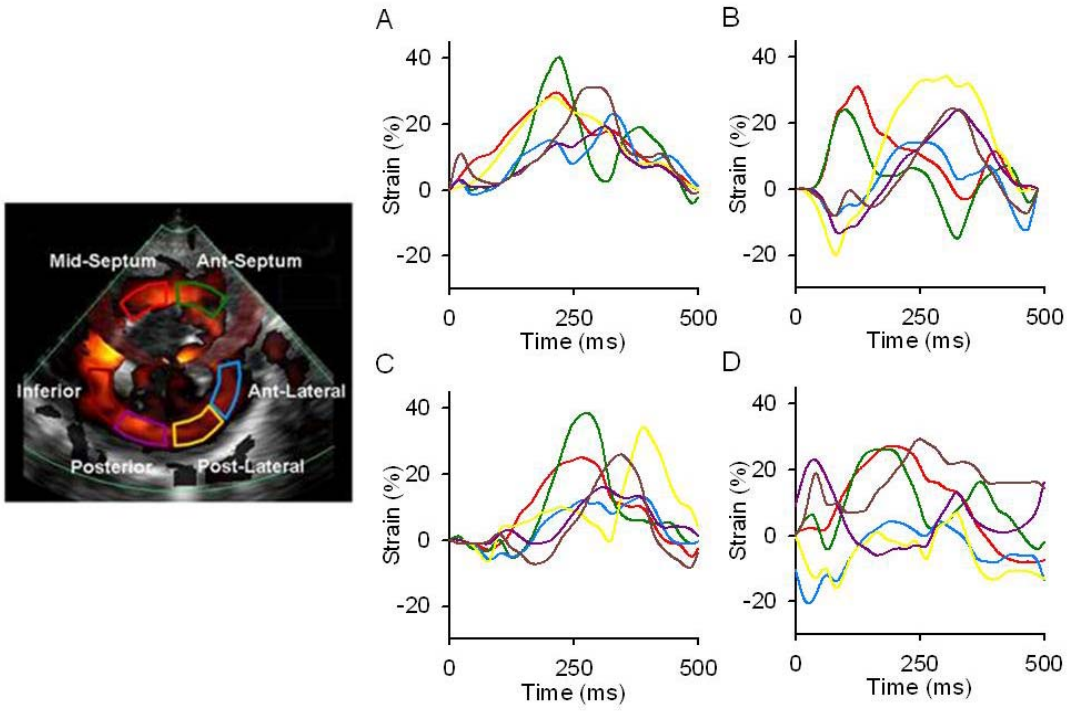

Figure 4-1. Tissue Doppler image and tissue Doppler-derived strain waveforms.

Left Panel: Short-axis TDI showing segmentation of mid-LV. **Right Panel:** Strain waveforms derived from velocity data were obtained at each of the six segments under four pacing modalities: **(A)** RA pacing, **(B)** RV pacing, **(C)** CRTa, and **(D)** CRTf; line colors of waveforms correspond to segments labeled in TDI. Abbreviations: TDI = tissue Doppler image; RA = right atrial; RV = right ventricular; CRTa = cardiac resynchronization therapy at LV apex; CRTf = cardiac resynchronization therapy at LV free-wall.

4.2.4 Contraction Synchrony Analysis

Regional radial synchrony was analyzed by implementing a newly developed algorithm on time-strain curves constructed from color-coded strain data at the mid-LV level. The new index derived from this algorithm was compared to other commonly used indices of dyssynchrony.

4.2.4.1 Cross-Correlation Synchrony Index

A new index of synchrony was developed in the time-domain via a pair-wise correlation analysis of radial strain waveforms over systole for six myocardial segments. The peak of the QRS wave on ECG defined the onset of systole. Off-line analysis of data indicated that global end-systole, defined by the dicrotic notch of aortic pressure waveform, and time of latest peak radial strain occurred in close proximity. Thus, end-systole was defined by the time of latest peak strain. Only the systolic portion of the strain waveforms was used for all cross-correlation analyses. Given that strain data were acquired for 6 segments, there are 15 segment pairs. For each segmental pair, multiple linear regression was performed to derive cross-correlation coefficients (range of -1.0:1.0 meaning maximum dyssynchrony: maximum synchrony) for a number of "time delays" using a custom written MATLAB (v. R2006a, The MathWorks, Inc.) program (see Appendix B.1). For each segmental pair, a cross-correlation spectrum was obtained by shifting one segment in time with respect to the other (Figure 4-2).

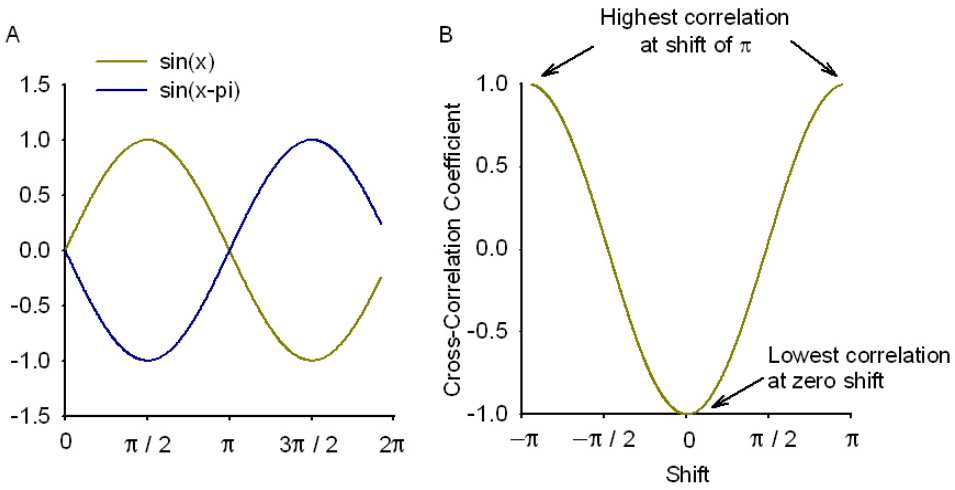

Figure 4-2. Example of cross-correlation spectrum.

(A) Raw data illustrated as two sine waveforms of various phases. **(B)** Cross-correlation spectra obtained for the pair of sine waveforms. Note that since the waveforms are mirror opposites in morphology, the cross-correlation coefficient is -1.0. However, if shifted by ±π, the waveforms now perfectly "line-up" and a cross-correlation coefficient of +1.0 are obtained.

From this cross-correlation spectrum, three values can be derived that could potentially describe the synchrony of contraction: (1) cross-correlation value at zero time-shift (corresponding to the raw, unshifted waveforms), (2) maximum cross-correlation value and (3) time shift corresponding to the maximum cross-correlation value which indicates the shift necessary to optimally "line-up" the two waveforms. Each of the values that were derived from the spectrum for all 15 segmental pairs were summed. For example, at zero time shift, all cross-correlation coefficients were summed and used as an overall index of synchrony; a value of 15 for this index would imply perfect synchrony and lower values would correspond to progressively greater dyssynchrony. An example of cross-correlation analysis for one segmental pair is shown in **Figure 4-3**.

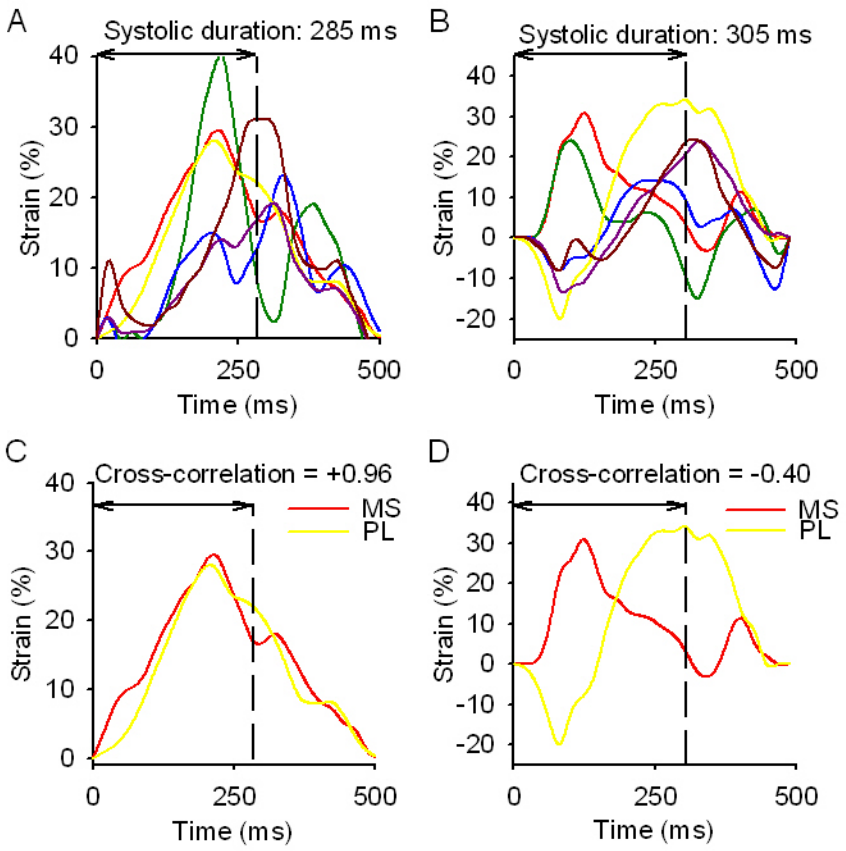

Figure 4-3. Example of cross-correlation method developed to analyze contraction synchrony.

Top Panels: Regional myocardial strain waveforms for all six segments under **(A)** RA pacing and **(B)** RV pacing. End systole was determined by the time to latest peak strain (dashed line). Waveform colors correspond to the segments labeled in **Figure 4-1**, left panel. **Bottom Panels:** Cross-correlation analysis applied to one segmental pair (MS-PL) over systole. **(C)** With RA pacing, the two segments are contracting almost synchronously, as indicated by high cross-correlation value (0.96) over the systolic duration. **(D)** In contrast, significant contraction dyssynchrony is evident with RV pacing manifested as mid-septal to postero-lateral contraction delay and a low cross-correlation value (-0.40) over the systolic duration. Abbreviations: MS = mid-septal; PL = postero-lateral; other abbreviations as in **Figure 4-1**.

4.2.4.2 Additional Synchrony Indices

Two commonly used indices of dyssynchrony were also calculated to provide a preliminary validation of our new index and to confirm that our findings were not a result of the specific algorithm used in the analysis. These two indices were: 1) maximal time delay of peak systolic strain calculated from data for multiple segments [42], and 2) standard deviation (SD) of time to

peak systolic strain calculated from data for multiple segments [85]. Although Yu *et al.* [85] used velocity instead of strain to calculate the SD index in their study; the conceptual underpinnings are the same – higher value of SD indicates a greater degree of dyssynchrony.

4.2.5 Global LV Performance Analysis

Indices of global performance (e.g., LV stroke volume, LV stroke work, LV dP/dt_{max} and dP/dt_{min}) were calculated from LV pressure-volume data obtained under steady-state apneic conditions for each pacing modality using standard formulae [84].

4.2.6 Statistical Analysis

Data are expressed as mean ± SEM. One-way analysis of variance (ANOVA) with repeated measures was used to evaluate the effects of different pacing modalities on regional LV synchrony and indices of global LV performance. Tukey-Kramer test was employed for *post hoc* pair-wise comparisons following each ANOVA. Significance was determined as $P<0.05$. Linear regression analysis was used to compare the newly developed index of contraction synchrony with the existing dyssynchrony indices.

4.3 RESULTS

4.3.1 Synchrony Indices Derived from Cross-Correlation Analysis

Although derivation of a cross-correlation spectrum was promising in theory, the complexity of physiological signals introduced certain challenges. For example, the two sine waves shown in **Figure 4-2** are mirror opposites of each other. However, with dyssynchrony, waveforms tend to exhibit complex patterns with multi-faceted behavior (i.e., thinning/thickening over different portions of the cardiac cycle). Therefore, two waveforms may never "line-up". Thus, although 3 different synchrony indices were derived from the cross-correlation spectrum (see **Section 4.2.4.1**), only the cross-correlation sum at zero time delay was used as an index of radial synchrony.

4.3.2 Induction of LV Contraction Dyssynchrony

RV pacing induced radial contraction dyssynchrony manifested as a significant decrease in the synchrony index from 11.1 ± 0.8 (RA pacing) to 4.8 ± 1.2 (P<0.01, **Figure 4-4**). Regional dyssynchrony was correlated with marked depression in LV pressures, volumes, and global LV functional indices [e.g., stroke volume (SV): 15 ± 2 to 10 ± 1 mL; cardiac output (CO): 2.0 ± 0.3 to 1.4 ± 0.1 $L \bullet min^{-1}$; stroke work (SW): 137 ± 22 to 60 ± 14 mJ; LV dP/dt_{max}: 1346 ± 144 to 1087±166 mm $Hg \bullet s^{-1}$; LV dP/dt_{min}: -1679 ± 221 to -1072 ± 165; all P<0.05]. Hemodynamic data and calculated variables under the control condition (RA pacing) and contraction dyssynchrony model (RV pacing) are presented in **Table 4-1**. Overall, RV pacing was associated with both marked radial dyssynchrony and depression of global LV performance.

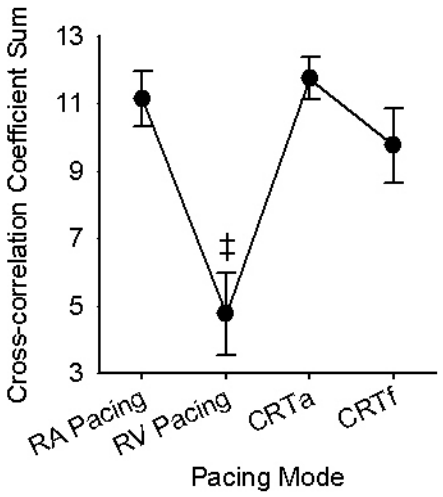

Figure 4-4. Mean values of radial synchrony index at mid-LV.

Compared to control (RA pacing), RV pacing resulted in a marked decrease in synchrony and both modes of CRT (i.e., CRTa and CRTf) restored synchrony to the control level (i.e., RA pacing). Data: mean ± SEM; n=7; ‡P<0.01 *vs*. RA pacing. Abbreviations as in **Figure 4-1**.

Table 4-1. Global LV performance values for different pacing modalities.

	RA Pacing	RV Pacing	CRTa	CRTf
HR (beats•min^{-1})	133 ± 6	133 ± 6	133 ± 6	133 ± 6
ΔHR			*0 ± 0 %*	*0 ± 0 %*
MAP (mm Hg)	91 ± 7	71 ± 7 §	71 ± 6	72 ± 7
ΔMAP			*2 ± 5 %*	*3 ± 7 %*
LV EDP (mm Hg)	11 ± 2	10 ± 2	10 ± 2	9 ± 2
ΔLV EDP			*-1 ± 9 %*	*-13 ± 3 %*
LV ESP (mm Hg)	96 ± 8	77 ± 8 §	77 ± 7	77 ± 8
ΔLV ESP			*1 ± 4 %*	*1 ± 5 %*
LV EDV (mL)	46 ± 7	41 ± 6 §	39 ± 7	39 ± 6
ΔLV EDV			*-8 ± 3 %*	*-5 ± 3 %*
LV ESV (mL)	31 ± 5	30 ± 6	23 ± 6 ‡	27 ± 6*
ΔLV ESV			*-36 ± 9 %*	*-12 ± 4 %*
SV (mL)	15 ± 2	10 ± 1 §	16 ± 2 ‡	12 ± 1**
ΔSV			*58 ± 16 %*	*13 ± 9 %*
CO (L•min^{-1})	2.0 ± 0.3	1.4 ± 0.1 §	2.1 ± 0.2 ‡	1.5 ± 0.2**
ΔCO			*58 ± 16 %*	*13 ± 9 %*
dP/dt$_{max}$ (mm Hg•s^{-1})	1346 ± 144	1087 ± 166 §	1109 ± 116	1144 ± 138
ΔdP/dt$_{max}$			*8 ± 8 %*	*9 ± 8 %*
dP/dt$_{min}$ (mm Hg•s^{-1})	-1679 ± 221	-1072 ± 165 §	-1218 ± 181	-1243 ± 216
ΔdP/dt$_{min}$			*17 ± 7 %*	*17 ± 9 %*
SW (mJ)	137 ± 22	60 ± 14 §	113 ± 13 ‡	75 ± 12*
ΔSW			*180 ± 94 %*	*65 ± 43 %*

Data: mean ± SEM; n=7. For CRT, below each performance index is the percentage change with respect to RV pacing. §P<0.05, RV pacing *vs.* RA pacing; ‡P<0.01, CRTa *vs.* RV pacing or CRTf *vs.* RV pacing; $^{*}P$<0.05, $^{**}P$<0.01, CRTf *vs.* CRTa. Abbreviations: HR = heart rate; MAP = mean arterial pressure; LV EDP, LV ESP = left ventricular end-diastolic and end-systolic pressure, respectively; LV EDV, LV ESV = left ventricular end-diastolic and end-systolic volume, respectively; SV = stroke volume; CO = cardiac output; dP/dt_{max}, dP/dt_{min} = maximum and minimum rate of change of LV pressure, respectively; SW = LV stroke work; RA = right atrial; RV = right ventricular; CRTa = cardiac resynchronization therapy at LV apex; CRTf = cardiac resynchronization therapy at LV free-wall.

4.3.3 Resynchronization with CRT

As illustrated in **Figure 4-4**, CRT using LV apical pacing (CRTa) restored radial synchrony to that seen with RA pacing, with the synchrony index increasing to 11.7 ± 0.6 (P<0.01 *vs.* RV

pacing and *P*=NS *vs*. RA pacing). Similarly, CRT using LV free-wall pacing (CRTf) also significantly improved radial synchrony by increasing the synchrony index to 9.8 ± 1.1 (*P*<0.01 *vs*. RV pacing and *P*=NS *vs*. RA pacing). The synchrony index was not significantly different between the two CRT modes (*P*=NS, CRTf *vs.* CRTa).

Although some scatter existed, the newly developed synchrony index (i.e., cross-correlation coefficient sum) was significantly correlated with two commonly used measures of dyssynchrony (**Figure 4-5A, B**). Quantification of dyssynchrony using these two indices (**Figure 4-5C, D**) yielded the same results as those obtained using the cross-correlation analysis (i.e., decreased synchrony with RV pacing and significant improvement of synchrony with both CRT modes).

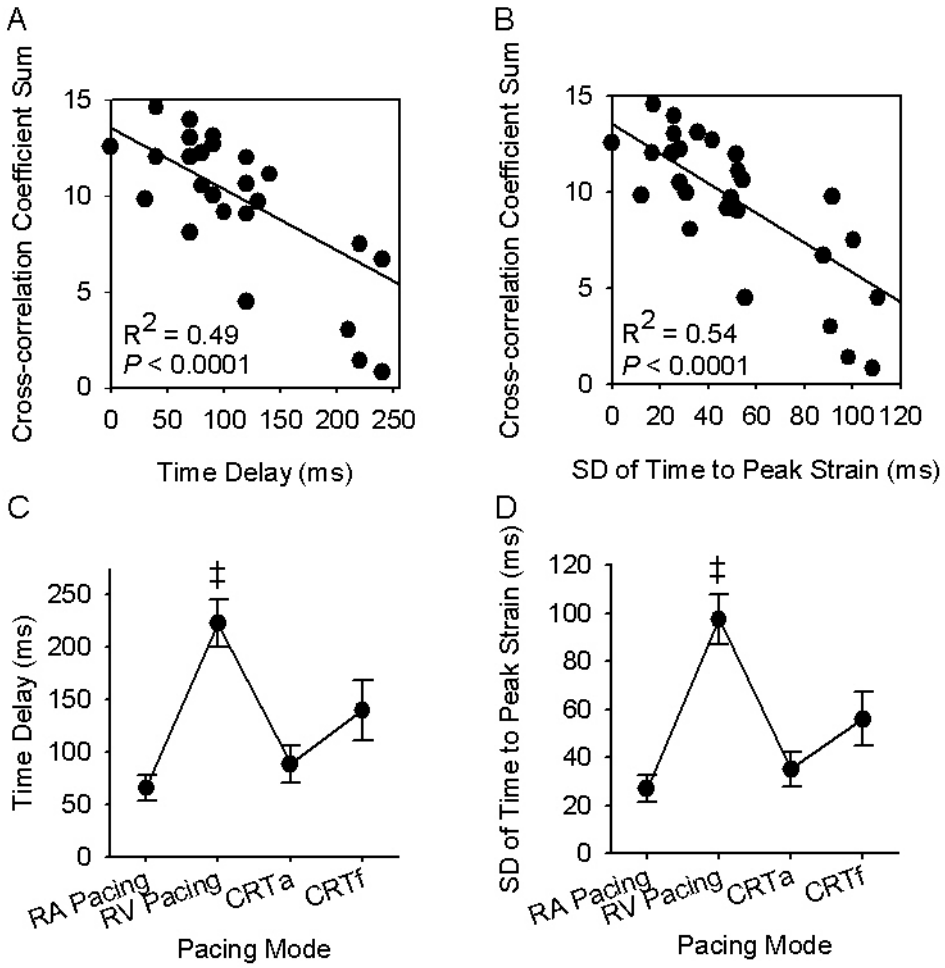

Figure 4-5. Comparison of the new synchrony index with two currently used indices.

Top Panels: Significant correlations were observed between the newly developed measure of synchrony (cross-correlation coefficient sum) and the two currently used indices [**(A)** time difference between earliest and latest peak segmental strain (Time Delay); **(B)** standard deviation (SD) of time to peak strain for six segments]. **Bottom Panels:** Mean values of commonly used dyssynchrony indices [**(C)** Time Delay; **(D)** SD of Time to Peak Strain] for each pacing mode. For both indices, compared to the control condition (RA pacing), RV pacing resulted in marked increase in contraction dyssynchrony, as indicated by increased values, and both CRT modes restored synchrony to RA values. Data: mean ± SEM; n = 7; ‡P<0.01 *vs*. RA pacing. Abbreviations as in **Figure 4-1**.

4.3.4 CRT and Global LV Performance

Hemodynamic data and calculated variables under RV pacing and both CRT modes (CRTa and CRTf) are presented in **Table 4-1**. Below each performance index is the percent change with respect to its value with RV pacing.

When CRTa was used to correct for RV pacing-induced contraction dyssynchrony, mean arterial pressure (MAP) and LV end-systolic pressure (ESP) did not change. However, global LV systolic performance was significantly improved with CRTa (SV: 16 ± 2 mL; CO: 2.1 ± 0.2 $L \bullet min^{-1}$; SW: 113 ± 13 mJ; all $P<0.01$, CRTa *vs*. RV pacing). The increase in CO was primarily a result of significantly lower LV end-systolic volume (ESV: 23 ± 6 mL; $P<0.01$, CRTa *vs*. RV pacing). Although most LV systolic performance indices were increased with CRTa, LV dP/dt_{max} did not change (P=NS, CRTa *vs*. RV pacing). Furthermore, diastolic performance was unaltered compared to the RV pacing mode as evidenced by unchanged LV dP/dt_{min} and end-diastolic volume (P=NS, CRTa *vs*. RV pacing).

Surprisingly, despite a significant improvement of radial synchrony with CRTf, global LV function was not altered with respect to RV pacing. Furthermore, SV, SW and CO were all significantly less with CRTf than with CRTa ($P<0.05$ *vs.* CRTa). Thus, there seems to be discordance between restoration of radial synchrony and global LV performance following CRTf.

The differential response with respect to the improvement in global LV systolic function between the two CRT modes can be better appreciated from the data illustrated in **Figure 4-5**. For CRTf, the changes in global LV systolic performance indices hovered around zero, even when there was significant improvement in radial synchrony. In contrast, CRTa resulted in improvements in both radial synchrony and global LV systolic performance. Despite the variability in global LV performance (especially for dP/dt_{max}), the changes in these indices were proportional to the improvements in radial synchrony with CRTa (**Figure 4-6**).

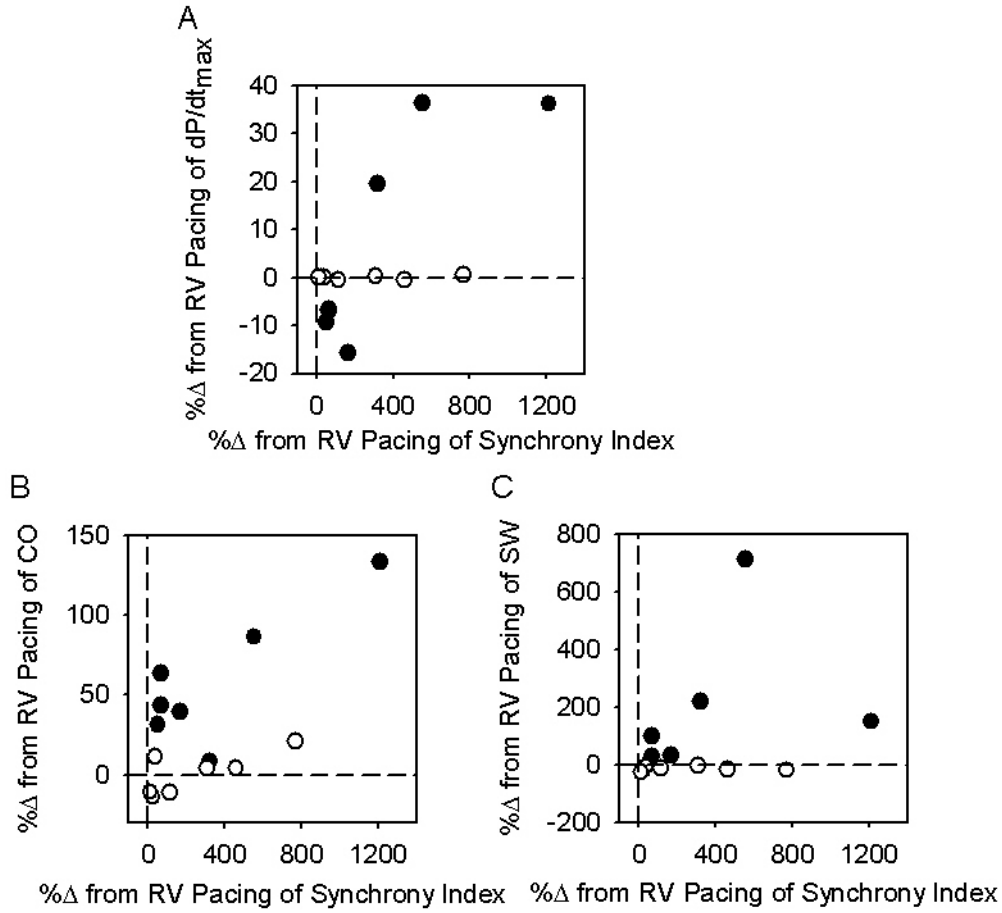

Figure 4-6. Percentage change in global LV performance indices and synchrony index.

Relationships between percentage changes in global performance indices [**(A)** dP/dt_{max}, **(B)** CO, **(C)** SW] and percentage changes in synchrony index. Percentage changes were calculated with respect to the values for RV pacing. Closed and open circles correspond to CRTa and CRTf values, respectively. As CRTa improves synchrony, there is a concordant improvement in global LV performance. However, despite increasing synchrony with CRTf, global LV performance is unaltered. Abbreviations as in **Figure 4-1 and Table 4-1**.

Representative pressure-volume loops for RV pacing and both CRT modes are shown in **Figure 4-7**. Compared to RV pacing (i.e., the dyssynchrony model), CRTa significantly decreased LV end-systolic volume, without any change in end-systolic pressure (**Table 4-1**), indicating augmented global LV contractile state. Although a similar pattern of changes in ESV and ESP was seen with CRTf, the decrease in ESV did not reach statistical significance (**Table 4-1**), indicating modest or no change in global LV contractility with respect to RV pacing.

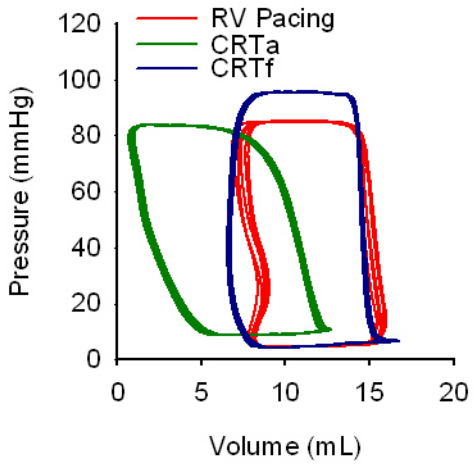

Figure 4-7. Representative P-V loops under dyssynchrony and CRT.

With respect to RV pacing (red), CRTa (green) resulted in significantly lower end-systolic volumes, with little change in end-systolic pressures, suggesting increased LV contractility with CRTa. In contrast, CRTf (blue) was associated with modest or no change in LV contractility as judged by the changes in end-systolic pressure-volume points (see **Table 4-1** for group average values). Abbreviations as in **Figure 4-1**.

4.3.5 Effects of LV Pacing Alone

Given that LV pacing can create dyssynchronous contraction by itself [18], we assessed radial dyssynchrony under LV apical (LVa) and LV free-wall (LVf) pacing alone (i.e., in the absence of simultaneous RV pacing). With LVa pacing alone, our synchrony index decreased slightly (9.8 ± 1.1); however this was not significantly different from the RA pacing value (11.1 ± 0.8; P=0.23). In contrast, LVf pacing alone significantly decreased the synchrony index to 4.5 ± 1.7 (P = 0.002, LVf *vs*. RA). Thus, the observation that CRTf failed to improve global LV systolic performance in spite of a significant improvement in radial synchrony may be a consequence of the dyssynchronous effects of LVf pacing alone. In addition, radial synchrony may not have been restored with CRTf at all cross-sectional planes (we only examined synchrony at the mid-LV level).

4.4 DISCUSSION

The current study reports three primary findings. (1) Although both modes of CRT (CRTa and CRTf) significantly restored radial synchrony, only CRTa increased global LV systolic function. (2) The improvement in global LV systolic function with CRTa appears to be driven by increased LV contractility, as indicated by an increase in SV with unchanged LV EDV, LV ESP, and HR. (3) The dissociation between changes in synchrony and global LV performance with CRTf suggests that regional analysis from a single plane may not be sufficient to adequately characterize contraction synchrony. We also report a new index to quantify LV synchrony using pair-wise cross-correlations of six LV wall regions. Before we discuss the current findings, we will first address certain methodological considerations.

4.4.1 Methodological Considerations

4.4.1.1 Dyssynchrony Model

Two relevant issues need to be noted here. First, we did not study the impact of dyssynchrony or CRT in the setting of chronic structural conduction abnormalities such as blockage of the His-Purkinje System or myocardial ischemia/infarction. Instead, we used RV pacing as a model of LBBB-like contraction pattern. Right ventricular pacing is known to produce delayed LV contraction [20] and consequently, LV contraction dyssynchrony, which has been shown to decrease stroke volume, stroke work, and LV pressures [42]. Although RV pacing-induced dyssynchrony has been used previously [19, 20, 42], functional differences in contraction resynchronization using an intact conduction system may not extrapolate to studies where

anatomical LBBB is present. Second, we studied the effect of dyssynchrony and CRT in healthy, non-failing hearts. Contractile and structural changes occur in heart failure that may alter the response of CRT. Future studies involving a heart failure model with structural defects will address these issues.

4.4.1.2 Consequence of Short A-V Delay

The animal model used in the current study involved an intact conduction system; therefore a short A-V delay was necessary to avoid intrinsic activation of the ventricles (i.e., fusion beats). However, a short A-V delay often leads to inefficient atrial emptying because the atrium is forced to contract against the closed mitral valve [86], which adversely affects A-V coupling by decreasing LV preload. Therefore, the observed lower end-diastolic volumes with RV pacing and CRT may be a consequence of the short A-V interval used in the current study. It should be noted, however, that our inferences regarding the differential effects of the modes of CRT (CRTa *vs*. CRTf) on LV global performance are not confounded by the short A-V delay because this short delay existed for all three conditions (RV pacing, CRTa, CRTf) that were included in the statistical analysis. Furthermore, in a previous study using this model we performed A-V nodal ablation and saw no differences in regional or global function with CRT as compared to the intact A-V node condition (data not shown).

4.4.2 Quantification of Dyssynchrony

Quantification of contraction dyssynchrony is an emerging interest in cardiology and several different indices have been reported to assess it. We developed a new algorithm to quantify LV

synchrony by pair-wise cross-correlation analysis of LV regional TD segmental strain. Previously, mechanical dyssynchrony has been quantified using time to peak systolic longitudinal velocity using TD from echocardiographic apical views and expressed principally as either the standard deviation of 12 segments or the maximum opposing wall delay [39, 43, 87, 88]. However, difficulties may exist with TD angle dependence, signal noise, translational effects of scar, and variations in heart rate [12, 38, 39, 41], which can make this approach less robust. Angle-corrected TD imaging minimizes some but not all of the angle dependence bias. Importantly, tissue strain echocardiography has the advantage over TD velocity with respect to differentiating active contraction from passive motion or tethering, which are important confounding variables in patients with ischemic heart disease [42].

Mid-ventricular cross-sectional radial strain has recently been shown to predict both acute and chronic clinical response to CRT using the maximal time delay between earliest and latest peak strain [43, 44]. Although our new index significantly correlated with this index, cross-correlation analysis is expected to be superior in assessing LV contraction synchrony. Our synchrony algorithm assesses the entire systolic portion of the time-strain waveform, and thus offers a more robust method in assessing contraction synchrony. It also overcomes the limitation of variations in heart rate because each region is compared to a common end-systole. However, because our new algorithm was applied to a non-ischemic, non-heart failure model, we cannot prove superiority over other indices at this time. Future studies involving an ischemic model will address this issue. Importantly though, as this algorithm is assessed, one limitation must be kept in mind: the inability of cross-correlation analysis to distinguish differences in amplitude. If heterogeneity of contractile state exists between segments that are temporally synchronous,

cross-correlation analysis will not identify the contractile disparity. However, this type of dyssynchrony may not be amenable to pacing therapy [89].

The current study used TD radial strain at a mid-papillary view to assess contraction dyssynchrony. Although twelve longitudinal segments were used to calculate the dyssynchrony index in other studies [85], we were limited to six segments in our analysis for two reasons: 1) Doppler calculations are not possible where the angle of incidence approaches 90º, and 2) increasing the number of segments in processing TD data increases the signal-to-noise ratio, which jeopardizes the reliability of the data. We plan to improve our analysis in future studies by using speckle-tracking algorithm of routine echocardiographic images, which will allow us to apply our cross-correlation analysis on more LV regions to better quantify contraction synchrony.

4.4.3 LV Pacing Sites: Implications for CRT and Contraction Synchrony Analysis

We saw significant improvements in global LV performance compared to RV pacing only with CRTa, even though both CRTa and CRTf significantly improved contraction synchrony. Thus, it appears that LV apical pacing is superior to LV free-wall pacing in CRT if no structural limitations to cardiac conduction co-exist. Recently Helm *et al.* [90] have reported that CRT response was better with LV apical pacing compared to more basal stimulation. They used a custom epicardial sock with 128 stimulating/recording electrodes and showed that mechanical synchrony and global LV function was better preserved as the LV pacing site was moved more apically. Similarly, Peschar *et al.* [91] and Prinzen *et al.* [92] reported beneficial effects on global LV performance following biventricular (RV apex + LV apex) pacing in healthy dogs. Furthermore, Vanagt *et al.* [93] showed that the LV apex was the optimal pacing site in both

canines and humans. Apical stimulation may be more beneficial to global LV function because it triggers mechanical activity closest to the intrinsic pattern of contraction. Propagation of electrical signals is fastest when the stimulation is nearest to the sites where the intrinsic impulses exit the Purkinje system [18]. Since impulses exit the Purkinje system in the lower third of the LV wall [94], apical stimulation should induce an activation pattern similar to intrinsic myocardial activation thus contributing to improved global LV performance.

We used changes in the end-systolic pressure-volume point to draw the conclusion that only CRTa significantly increased LV contractile state as compared to RV pacing. It is acknowledged that the entire end-systolic pressure-volume relationship (ESPVR) would have been better for this purpose. However, significant reductions in LV ESV with little or no change in ESP provide a reasonably sound basis for our conclusion. Although ESPVR has been used to quantify changes in LV contractile state following restoration of synchrony [52, 95], most previous studies have used dP/dt_{max} as the index of LV contractility. In the present study, CRTa did not increase the group average value of dP/dt_{max}, but this response was variable among different experiments (**Figure 4-6**). We attribute this variability to concomitant changes in LV end-diastolic volume, which, together with LV contractility, can affect LV dP/dt_{max} [96].

In contrast to our results regarding CRTf, some studies have reported a benefit in LV global function with LV free-wall pacing. Leclercq *et al.* [81] induced LBBB via radiofrequency ablation in canines, and showed that both single-site and multi-site LV free-wall pacing significantly increased dP/dt_{max} and aortic pulse pressure compared to their LBBB mode. Verbeek *et al.* [46] also showed increases in dP/dt_{max} and stroke work with LV free-wall pacing relative to LBBB values. The differences in the dyssynchrony model may contribute to the discrepant observations. Whereas we used a pacing-induced model of dyssynchrony, Leclercq *et*

al. and Verbeek *et al.* used a structural insult to induce dyssynchrony. However, it is important to note that several other studies have supported our finding that LV free-wall pacing is an inferior pacing site in the context of resynchronization [90-93]. The conflicting results concerning benefit of LV free-wall pacing remain an unresolved issue in CRT research that needs further clarification.

We were also surprised to find that improvements in regional contraction synchrony with CRTf were not accompanied by improvements in global LV function (**Figure 4-6**). This apparent disconnect may be due to the limitations of synchrony analysis using single-plane views. Because the LV free-wall pacing site was in the same cross-sectional plane (mid-LV) as that used for TD imaging, it is not surprising that electrical stimulation synchronized contraction in this plane. However, due to slow conducting myocardium [18], delayed activation of the remainder of the LV free-wall may have failed to correct contraction dyssynchrony at other planes. Therefore, the failure of global function to improve with CRTf may be a result of continued presence of contraction dyssynchrony at sites outside of the mid-LV plane. Multi-plane assessment of synchrony is necessary for a more comprehensive characterization.

4.5 CONCLUSIONS

Following RV pacing-induced LBBB-like contraction patterns, differential effects were observed with two different LV pacing sites during CRT. Although both modes of CRT significantly improved radial contraction synchrony, only CRTa improved global LV performance, likely due to increased global LV contractility. Thus, the LV apex appears to be a superior pacing site in the context of cardiac resynchronization therapy. The observed dissociation between changes in

regional contraction synchrony and changes in global LV performance with CRTf suggests that regional contraction data obtained from a single cross-sectional plane may not be sufficient to adequately characterize contraction synchrony of the LV as a whole; 3D dataset may be necessary.

In summary, the current study introduced the utility of cross-correlation algorithm as a robust tool to quantify radial contraction dyssynchrony. Unfortunately, we found a disconnect between regional and global LV function with CRTf possibly due to inadequate characterization of LV contraction afforded by TD-derived strain at the mid-LV. The next study aims to better characterize regional LV function using cross-correlation analysis on speckle-derived radial strain at multiple LV short-axis levels and investigate the mechanism of changes in global LV performance with resynchronization.

5.0 STUDY 3: A METHOD TO QUANTIFY SEGMENTAL CONTRIBUTIONS TO THE INTEGRATED MEASURE OF CONTRACTION SYNCHRONY

Specific Aim 3. To investigate the *link between regional and global LV function* under different contraction patterns induced by ventricular pacing at various sites.

Specific Aim 4. To apply cross-correlation analysis to a multi-plane dataset to quantify integral and segmental synchrony for a *comprehensive characterization of regional LV function*.

5.1 INTRODUCTION

The COMPANION and CARE-HF trials firmly established the therapeutic benefit of CRT in patients with refractory heart failure [7, 9]; however, as previously mentioned, about 30% of patients still do not respond to this therapy [4, 26]. These disappointing results have prompted investigators to develop better criteria that identify responders before pacemaker implantation. Despite its use as an indicator for CRT [2], QRS duration poorly predicts response to CRT [24, 25]. With this knowledge, emphasis has recently shifted towards refining dyssynchrony criteria for CRT by using a mechanical index of dyssynchrony instead of an electrical marker.

Several small single-center studies have shown that echocardiographic-derived mechanical markers of dyssynchrony demonstrate the ability to predict short-term [24] and long-

term [26-29] response to CRT. However, despite these promising results, when twelve different echocardiographic parameters were used to quantify ventricular dyssynchrony in a prospective, multicenter, nonrandomized clinical trial (PROSPECT trial), none of these measures were able to distinguish responders from non-responders to CRT to a significant degree [63]. The discrepancy between the PROSPECT trial and other small, single-center studies may be a result of several factors: (1) technological issues surrounding TDI methods that lead to significant interobserver variability, (2) high variability with measures derived from longitudinal imaging [97], and/or (3) variable definitions for study end points that identified responders (e.g., end point defined as a clinical status parameter or as an echocardiographic variable such as a reduction in end-systolic volume (i.e., reverse remodeling)). More importantly, it is clear that dyssynchrony is a dynamic process and a single measurement may not represent the entire burden of this mechanical disease. Most mechanical indices use an integrated measure to quantify dyssynchrony, but information may be lost in using this "global" approach, masking the mechanisms underlying changes in contraction patterns.

In the previous study, a disconnect was observed between regional and global LV function with CRTf possibly due to inadequate characterization of LV contraction afforded by TD-derived strain at the mid-LV. The current study attempted to address this dissociation by assessing regional contraction patterns at multiple cross-sectional radial levels to more adequately characterize synchrony of the LV as a whole. In addition, a method to quantify segmental contributions to the integrated measure of contraction synchrony was developed to offer better insight into contraction patterns. Lastly, the current study better quantified global LV mechanical contractility under different ventricular pacing modalities.

5.2 METHODS

5.2.1 Preparation

The protocol was approved by the Institutional Animal Care and Use Committee and conformed to the position of the American Physiological Society on research animal use. Eight mongrel dogs, weighing 20.6 ± 1.5 kg were studied after an overnight fast. The same preparation as described in **Section 4.2.1** was performed. The placement of ventricular pacing leads is shown in the schematic in **Figure 1A, B** (star symbols).

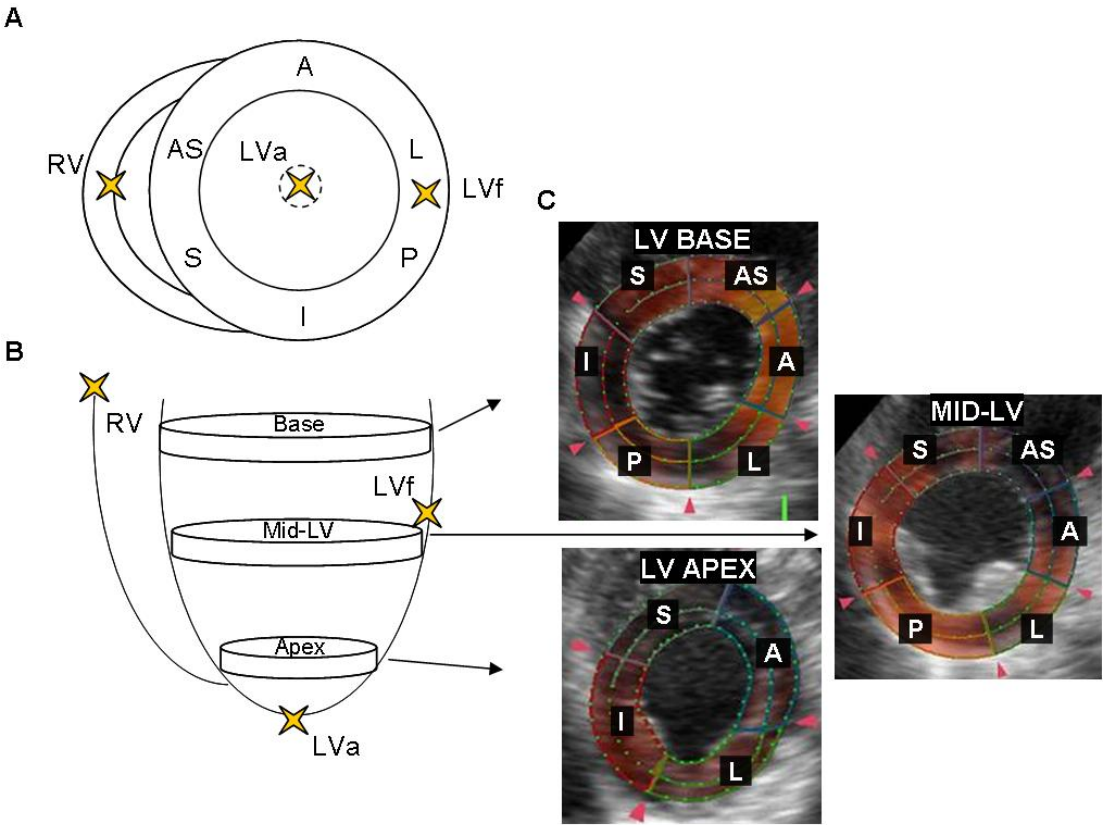

Figure 5-1. Schematic of pacing sites and short-axis echocardiographic imaging levels.

Ventricular pacing leads were placed at the RV outflow tract, LV free-wall, and LV apex (stars), shown for LV **(A)** short-axis and **(B)** long-axis views. **(C)** Echocardiographic short-axis images at the LV base, mid-LV, and LV apex showing radial segmentation. Note that the LV apex was segmented into only 4 regions instead of 6 because the LV tapers as it approaches the apex. Abbreviations: LV = left ventricular; RV = right ventricular; LVa = LV apex; LVf = LV free-wall; I = inferior; P = posterior; L = lateral; A = anterior; AS = antero-septal; S = septal.

5.2.2 Protocol

The protocol described in **Section 4.2.2** was utilized with the exception of using an A-V delay of 20 ms. In addition to steady-state conditions, data was obtained during inferior vena caval (IVC) occlusion to evaluate global LV intrinsic properties.

5.2.3 Echocardiographic Imaging and Speckle Tracking Analysis

An echocardiographic system (Aplio 80, Toshiba Medical Systems Corp, Tokyo, Japan) was used to obtain images with a 3.0 MHz transducer directly applied to the heart. Digital routine gray-scale 2D images from 3 consecutives beats were obtained at end-expiratory apnea from the LV basal, mid-LV, and LV apical short axis views at depths of 8 cm using a fixed transducer position. The three short-axis views were identified using the following anatomical landmarks: LV base, mitral valve; mid-LV, papillary muscle; and LV apex, below the papillary muscle but before the end of the LV cavity. Great care was taken to orient the images to the most circular geometry possible. Gray scale images were collected at frame rates of 49 Hz and gain settings were adjusted to optimize endocardial definition. Importantly, images were collected without LV conductance- or pressure catheters to eliminate the shadowing effects associated with these instruments.

Speckle tracking analysis [98] was used to generate regional LV strain-time waveforms [44] from routine B-mode gray scale echocardiographic images at each of the three LV short-axis levels. Strain-time waveforms were generated using novel software (Toshiba Medical

Systems Corporation, Tokyo, Japan) for frame-by-frame movement of stable patterns of natural acoustic markers present in ultrasound tissue images over the cardiac cycle as previously described [44]. Briefly, a circular region of interest was traced on the endocardial and epicardial border of each LV short axis image, using a point-and-click approach. The software automatically divided the region of interest into 6 equal radial segments: inferior (I), posterior (P), lateral (L), anterior (A), antero-septal (AS), and septal (S) (**Figure 5-1C**). The LV tapers as it approaches the apex, so only 4 strain-time waveforms (I, L, A, and S; **Figure 5-1C**) were calculated for the apical short-axis view as recommended by the Cardiac Imaging Committee of the Council on Clinical Cardiology of the American Heart Association [99]. The segments automatically created by the software were adjusted as needed, and speckles within each segment were tracked in subsequent frames by the imaging software. The location shift of these speckles from frame to frame represented tissue movement and provided the spatial and temporal data. Radial strain was calculated as change in length/initial length between speckles as $\Delta L/L_o$. Myocardial thickening was represented as positive strain and thinning was represented as negative strain. Radial strain values from multiple circumferential points within each segment were calculated and averaged into segmental strain-time curves, as previously validated in humans [44]. Quantification of radial synchrony was then performed offline.

5.2.4 Integrated and Segmental Synchrony Analyses

Radial synchrony was quantified by analyzing the speckle-derived strain waveforms with our proprietary algorithm "Cross-Correlation Analysis: A Novel Bedside Tool to Quantify Left Ventricular Contraction Dyssynchrony" (©2008 University of Pittsburgh). This algorithm has been described in detail elsewhere [74] (also see **Appendix B.1**). Briefly, an index of radial

synchrony (i.e., cross-correlation synchrony index, CCSI) was calculated in the time-domain via pair-wise correlation analyses of radial strain waveforms over systole for all myocardial segments at each LV short-axis level (*integrated synchrony analysis*). Next, to quantify segmental contributions to the integrated measure of synchrony, a single CCSI was calculated for each segment within its respective short-axis level (*segmental synchrony analysis*).

5.2.4.1 Integrated Synchrony Analysis

Pair-wise cross-correlation analysis of regional strain waveforms was used to develop an integrated cross-correlation synchrony index ($CCSI_{int}$) for each of the three cross-sectional levels (i.e., LV basal, mid-LV, and LV apical short-axis levels). Given that strain data were acquired for 6 segments at the LV base and mid-LV, there are 15 segment pairs for each of those levels. Within each level, cross-correlation coefficients were obtained for each of the 15 pair-wise correlations, summed and normalized to the number of correlations (i.e., 15 for the base and mid-LV). A value of 1.0 for $CCSI_{int}$ would imply perfect synchrony and lower values would correspond to progressively greater dyssynchrony. The 15 pair-wise correlations used to derived mid-LV $CCSI_{int}$ are shown in Figure 5-2. The same correlations were used to derive LV basal $CCSI_{int}$, however, the LV apical view possessed only 4 segments, giving 6 pair-wise correlations for derivation of LV apical $CCSI_{int}$: (1) I *vs.* L; (2) I *vs.* A; (3) I *vs.* S; (4) L *vs.* A, (5) L *vs.* S; (6) A *vs*. S (Figure 5-2).

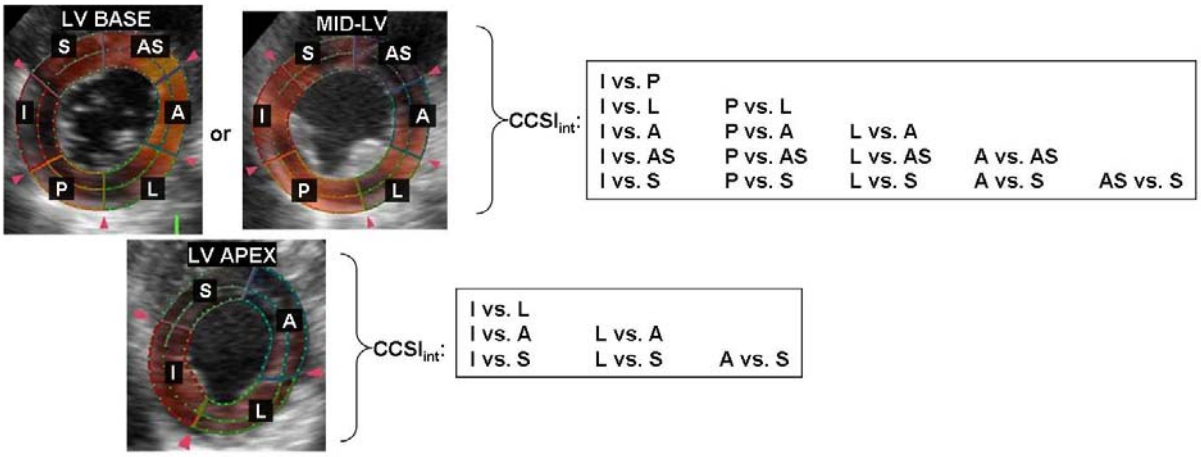

Figure 5-2. Pair-wise correlations used to derive integrated measures of synchrony ($CCSI_{int}$).

Pair-wise correlations (in boxes) for derivation of $CCSI_{int}$ at each short-axis level. For the derivation of either basal or mid-LV $CCSI_{int}$, 15 correlations are used. However, there are only 6 pair-wise correlations for the derivation of LV apical $CCSI_{int}$, since this level possesses only 4 segments. Abbreviations: $CCSI_{int}$ = integrated cross-correlation synchrony index; other abbreviations as in **Figure 5-1**.

5.2.4.2 Segmental Synchrony Analysis

For the segmental analysis, a CCSI was calculated for each segment ($CCSI_{seg}$) from pair-wise correlations of that segment with all other segments within the same cross-sectional level. For example, $CCSI_{seg}$ for segment I (i.e., $CCSI_{seg\ I}$)at the mid-LV level contained the following pair-wise correlations: (1) I *vs.* P, (2) I *vs.* L, (3) I *vs.* A, (4) I *vs.* AS, and (5) I *vs.* S (Figure 5-3A). Cross-correlation coefficients derived for each of these pairs were then summed and normalized by the total number of correlations (i.e., 5). A value of 1.0 for $CCSI_{seg}$ would imply perfect synchrony for a given segment with respect to all other segments within the same cross-sectional level, and lower values would correspond to progressively greater segmental dyssynchrony. This was repeated for the other 5 segments within its respective level to obtain 6 $CCSI_{seg}$ for the mid-LV. This was repeated for the LV basal level. However, since the LV apex was divided into 4

segments instead of 6, $CCSI_{seg}$ for each segment had 3 pair-wise correlations instead of 5 as with the mid-LV or LV basal $CCSI_{seg}$ (Figure 5-3B).

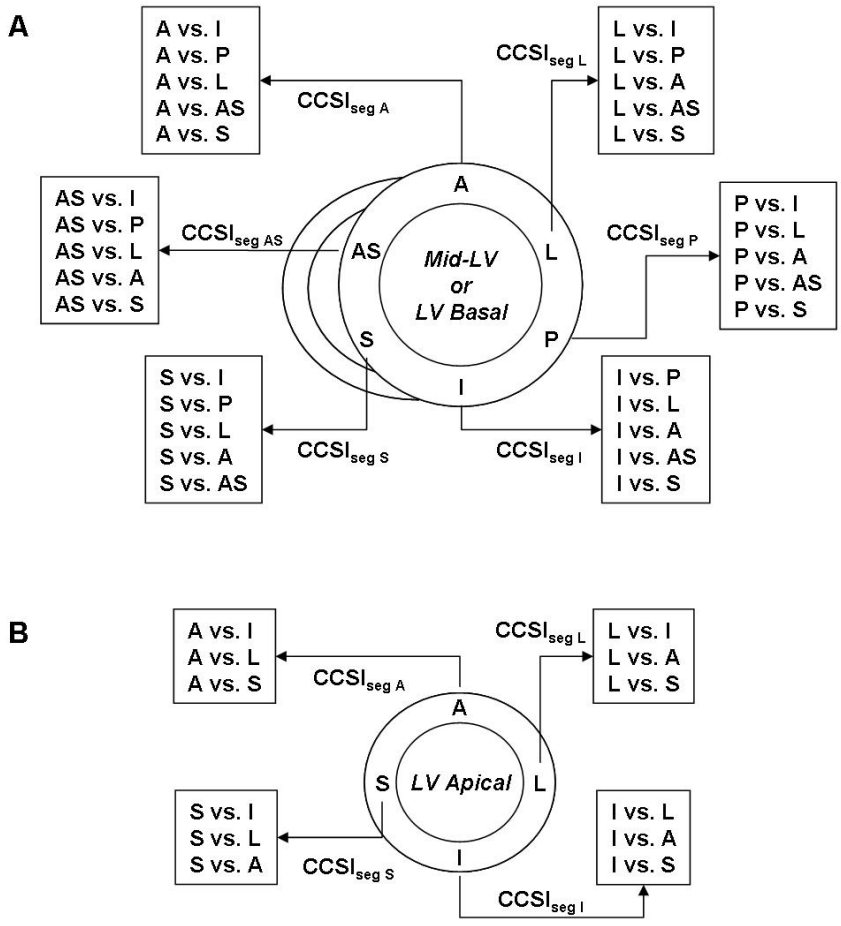

Figure 5-3. Pair-wise correlations used to derive segmental measures of synchrony ($CCSI_{seg}$).

(A) Each segment is associated with 5 pair-wise correlations for the mid-LV or LV base. **(B)** For the LV apex, each segment is associated with 3 pair-wise correlations since the LV is divided into 4 segments at this level.
Abbreviations: $CCSI_{seg}$ = segmental cross-correlation synchrony index; other abbreviations as in **Figure 5-2**.

5.2.5 Global LV Mechanical Property Analysis

Transient pressure-volume data obtained during IVC occlusion were used to quantify LV intrinsic mechanical properties. Specifically, LV contractility was quantified in terms of end-systolic pressure (ESP)-volume (ESV) relationship, ESPVR [$ESP = E_{es}(ESV - V_d)$, where E_{es}

and V_d are parameters]. The slope of ESPVR, or end-systolic elastance (E_{es}), is commonly used as an index of contractility [56]. However, we found several hearts with increased E_{es} for conditions wherein LV contractility was clearly depressed, as indicated by a rightward shift of ESPVR over the entire operating range (**Figure 5-4**, solid *vs.* dashed lines). Thus, we proposed a new index that simultaneously considered both slope (E_{es}) and intercept (V_d) values for proper evaluation of contractile state. LV contractility was quantified by the area enclosed by ESPVR and Y-axis over the end-systolic pressure range of 60-120 mmHg. This range was chosen based upon the working end-systolic pressure range identified throughout the entire study. A larger area (e.g. rightward shift of ESPVR) would correspond to lower contractility and *vice versa* (**Figure 5-4**, shaded areas).

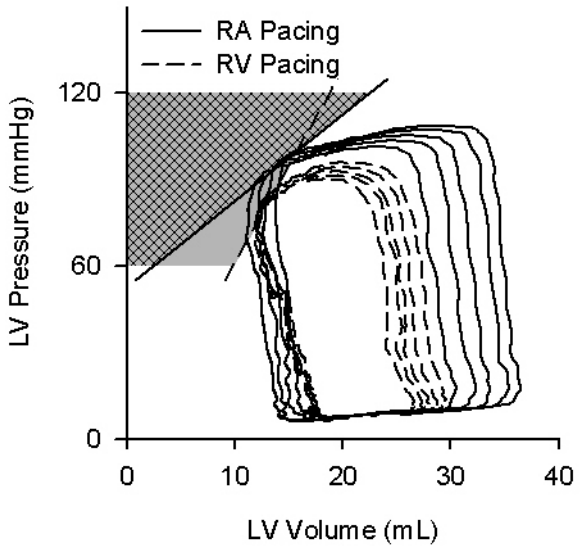

Figure 5-4. Example of calculation of ESPVR area.

Compared to RA pacing (solid line), ESPVR for RV pacing (dashed line) has a greater slope. However, ESPVR for RV pacing is shifted to the right and pressure-volume loops are smaller signifying a more depressed ventricle. To quantify the contractility by taking both ESPVR slope and intercept into account, ESPVR area calculated from the RV pacing ESPVR to Y-axis (grey) is larger than that for RA pacing (grey hatched). The greater ESPVR area indicates depressed contractility. Abbreviations: RA = right atrial; RV = right ventricular; LV = left ventricular; ESPVR = end-systolic pressure-volume relationship.

5.2.6 Statistical Analysis

Data are expressed as mean ± SEM. One-way analysis of variance (ANOVA) with repeated measures was used to evaluate the effects of different pacing modalities on regional LV synchrony and indices of global LV performance. Tukey-Kramer test was employed for *post hoc* pair-wise comparisons following each ANOVA. Significance was determined as $P<0.05$. Linear regression analysis was used to compare $CCSI_{int}$ with a commonly used dyssynchrony index. In addition, multiple linear regression analysis was performed to investigate whether additional regional information at the basal level (i.e., basal LV $CCSI_{int}$) improved the predictive power of integrated cross-correlation analysis to identify response to CRT.

5.3 RESULTS

Although all echocardiographic images were of acceptable quality, strain data from one animal were associated with significant noise, reflecting poor speckle tracking. Therefore, only 7 of 8 strain datasets were used for synchrony analysis. In addition, due to technical challenges, accurate steady-state LV pressure-volume data were available in only 7 of 8 experiments and inferior vena-caval occlusion data were collected in only 6 of 8 experiments.

5.3.1 Integrated Synchrony Analysis

Using the integrated approach, a synchronous contraction pattern was observed with RA pacing as indicated by a $CCSI_{int}$ near 1.0 at the LV base (**Figure 5-5A**, closed circles). Synchrony was

adversely affected with RV pacing reflected by a significant decrease in basal $CCSI_{int}$ compared to RA pacing [0.95±0.02 to 0.64±0.14; $P<0.05$ RA to RV pacing]. Interestingly, resynchronization was only successful with CRTa as shown by an increase in $CCSI_{int}$ at the LV base [0.93±0.03; $P<0.05$ *vs.* RV pacing]. Although CRTf tended to improve synchrony compared to RV pacing, the increase in basal $CCSI_{int}$ did not reach statistical significance. Similar changes in $CCSI_{int}$ were observed at the mid-LV level; compared to RA pacing, mid-LV $CCSI_{int}$ markedly decreased with RV pacing, and only CRTa restored synchrony compared to RV pacing (**Figure 5-5A**, open circles). Although it appeared that all ventricular pacing modes (i.e., RV pacing, CRTa, and CRTf) were associated with some radial dyssynchrony at the apex, differences in LV apical $CCSI_{int}$ did not reach statistical significance for any pacing modality (**Figure 5-5B**; $P=0.32$).

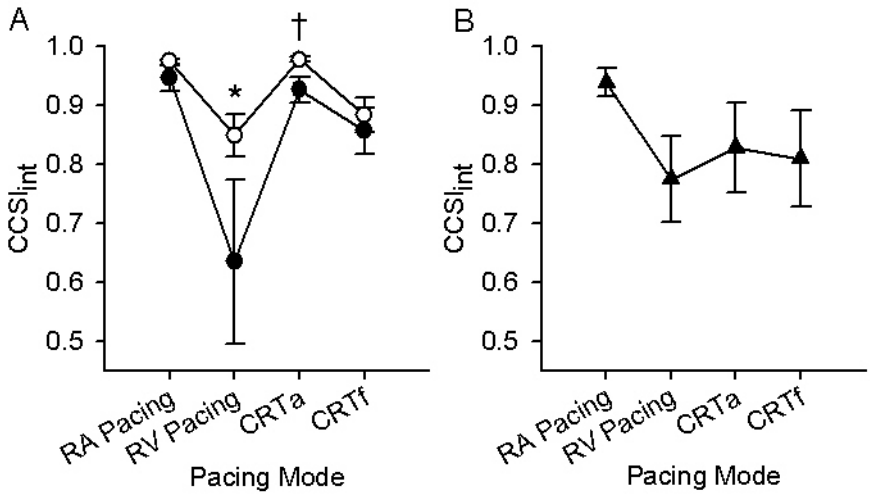

Figure 5-5. Integrated measure of synchrony ($CCSI_{int}$) for each short-axis view.

$CCSI_{int}$ for **(A)** LV base (closed-circles), mid-LV (open circles), and **(B)** LV apex. Data: mean ± SEM, n=7, *$P<0.05$ vs. RA pacing, †$P<0.05$ vs. RV pacing. Abbreviations: $CCSI_{int}$ = integrated cross-correlation synchrony index; RA = right atrial; RV = right ventricular; CRTa = resynchronization at the LV apex; CRTf = resynchronization at the LV free-wall..

Although some scatter was present, both the basal and mid-LV $CCSI_{int}$ significantly correlated with a commonly used measure of dyssynchrony: time delay between earliest and

latest peak strain derived from data at the LV base and mid-LV, respectively (**Figure 5-6A, B**). A significant correlation between time delay and $CCSI_{int}$ was not observed at the apical level due to a great degree of scatter (R^2=0.12, P=0.08; data not shown). Trends for group comparisons using time delay as an index of dyssynchrony were similar those observed with $CCSI_{int}$ for both basal and mid-LV, however, a discrepancy was observed with one pacing modality (**Figure 5-6C, D**). Specifically, synchrony appeared to significantly improve with CRTf when quantified by time delay indices for the base and mid-LV (**Figure 5-6C, D**), whereas $CCSI_{int}$ was not statistically different than RV pacing for either cross-sectional level (**Figure 5-5A**).

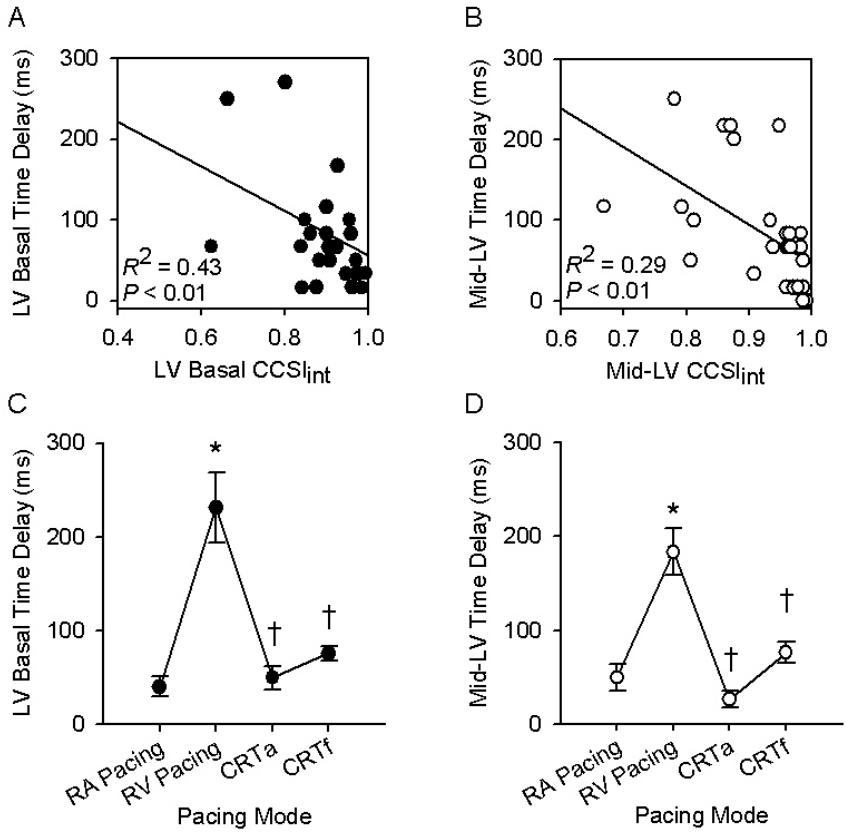

Figure 5-6. Correlation of new and standard (dys)synchrony indices and trends of standard measures of dyssynchrony for each pacing modality.

Correlation of standard dyssynchrony index (i.e., time delay between earliest and latest peak strain) and $CCSI_{int}$ at two LV short-axis levels (**A:** LV base, **B:** mid-LV). Also shown are mean (±SEM) standard dyssynchrony measures for the **(A)** LV base and **(B)** mid-LV. **(A), (B)**: Data shown are for all pacing modes (RA, RV, CRTa, and CRTf). **(C), (D)**: Data: mean ± SEM, n=7, **P*<0.05 vs. RA pacing, †*P*<0.05 vs. RV pacing. Abbreviations as in **Figure 5-5**.

5.3.2 Segmental Synchrony Analysis

The synchronous contraction pattern observed with RA pacing can be better appreciated from the data presented in **Figure 5-7A** (left panel), where all $CCSI_{seg}$ are similar with relatively high values around 1.0. To better illustrate this pattern, mean $CCSI_{seg}$ are color-coded and displayed in a Bull's Eye representation shown in **Figure 5-7A** (right panel), with basal and mid-LV segments circling the outer ring and inner rings, respectively. Note that apical $CCSI_{seg}$ are not shown because significant changes in $CCSI_{int}$ were not observed at the apex. A relatively homogeneous yellow Bull's Eye plot is shown for RA pacing indicating almost perfect synchrony (**Figure 5-7A**, right panel). Unlike the pattern observed with RA pacing, $CCSI_{seg}$ values are less in value and uniformity with RV pacing (**Figure 5-7B**, left panel), reflected by the darker heterogeneous colors in the Bull's Eye plot (**Figure 5-7B**, right panel). Note that $CCSI_{seg}$ for the antero-septal (AS) and septal (S) segments at the LV base were less than that of the other segments, reflected by the darkest color in the Bull's Eye plot. However, these values were not significantly different than other $CCSI_{seg}$ within the basal level. As stated above, CRTa improved the integrated synchrony measure ($CCSI_{int}$) at both the basal and mid-LV short-axis levels. Therefore, it was not surprising that $CCSI_{seg}$ values were not different from each other following CRTa (**Figure 5-7C**, left panel), which gave a relatively homogenous yellow Bull's Eye plot (**Figure 5-7C**, right panel). In contrast, a heterogeneous pattern was observed with CRTf, such that $CCSI_{seg}$ for the inferior (I) segment was significantly less than that for all other segments (**Figure 5-7D**, left panel). This segment at the LV base and mid-LV is easily identified by the darkest orange colors on the Bull's Eye plot, reflecting the most dyssynchronous segment (**Figure 5-7D**, right panel).

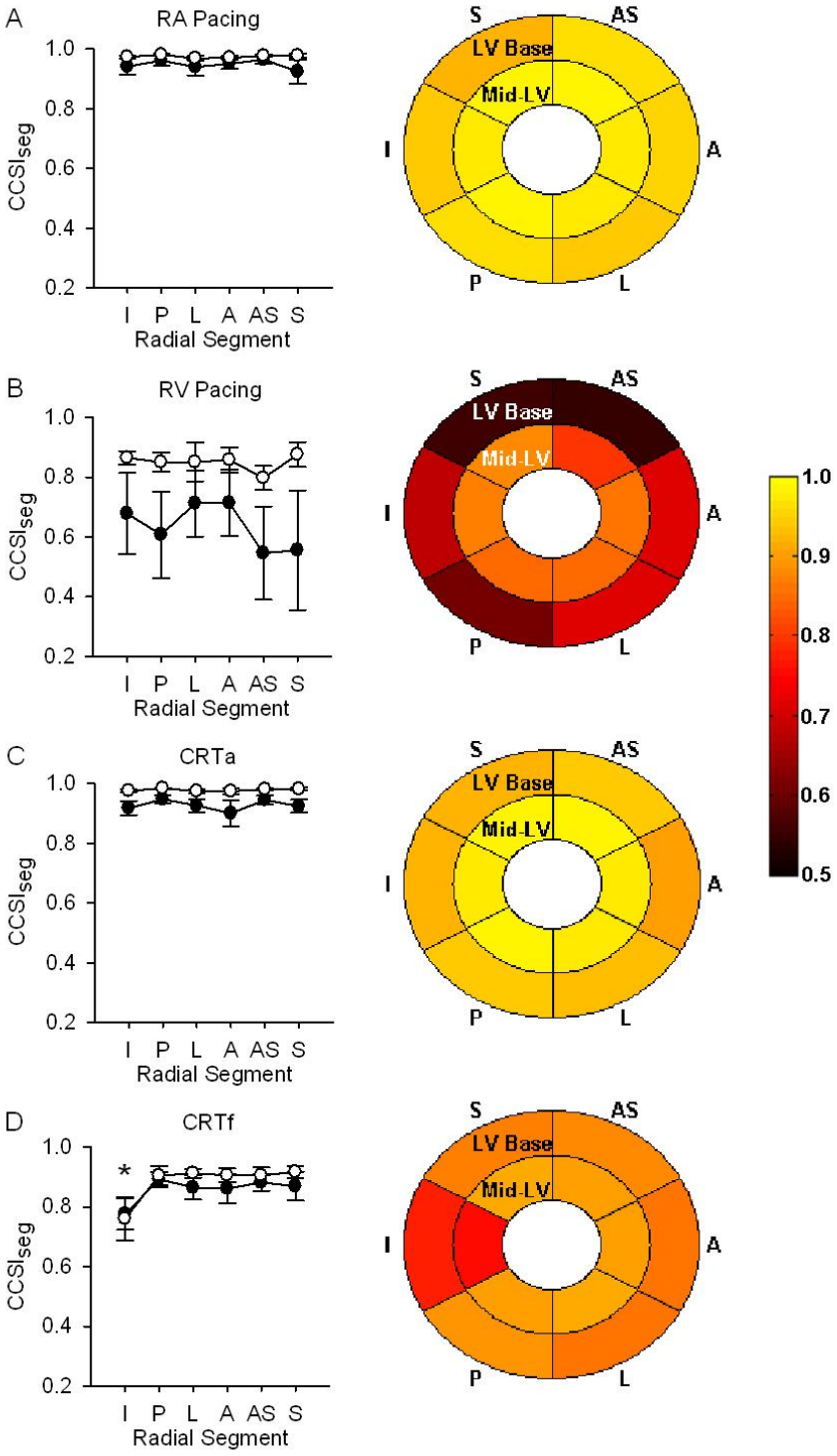

Figure 5-7. Segmental synchrony indices ($CCSI_{seg}$) and corresponding Bull's Eye plots.

$CCSI_{seg}$ at the LV base (closed circles) and mid-LV (open circles) under **A:** RA pacing, **B:** RV pacing, **C:** CRTa, and **D:** CRTf. Color-coded representations of $CCSI_{seg}$ are to the right of each plot with black corresponding to values ≤0.5 and yellow representing 1.0. Data: mean ± SEM, n=7, **P*<0.05. $CCSI_{seg}$ = segmental cross-correlation synchrony index; other abbreviations as in **Figure 5-1** and **Figure 5-5**.

In order to compare the performance of $CCSI_{seg}$ to commonly used dyssynchrony indices, we applied the same method of analysis to the time delay index (i.e., maximum time delay between earliest and latest peak strain) at the LV base and mid-LV. Specifically, a time delay for each segment with respect to the remaining segments in the same cross-sectional level was calculated, and from these 5 calculated delays, an average delay for that segment was derived. This procedure was used to derive an average delay for each of the 6 segments at the LV base and mid-LV.

Following RA pacing and CRTa, patterns similar to those observed with $CCSI_{seg}$ were observed using the average time delay as a segmental index of synchrony (**Figure 5-8A, C**). Relatively homogenous, synchronous (i.e., low) delays for each segment were observed with both RA pacing and CRTa. Although statistical significance was not reached, the LV basal inferior segment was associated with greatest dyssynchrony during RV pacing (**Figure 5-8B**). This observation cannot be physiologically reconciled with ease since RV outflow tract pacing mainly induces septal disparities. Importantly, the $CCSI_{seg}$ data presented in **Figure 5-7B** above revealed that the antero-septal and septal segments were associated with the most segmental dyssynchrony with RV pacing, which is consistent with physiological reasoning. In addition, the mean time delay for segmental dyssynchrony failed to identify the significant disparity associated with CRTf at the inferior region (**Figure 5-8D**) that was observed using $CCSI_{seg}$ (**Figure 5-7D**).

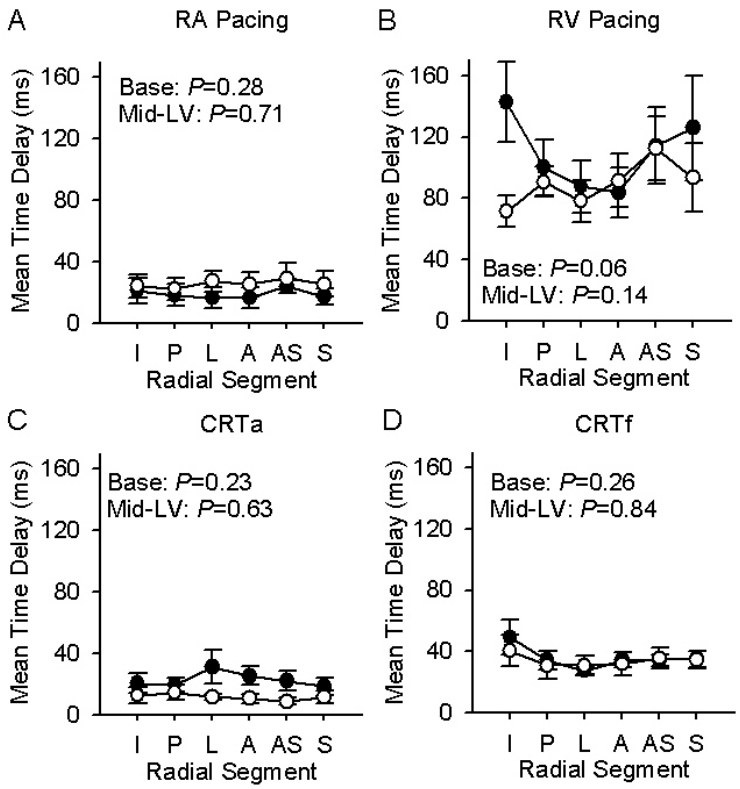

Figure 5-8. Segmental time delay dyssynchrony indices.

Segmental time delay at the LV base (closed circles) and mid-LV (open circles) under **A:** RA pacing, **B:** RV pacing, **C:** CRTa, and **D:** CRTf. Data: mean ± SEM, n=7. Abbreviations as in **Figure 5-1** and **Figure 5-5**.

5.3.3 Global LV Performance Analysis

It is important to note that a short A-V delay adversely affects diastolic filling with ventricular pacing. Therefore, pair-wise statistical comparisons did not include intrinsic RA pacing. However, since RV pacing was used as a model of dyssynchrony, it was important to show that this pacing modality adversely affected global LV function. Therefore, we compared RA and RV pacing only, with awareness that some depression may be due to short A-V delay effects. RV pacing significantly impaired global LV performance as indicated by marked decreases in

cardiac output [CO: 2.9 ± 0.3 to 2.3 ± 0.2 L•min^{-1}; P<0.05] and stroke work [SW: 252 ± 23 to 151 ± 24 mJ; P<0.05] as well as other global LV performance indices (**Table 5-1**).

Similar to the patterns observed with regional synchrony, global LV performance was improved with only CRTa (**Table 5-1**). Compared to RV pacing, end-systolic volume was significantly improved with CRTa which led to a marked increase in CO [3.2 ± 0.2 L•min^{-1}; P<0.05 vs. RV pacing] and SW [240 ± 19; P<0.05 vs. RV pacing]. However, following CRTf, the only global LV performance index that showed improvement compared to RV pacing was dP/dt_{min} (**Table 5-1**).

Table 5-1. Global LV performance values for different pacing modalities.

	Dyssynchrony			***Resynchronization***		
	RA Pacing	**RV Pacing**	***P*-value**	**CRTa**	**CRTf**	***P*-value**
HR (beats•min^{-1})	139 ± 3	139 ± 3	*0.2437*	139 ± 3	139 ± 3	*0.8223*
LV ESP (mmHg)	109 ± 3	92 ± 5*	*0.0041*	94 ± 2	95 ± 3	*0.611*
LV EDP (mmHg)	12 ± 2	11 ± 2*	*0.0241*	9 ± 2†	10 ± 2	*0.0099*
MAP (mmHg)	96 ± 4	78 ± 5*	*0.0012*	83 ± 4	83 ± 4	*0.1829*
EDV (mL)	40 ± 1	34 ± 2*	*0.0022*	34 ± 2	34 ± 2	*0.9771*
ESV (mL)	19 ± 2	18 ± 2	*0.3075*	11 ± 2†	16 ± 2	*0.0014*
SV (mL)	21 ± 2	17 ± 2*	*0.0096*	23 ± 1†	18 ± 2	*0.0095*
CO (L•min^{-1})	2.9 ± 0.3	2.3 ± 0. 2*	*0.0132*	3.2 ± 0.2†	2.5 ± 0.2	*0.007*
dP/dt_{max}(mmHg•s^{-1})	2063 ± 172	1603 ± 160*	*0.0001*	1946 ± 244†	1699 ± 163	*0.0317*
dP/dt_{min} (mmHg•s^{-1})	-2325 ± 175	-1684 ± 182*	*0.0001*	-2061 ± 166†	-1973 ± 178†	*0.0022*
SW (mJ)	252 ± 23	151 ± 24*	*0.0019*	240 ± 19†	175 ± 18	*0.0073*

Data: mean ± SEM, n=7; *P<0.05 vs. RA pacing, †P<0.05 vs. RV pacing. Abbreviations: RA = right atrial; RV = right-ventricular; CRTa = biventricular apical; BiVf = biventricular free-wall; HR = heart rate; LV = left ventricular; ESP = end-systolic pressure; EDP = end-diastolic pressure; MAP = mean arterial pressure; EDV = end-diastolic volume; ESV = end-systolic volume; SV = stroke volume; CO = cardiac output; dP/dt_{max} = maximum rate of pressure rise; dP/dt_{min} = minimum rate of pressure rise; SW = stroke work.

5.3.4 Global LV Mechanical Property Analysis

Compared to RA pacing, the commonly used index of contractility, E_{es}, increased with RV pacing [2.7 ± 0.5 to 5.1 ± 0.7 mmHg•mL^{-1}; P<0.05; **Figure 5-9A**], a pattern inconsistent with changes in global LV performance. In contrast, the volume-axis intercept of ESPVR, V_d, was significantly shifted to the right with RV pacing [-26 ± 5 to -2 ± 5 mL, RA to RV pacing; P<0.05; **Figure 5-9B**], thus, making it difficult to quantify global LV contractility using E_{es} alone. However, ESPVR area, which simultaneously considers E_{es} and V_d, increased with RV pacing [697 ± 153 to 1019 ± 202 mmHg•mL, RA to RV pacing; P<0.05; **Figure 5-9C**]. Therefore, compared to RA pacing, RV pacing was associated with depressed contractility as quantified by ESPVR area.

The effect of resynchronization on global LV mechanics was also not clear when comparing E_{es} or V_d (**Figure 5-9A, B**). Compared to RV pacing, CRTa decreased both the slope (i.e., E_{es}) and intercept (i.e., V_d) of ESPVR. However, when quantified using our new index, ESPVR area, LV contractility improved with CRTa compared to RV pacing, such that ESPVR area was less with CRTa than with RV pacing (**Figure 5-9C**). This pattern was more consistent with changes in global LV performance and synchrony during CRTa. As observed with regional function, CRTf was associated with contractility similar to that observed with RV pacing; ESPVR slope, ESPVR intercept, or ESPVR area were not different than RV pacing (**Figure 5-9A-C**).

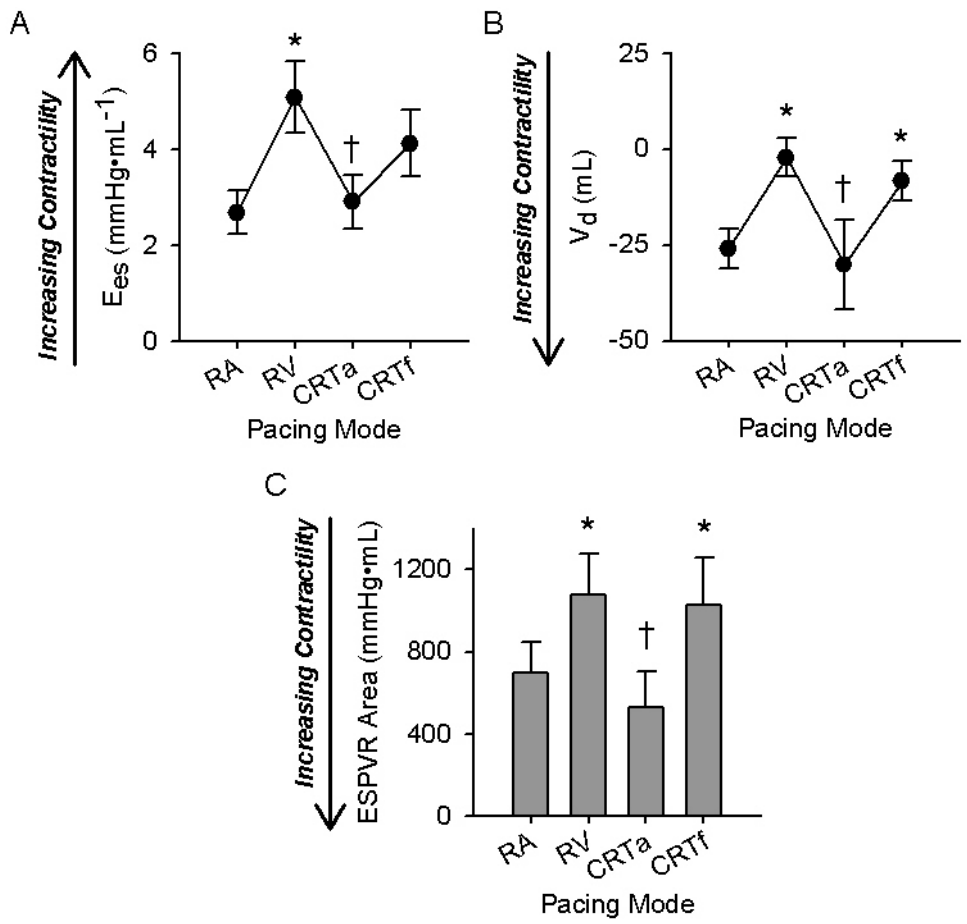

Figure 5-9. Indices of global LV mechanical properties.

Compared to RV pacing, E_{es} was lower with CRTa **(A)**, indicating depressed LV contractility; however, the volume-axis intercept was lower with CRTa **(B)**, suggesting improved mechanics. With a combined index of E_{es} and V_d, ESPVR area was significantly less than that with RV pacing **(C)**, indicating improved contractility, a pattern consistent with regional synchrony and global LV performance. Data: mean ± SEM, n=6; **P*<0.05 vs. RA pacing , †*P*<0.05 vs. RV pacing. Abbreviations as in **Figure 5-4** and **Figure 5-5**.

5.3.5 Correlation of Global and Regional Changes

We first investigated whether the CRT-induced changes in integrated synchrony measures ($CCSI_{int}$) correlated with the changes in global LV performance (i.e., SW, **Figure 5-10A**) and contractility (i.e., ESPVR area, **Figure 5-10B**). All CRT-induced changes were calculated with respect to the values with RV pacing. The univariate analysis revealed that neither mid-LV nor

basal $CCSI_{int}$ was significantly correlated with SW or ESPVR area (**Table 5-2**). The multivariate analysis using mid-LV and basal $CCSI_{int}$ as two independent variables did not improve the correlation (**Table 5-2**).

Since the segmental cross-correlation analysis provided useful information that identified particular segments that were responsible for the failure to resynchronize with CRTf, we also investigated whether this analysis provided a better link between changes in global LV function and contraction dyssynchrony. Specifically, the change in $CCSI_{seg}$ was calculated for the most dyssynchronous segment during CRT with respect to its value at RV pacing, and was compared to the change in global LV function. Univariate analysis revealed that neither mid-LV nor basal $CCSI_{seg}$ was significantly correlated with SW (**Table 5-2**). Mid-LV $CCSI_{seg}$ did not predict changes in ESPVR area either, however, basal $CCSI_{seg}$ significantly correlated with changes in ESPVR (**Table 5-2**). Accordingly, the multivariate analysis using mid-LV and basal $CCSI_{seg}$ as two independent variables improved the correlation (**Table 5-2**).

Table 5-2. Regression statistical outputs for univariate and multivariate analyses.

			Univariate Analysis		Multivariate Analysis
			LV Base	Mid-LV	LV Base and Mid-LV
$\Delta CCSI_{int}$	%Δ SW	R^2	0.03	0.03	0.04
		P	0.60	0.57	0.83
	%Δ ESPVR Area	R^2	0.19	0.23	0.28
		P	0.16	0.12	0.23
$\Delta CCSI_{seg}$	%Δ SW	R^2	0.002	0.04	0.12
		P	0.88	0.52	0.57
	%Δ ESPVR Area	R^2	0.68	0.18	0.74
		P	0.0009	0.18	0.003

Statistical analyses performed on data calculated from percent changes of CRTa and CRTf compared to RV pacing (n=6). Abbreviations: CCSIint, seg = integrated and segmental cross-correlation synchrony index, respectively; SW = stroke work; ESPVR = end-systolic pressure-volume relationship; LV = left ventricle.

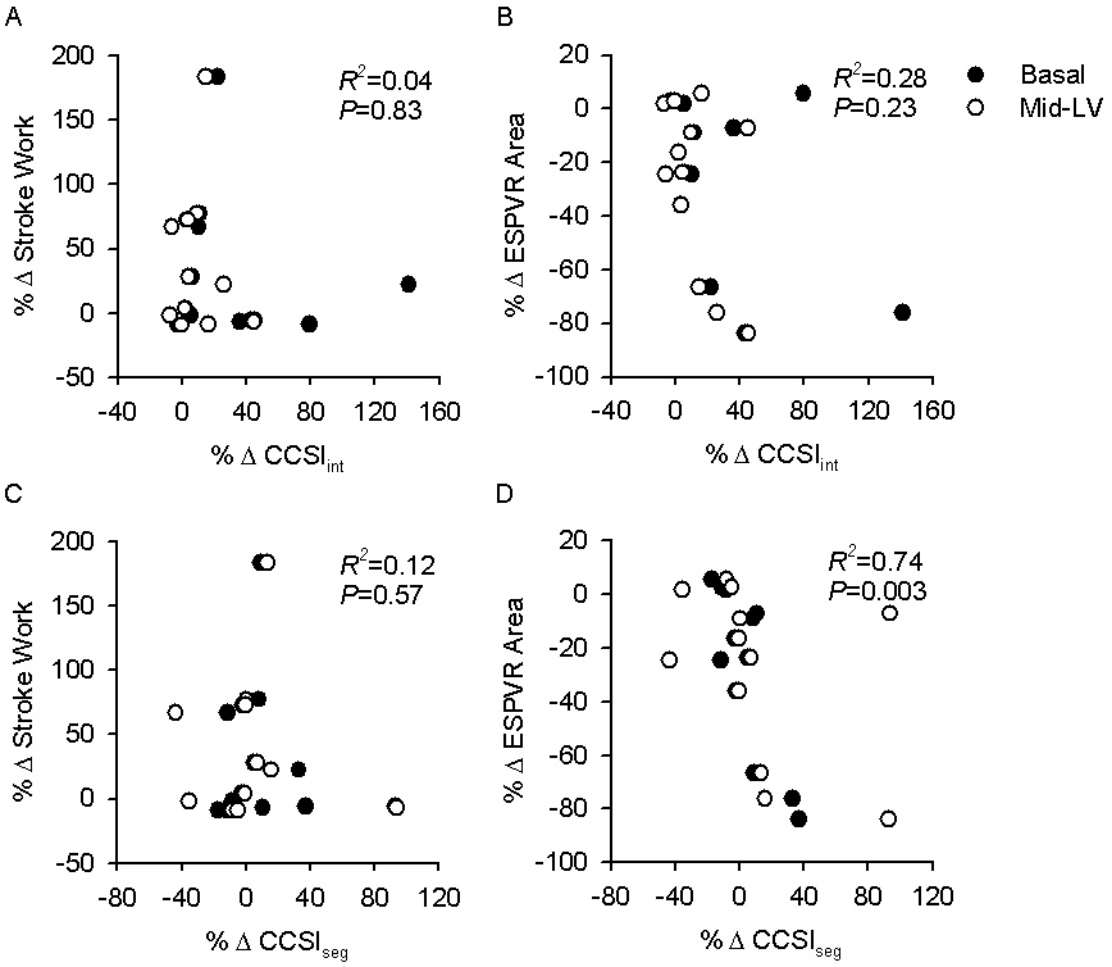

Figure 5-10. Correlation of global and regional LV function.

Percent change in basal LV $CCSI_{int}$ (closed circles) and mid-LV $CCSI_{int}$ (opened circles) compared to percent change in stroke work **(A)** or ESPVR area **(B)**. Also, percent change in the most dyssynchronous basal and mid-LV $CCSI_{seg}$ were compared to percent change in stroke work **(C)** or ESPVR area **(D)**. Regression statistics are shown for multivariate analysis. Abbreviations: $CCSI_{int, seg}$ = integrated and segmental cross-correlation synchrony index, respectively; ESPVR = end-systolic pressure-volume area.

5.4 DISCUSSION

The current study reports three primary findings. (1) The proposed segmental synchrony analysis provided insight into changes in the integrated contraction pattern of the LV. (2) In the setting of contraction dyssynchrony, ESPVR area is a better index of contractility than E_{es} alone.

(3) The addition of regional information at the basal LV level to that of the mid-LV level did not improve the predictive response of integrated synchrony index (i.e., $CCSI_{int}$) to identify global LV improvement. However, changes in the most dyssynchronous segment reflected as the segmental cross-correlation index ($CCSI_{seg}$) significantly correlated with changes in global LV contractility. Before we discuss these findings in detail, we will address an inconsistency encountered from our previous canine study.

5.4.1 Tissue Doppler- vs. Speckle Tracking-Derived Strain

In the previous study, we observed a disconnect between changes in global and regional LV function such that CRTf resynchronized contraction without improving global LV performance (see **Section 4.0**). It appeared that evaluation of regional wall motion at the mid-LV using TD-derived strain was not sufficient to completely characterize synchrony of the entire LV. However, in the current study, dyssynchrony was observed with CRTf at both the LV base and mid-LV as characterized by speckle tracking-derived strain data. The lack of a significant correlation between regional and global LV function may suggest a disconnect in the current study, however, the failure to resynchronize with CRTf was consistent with the depression in global LV performance. The discrepancy in observations of synchrony patterns with CRTf may be due to the different echocardiographic methods (i.e., color-coded TD vs. speckle tracking) used to derive strain in the two studies.

In the current study, it appeared that speckle-tracking algorithm more accurately characterized contraction patterns occurring across the entire circumference of the myocardium than did TD-derived strain in the previous study. To further investigate this, we derived $CCSI_{seg}$ for TD-derived strain waveforms from the previous study. Consistent with the current study,

analysis of the $CCSI_{seg}$ data revealed that RA pacing was not associated with any significant disparities across segments; however, $CCSI_{seg}$ indices were lower than expected for a control condition (**Figure 5-11A**). Similar to the current study, RV pacing induced significant dyssynchrony at the mid- and antero-septal (MS and AS, respectively) segments (**Figure 5-11B**). However, resynchronization appeared to be successful with both CRTa and CRTf as indicated by nearly homogenous $CCSI_{seg}$ within both pacing modalities (**Figure 5-11C, D**). Therefore, unlike the current study, disparities at the inferior region with CRTf were not identified when using TD derived strain to quantify myocardial contraction. We therefore concluded that speckle tracking derived strain in the current study more accurately quantified contraction patterns than TD derived strain in the previous study.

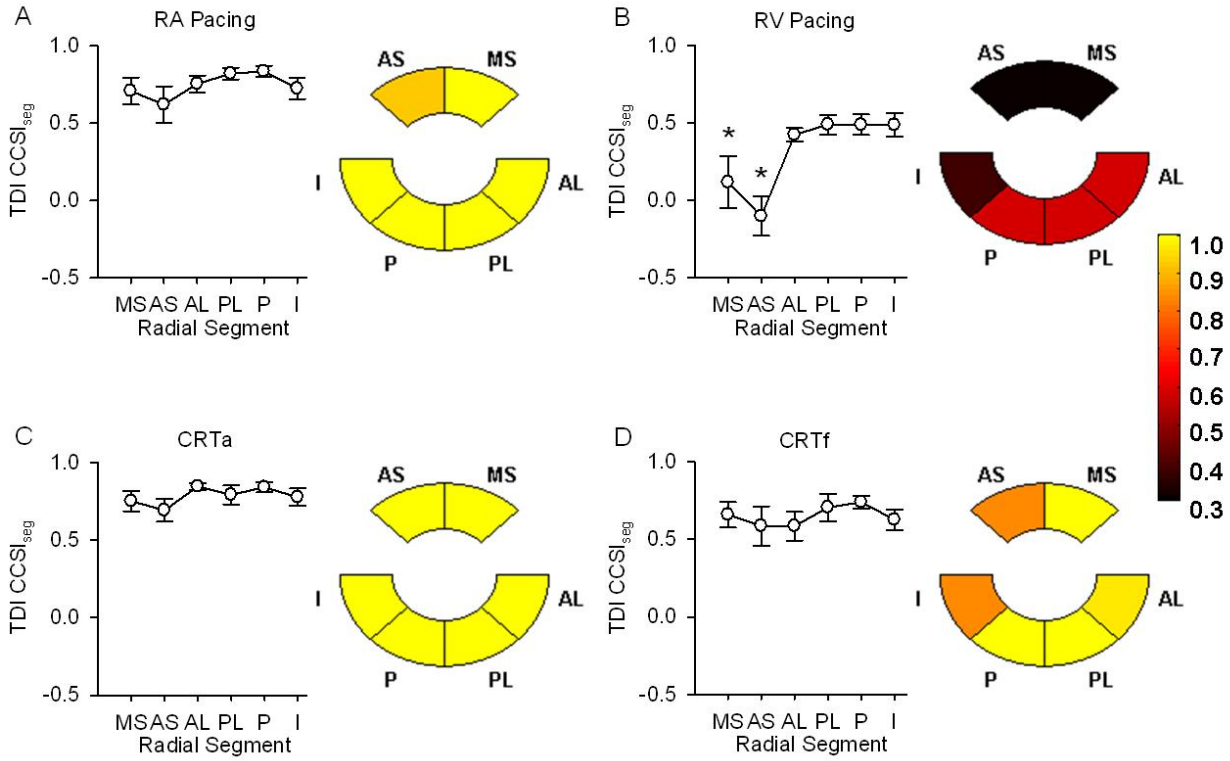

Figure 5-11. CCSI$_{seg}$ and corresponding Bull's Eye plot for TD derived strain.

CCSI$_{seg}$ at the mid-LV for TD derived strain under **A:** RA pacing, **B:** RV pacing, **C:** CRTa, and **D:** CRTf. Color-coded representations of CCSI$_{seg}$ are to the right of each plot with black corresponding to values ≤0.3 and yellow representing 1.0. Data: mean ± SEM, n=7, *P<0.05. Abbreviations: I = inferior; P = posterior; PL = postero-lateral; AL = antero-lateral; MS = mid-septum; AS = antero-septal; other abbreviations as in **Figure 5-7**.

A major limitation of TD imaging is that sectors are masked where the angle of incidence approaches 90º; therefore myocardial wall motion cannot be quantified for those masked regions (**Figure 5-11A**) [42]. However, speckle-tracked-derived strain may prove superior because it is angle independent [100], therefore the entire circumference of the myocardial can be segmented (**Figure 5-11B**). Interestingly, in the previous study, the inferior segment borders one of the regions masked by the angle of incidence (**Figure 5-11A**). Importantly, regions that approach the angle of incidence are more difficult to image, which may have contributed to a less accurate tracing with TD-derived strain in the previous study. In contrast, when speckle tracking algorithm was applied to standard 2D echocardiographic images in the current study, tracing at

the inferior region was not compromised due to the angle independent advantage of this modality, therefore allowing for more accurate imaging and strain derivation at this region.

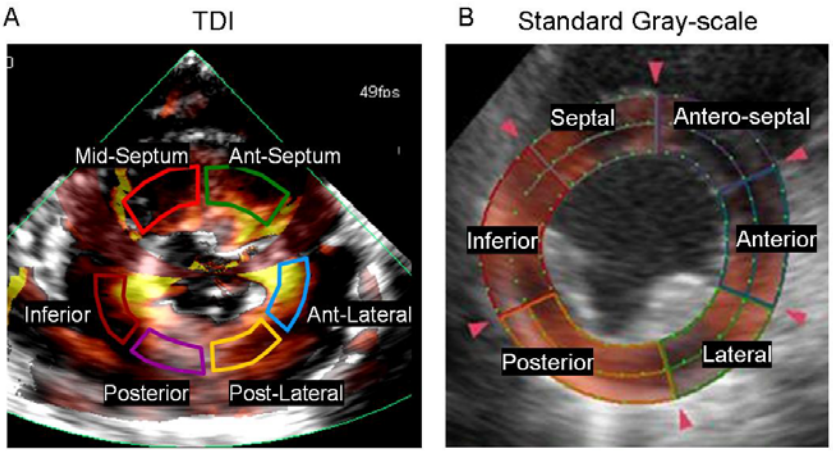

Figure 5-12. Comparison of image modalities.

(A) Short-axis Tissue Doppler (TD) image at mid-LV showing that segmentation is not possible at angles approaching 90° from the Doppler beam. **(B)** Standard gray-scale short-axis 2D image at the mid-LV showing that segmentation is possible across the entire circumference of the myocardium with speckle tracking algorithm.

5.4.2 Quantification of Synchrony: Integrated vs. Segmental Approach

Most echocardiographic-derived measures use an integrated approach to quantify dyssynchrony. For example, dyssynchrony metrics have been derived from time to peak systolic velocity using TDI from echocardiographic apical or short-axis views and expressed principally as either the standard deviation of 12 segments or the maximum opposing wall delay [39, 43, 87, 88]. However, using these integrated measures, it is difficult to determine the role of individual segments in overall synchrony. For example, the time delay index uses information from only the two extreme peak values (i.e., earliest and latest). To address this issue, we developed a method to quantify segmental contributions to the integrated measure of contraction synchrony. An advantage of the $CCSI_{seg}$ index derived from this methodology is that it characterizes the

synchrony of a particular segment with respect to all other segments within the same cross-sectional level. Importantly, the segmental cross-correlation approach offers insight into the mechanism behind overall synchrony patterns. For example, in the current study, we determined that the basal antero-septal and septal segments may be responsible for the overall decrease in synchrony with RV pacing and that resynchronization failure with CRTf was due to contraction disparities at the basal and mid-LV inferior segments. Furthermore, the color-coded plot of $CCSI_{seg}$ offers a visual representation of those segments responsible for dyssynchrony; this presentation has potential clinical applications for ease of interpretation.

Although many studies have focused on developing echocardiographic-derived measures to quantify dyssynchrony and identify patients for CRT [26, 29, 35, 43, 44], due to conflicting results, a standard approach to quantifying dyssynchrony has yet to be established. It is therefore not surprising that utilization of an echocardiographic-derived dyssynchrony parameter is presently not recommended to identify patients for CRT [101]. Metrics used in these studies have used an integrated approach as mentioned above, however, some segmental disparities may be diluted when all pieces are incorporated into a single index. The loss of this information may contribute to the lack of correlation with integrated dyssynchrony measures and response to CRT. Although we failed to find a significant correlation between change in global LV function and change in $CCSI_{int}$, changes in the most dyssynchronous segment as determined by $CCSI_{seg}$ predicted changes in global LV contractility. The use of $CCSI_{int}$ appears to be advantageous in assessing overall trends, however changes in the integrated measures of radial synchrony at a single or multiple cross-sectional levels are unable to consistently predict the changes in global LV function. These results indicate that multi-faceted dyssynchrony analysis (perhaps, one that includes measures of longitudinal dyssynchrony) is necessary for establishing a better link

between contraction dyssynchrony and global LV function. Regardless, it is clear that application of cross-correlation analysis to individual segments (i.e., derivation of $CCSI_{seg}$) allows one to identify the mechanism behind contraction patterns. Furthermore, improvement in global LV contractility appeared to be dependent on resynchronization of the most dyssynchronous segment (i.e., changes in the lowest $CCSI_{seg}$). We expect this new methodology to have clinical application in that evaluation of individual segments using cross-correlation analysis may offer insight into the underlying response or non-response to CRT.

5.4.3 Quantification of Global LV Contractility: Ees vs. ESPVR Area

The slope of ESPVR, or end-systolic elastance (E_{es}), is commonly used as an index of contractility. However, in the current study, LV contractility was not always adequately described using E_{es}. For example, there were several instances where both E_{es} and V_d increased (**Figure 5-4**, dashed ESPVR). Based on E_{es} alone, this would imply increased contractility, but a rightward shift of ESPVR (i.e., increased V_d) indicates depressed contractility. Recently, Burkhoff *et al*. noted that LV contractility should only be assessed using E_{es} alone in well-defined conditions [102]. Deviations from ideal conditions (e.g., dyssynchronous contraction as in the current study) warrant evaluation of LV contractility using both E_{es} and V_d together. Analysis of co-variance (ANCOVA) can be used to simultaneously assess changes in two parameters [102]. Although this approach will identify changes in E_{es} and/or V_d, it does not rank-order the contractile states of two conditions. To address this issue, we developed a new method that considers the entire ESPVR over the operating range and quantifies contractility in terms of a single number. Importantly, this new index, ESPVR area, better quantified changes in LV contractility than E_{es} alone.

Quantification of LV contractility with ESPVR area clearly and consistently showed a decrease in LV contractility (i.e., larger area) with RV pacing in the current study. Others have also reported a detriment in LV contractility following RV pacing in canines [51, 79]. However, one study observed a decrease in E_{es} with little change in V_d [79] and the other study noted a rightward shift of ESPVR (i.e., increased V_d) without a change in E_{es} [51]. This further supports the use of ESPVR area to simultaneously account for E_{es} and V_d in quantifying LV contractility.

5.5 CONCLUSIONS

Compared to RA pacing, RV pacing induced a significant decease in the integrated measure of synchrony ($CCSI_{int}$) and only CRTa improved synchrony at both the basal and mid-LV levels. Application of cross-correlation algorithm to individual segments revealed that the inferior segment was responsible for the failure to resynchronize with CRTf at both the LV basal and mid-LV levels; however, a similar approach using standard time delay indices could not distinguish any segmental contraction disparity with this pacing modality. Thus, the proposed segmental synchrony analysis using cross-correlation algorithm provided better insight into changes in the integrated contraction pattern of the LV. The utility of this segmental approach was further emphasized by the finding that improvement in global LV contractility appeared to be dependent on the degree of resynchronization of the most dyssynchronous segment. Finally, it was shown that both the slope (E_{es}) and intercept (V_d) of ESPVR must be considered simultaneously to accurately quantify LV contractility when contraction dyssynchrony is present. Therefore, ESPVR area is a better index of contractility than the traditional E_{es} under conditions of dyssynchrony.

The current study addressed some of the questions raised in **Study 2**. First, we derived a method to better quantify global LV contractility by incorporating both the slope and intercept of ESPVR into a single index (i.e., ESPVR area). Second, although we did not observe the disassociation between regional and global LV function that was reported in the previous study with CRTf when comparing average trends, changes in integrated measures of radial synchrony at a single or multiple cross-sectional levels were unable to consistently predict the changes in global LV function. These results indicate that multi-faceted dyssynchrony analysis (perhaps, one that includes measures of longitudinal dyssynchrony) is necessary for establishing a better link between contraction dyssynchrony and global LV function.

6.0 STUDY 4: SYNCHRONY ANALYSIS IN THE SETTING OF HEART FAILURE

Specific Aim 5. To assess *global LV function and synchrony patterns* in a tachycardia pacing-induced model of *heart failure*.

6.1 INTRODUCTION

In the previous two studies, we assessed the differential effects of pacing sites on regional LV synchrony and global LV performance and contractility. Specifically, we showed in healthy hearts that RV outflow tract pacing induced significant radial dyssynchrony at the LV base and mid-LV mainly due to underlying disparities at the antero-septal and septal regions. In addition, we showed that global LV performance and contractility were depressed with RV pacing. In an attempt to counteract this dyssynchronous contraction pattern, we showed that LV free-wall pacing (i.e., CRTf) failed to resynchronize the LV due to disparities at the inferior region. Furthermore, we did not observe any improvements in hemodynamic function or LV intrinsic contractile properties with resynchronization using LV free-wall pacing. Although cardiac pacing is often used in patients with normal or near-normal cardiac function, CRT is a unique pacing therapy that targets patients with dyssynchrony in refractory heart failure [2]. Therefore, the goal of the present study was to investigate how the presence of heart failure (HF) influences

the link between LV contraction dyssynchrony and global mechanical behavior. A canine model of HF induced by chronic tachycardia pacing was used for this purpose.

6.2 METHODS

6.2.1 Pacemaker Implantation and Heart Failure Model

The protocol was approved by the Institutional Animal Care and Use Committee and conformed to the position of the American Physiological Society on research animal use. Five mongrel dogs, weighing 19.9 ± 0.6 kg were studied over a period of 8 weeks. During a thorocotomy, pacing leads were epicardially sewn into the right atrium, right ventricular outflow tract, and left ventricular free-wall. An endocardial lead was also screwed into the right ventricular apex for tachycardia-induced heart failure. One week after the surgery, baseline echocardiographic evaluation was performed (referred to as Day 0, **Figure 6-1**). Tachycardia pacing was initiated after baseline data was collected. Each dog was endocardially paced at the RV apex at 200 beats•min^{-1} for 5 weeks to induce HF, and thereafter, tachycardia stimulation was permanently discontinued to allow recovery for 3 weeks.

6.2.2 Pacing Protocol and Echocardiography

Subjects were serially studied every week over an eight week period (**Figure 6-1**). During each study, subjects were pre-medicated with intramuscular injection of acepromazine [0.2 mL] 30-60 minutes prior to the study. Tachycardia pacing was confirmed with a pulse oxymeter and

temporally discontinued before the induction of isoflurane. Anesthesia was performed using masked isoflurane initially at 3-3.5%, and subjects were quickly weaned to 1.5-2%. Echocardiographic images were collected and strain was derived using speckle tracking algorithm as described in **Section 5.2.3**. Images were collected under control RA pacing, dyssynchronous RV pacing, and biventricular free-wall pacing (i.e., RV + LV free-wall pacing; CRTf). Importantly, ventricular stimulation was associated with simultaneous RA pacing to control for heart rate across pacing conditions. In addition, an A-V delay of 20 ms was used to prevent fusion beats. After echocardiographic data was obtained, tachycardia pacing was initiated until the following week. Note that after Day 35, tachycardia pacing was permanently discontinued, and the subject was allowed to "recover" for three weeks. Indices of global LV function were derived from standard echocardiographic techniques and included end-diastolic volume, end-systolic volume, and ejection fraction.

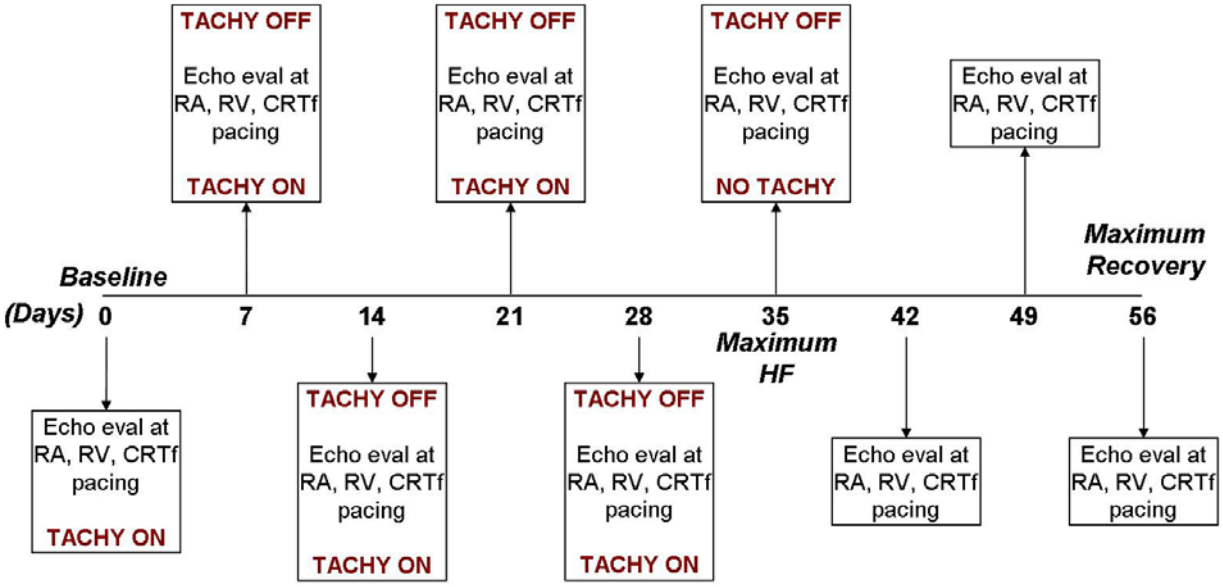

Figure 6-1. Chronic heart-failure model study design.

At Day 0, after baseline echocardiographic data was obtained, tachycardia pacing was initiated. Note that during each echocardiographic study, tachycardia pacing was temporally discontinued. The duration of chronic tachycardia pacing was 35 days, followed by 21 days of recovery without tachycardia pacing. Abbreviations: RA = right atrial; RV = right ventricular; CRTf = resynchronization at the LV free-wall; HF = heart failure.

6.2.3 Regional Analysis: Quantification of Synchrony

Radial strain waveforms were derived from standard echocardiographic grey scale images for 6 radial segments at the base and mid-LV and 4 at the apical level as described in **Section 5.2.3**. However, due to poor image quality at the LV base and apical-LV short-axis views, dyssynchrony analyses were only applied at the mid-LV level. Cross-correlation analysis was performed at both the integrated and segmental levels to quantify synchrony by $CCSI_{int}$ and $CCSI_{seg}$, respectively, as described in **Section 4.2.4**. In addition, dyssynchrony was quantified using current measures such as the maximum time delay between earliest and latest peak strains and the standard deviation of time to peak strains.

6.2.4 Statistical Analysis

Data are presented as mean ± SEM. The effect of pacing on global LV function and synchrony at baseline, maximum deterioration, and maximum recovery (i.e., Day 0, Day 35, and Day 56, respectively) was compared by two-way repeated measures ANOVA with Fisher's LSD post-hoc test. Significance was determined as $P<0.05$.

6.3 RESULTS

6.3.1 Heart Failure Model

A homogeneous model of heart failure was created by chronic tachycardia pacing as illustrated by the data in **Figure 6-2** during control RA pacing. Note that tachycardia pacing was temporally discontinued during echocardiographic data collection. Synchrony patterns did not change during the induction or reversal of heart failure as indicated by relatively homogeneous mid-LV $CCSI_{int}$ values throughout the entire protocol (**Figure 6-2D**). Consistent with other heart failure models, end-diastolic and end-systolic volumes both increased during tachycardia pacing (Day 0-35), resulting in an overall decrease in ejection fraction (**Figure 6-2A-C**). Interestingly, the decrease in EF occurred almost immediately with a significant depression observed after only one week of tachycardia pacing. After Day 35, tachycardia pacing was permanently discontinued, changes in global and regional LV patterns were symmetric to those for the heart failure evolution such that end-diastolic and end-systolic volumes decreased and ejection fraction improved from Day 35-56. However, global LV function did not return to

baseline values at maximum recovery (i.e., Day 56). In summary, these data confirm the establishment of a reliable, consistent model of heart failure induced by chronic tachycardia pacing that was reversible once tachycardia pacing was permanently discontinued.

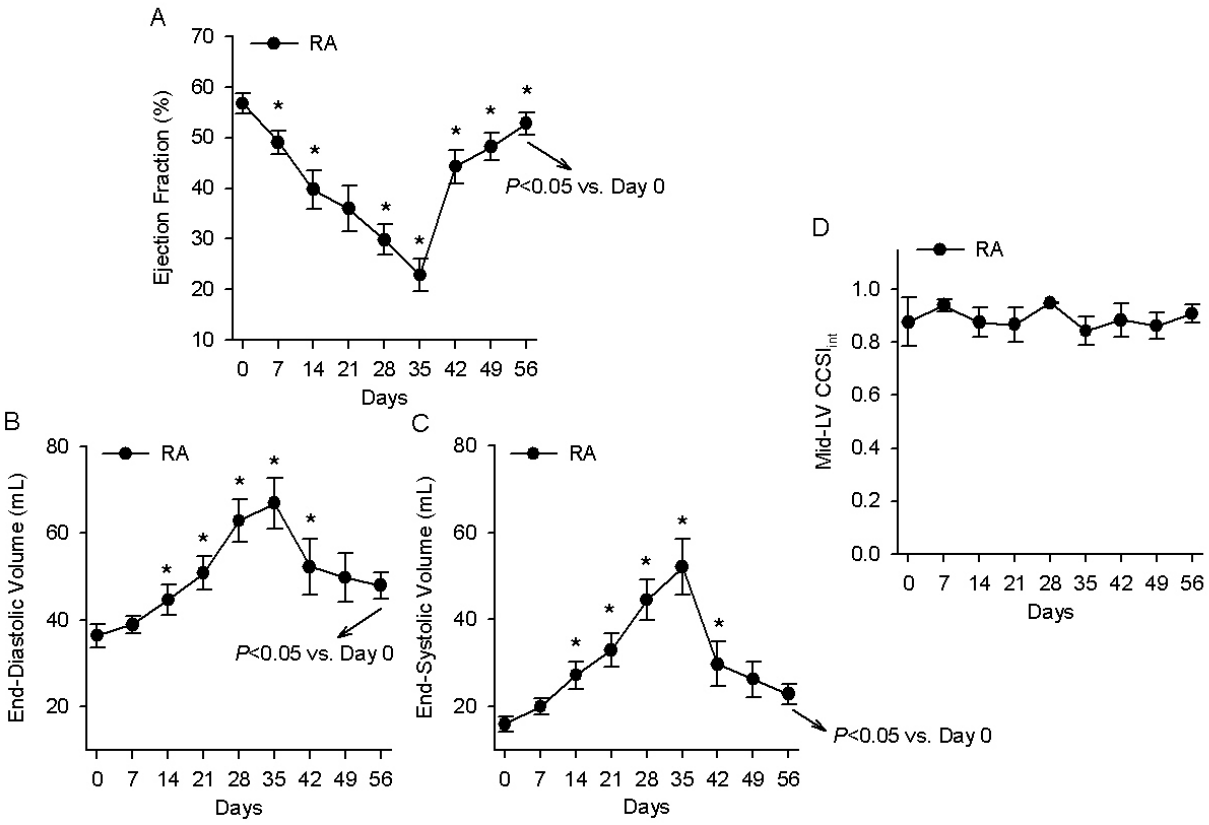

Figure 6-2. Heart failure model induced by tachycardia pacing.

Effects of tachycardia induced heart failure on **(A)** ejection fraction, **(B)** end-diastolic volume, **(C)** end-systolic volume, and **(D)** $CCSI_{int}$ at the mid-LV with control RA pacing. Global LV function declined with progressive LV dilation and increased end-systolic volumes during tachycardia pacing (Day 0-35), confirming the tachycardia pacing-induced model of heart failure. In addition, once tachycardia pacing was permanently discontinued, global LV function improved (Day 35-56). Note that synchrony patterns did not change during induction or reversal of HF indicating a homogeneous HF model. Data: mean ± SEM, n = 5 for Day 0-28 and n = 4 for Day 35-56; **P*<0.05 *vs.* previous week. Abbreviations: RA = right atrial; LV = left ventricular; $CCSI_{int}$ = integrated cross-correlation synchrony index.

6.3.2 Dyssynchrony at Various Degrees of Heart Failure

In the presence of heart failure, the effects of dyssynchrony were exaggerated with RV pacing as indicated by progressively lower mid-LV $CCSI_{int}$ with worsening heart failure (**Figure 6-3D**). This suggests that sicker hearts were more sensitive to RV pacing-induced dyssynchrony. In addition, compared to control RA pacing, RV pacing was associated with similar end-diastolic volumes and slightly higher end-systolic volumes resulting in lower ejection fraction for various degrees of heart failure (**Figure 6-3A-C**). Since the change in absolute values were similar during all degrees of HF, the downward parallel shift observed with EF (**Figure 6-3A**) indicated that the percent change between RA and RV pacing was greater at the maximum degree of HF (Day 35) compared to baseline (Day 0). This message is better illustrated by the data presentation in **Figure 6-3E**. Therefore, RV pacing-induced dyssynchrony and its adverse functional effects were exaggerated as heart failure progressed.

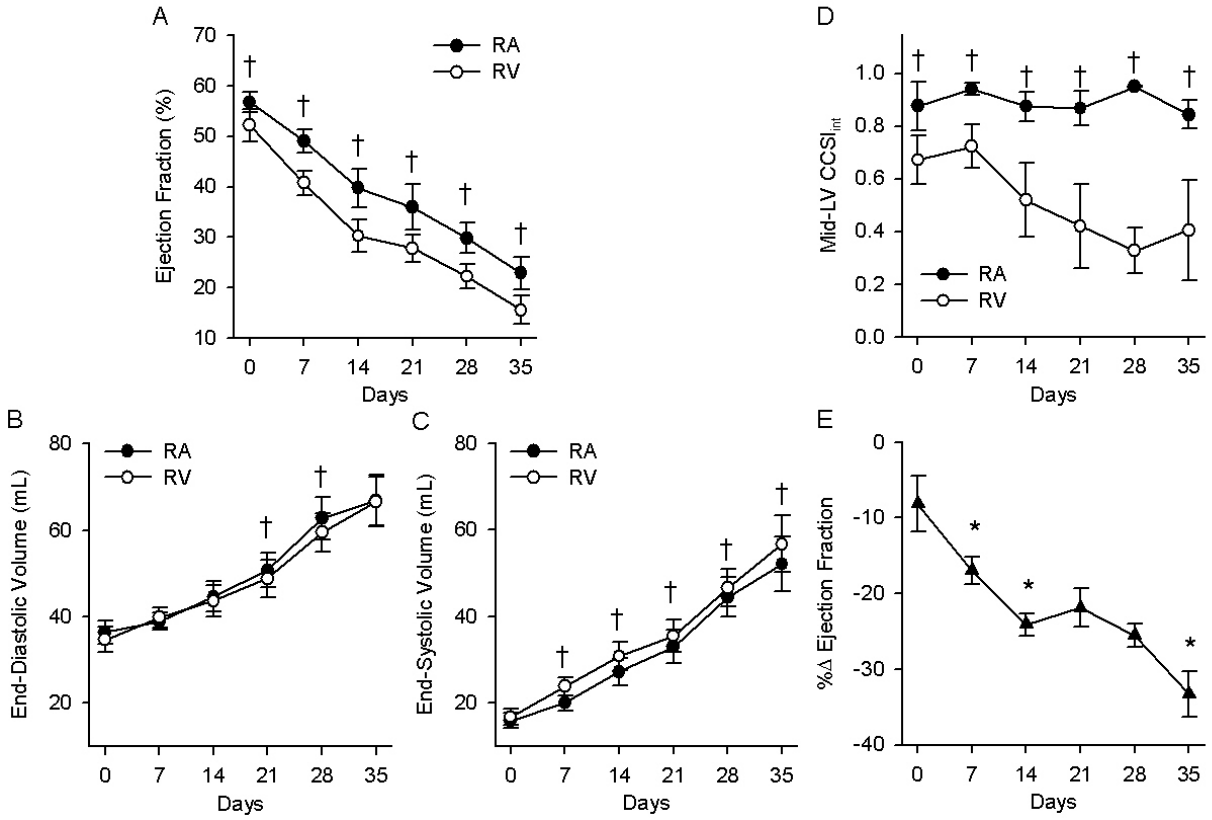

Figure 6-3. Trends in global and regional LV function with dyssynchrony in HF.

Effects of RV pacing on **(A)** ejection fraction, **(B)** end-diastolic volume, **(C)** end-systolic volume, and **(D)** $CCSI_{int}$ at the mid-LV during various degrees of heart failure. RV pacing-induced dyssynchrony and its adverse functional effects were exaggerated as heart failure progressed. **(E)** Percent change of ejection fraction between RA and RV pacing. Data: mean ± SEM, n = 5 for Day 0-28 and n = 4 for Day 35-56; †P<0.05 *vs.* RA pacing for the same week; *P<0.05 *vs.* previous week. Abbreviations as in **Figure 6-2**.

6.3.3 Resynchronization at Various Degrees of Heart Failure

Resynchronization was successful regardless of the degree of HF with LVf pacing (i.e., CRTf) as indicated by an increase in mid-LV $CCSI_{int}$ to a relatively homogeneous value compared to RV pacing during Day 0-35 (**Figure 6-4D**). In addition, synchrony was restored with CRTf to levels similar to that observed during control RA pacing. Furthermore, CRTf did not adversely affect global LV function. Specifically, with CRTf, end-diastolic volumes were similar and end-systolic volumes were lower than during RV pacing, resulting in higher ejection fraction (**Figure**

6-4A-C). The upward parallel shift indicates that resynchronization with CRTf resulted in greater percent change in EF compared to RV pacing at maximum HF (Day 35). Importantly, CRTf resulted in global LV function that was similar to that with RA pacing (**Figure 6-4A-C**). In addition, with respect to values during RV pacing, the degree of improvement in global LV function with CRTf significantly correlated with the level of resynchronization (**Figure 6-4E**; R^2=0.40, P<0.001).

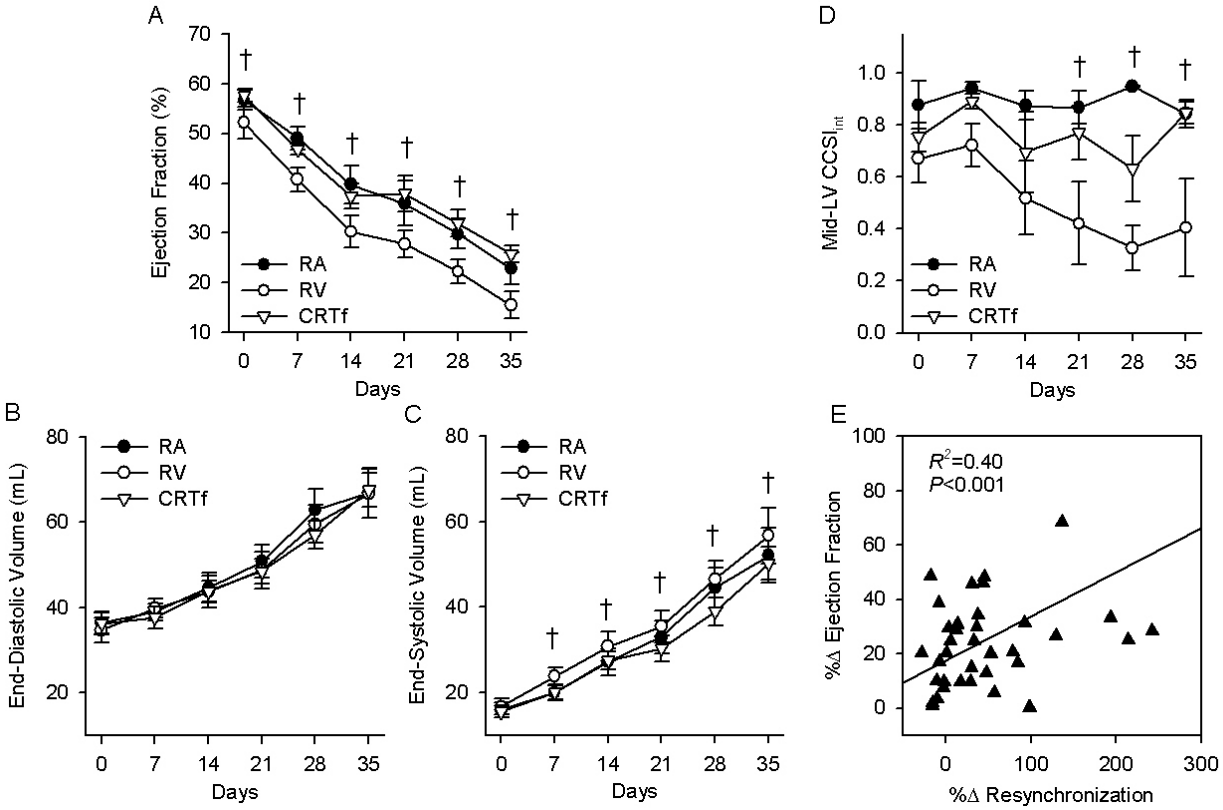

Figure 6-4. Trends in global and regional LV function with resynchronization in HF.

Effects of CRTf on **(A)** ejection fraction, **(B)** end-diastolic volume, **(C)** end-systolic volume, and **(D)** $CCSI_{int}$ at the mid-LV at various degrees of HF. CRTf was equally efficacious regardless of the level of heart failure. In addition, the degree of global LV improvement with CRTf, significantly correlated with the degree of resynchronization. Data: mean ± SEM, n = 5 for Day 0-28 and n = 4 for Day 35-56; †P<0.05 CRTf *vs.* RV pacing for the same week. Abbreviations as in **Figure 6-2**.

6.3.4 Observations During the Recovery from Heart Failure

When tachycardia pacing was permanently discontinued after Day 35, patterns in regional and global LV function during dyssynchrony and resynchronization were symmetric to those observed during HF. Specifically, during recovery, the effect of RV pacing on dyssynchrony became less exaggerated and resynchronization with CRTf was equally efficacious regardless of the state of global LV function (**Figure 6-5D**). In addition, end-systolic volumes were greater during RV pacing resulting in depressed EF compared to RA pacing (**Figure 6-5A-C**). Again, similar to the patterns observed during heart failure, global LV function during CRTf was similar to that during RA pacing.

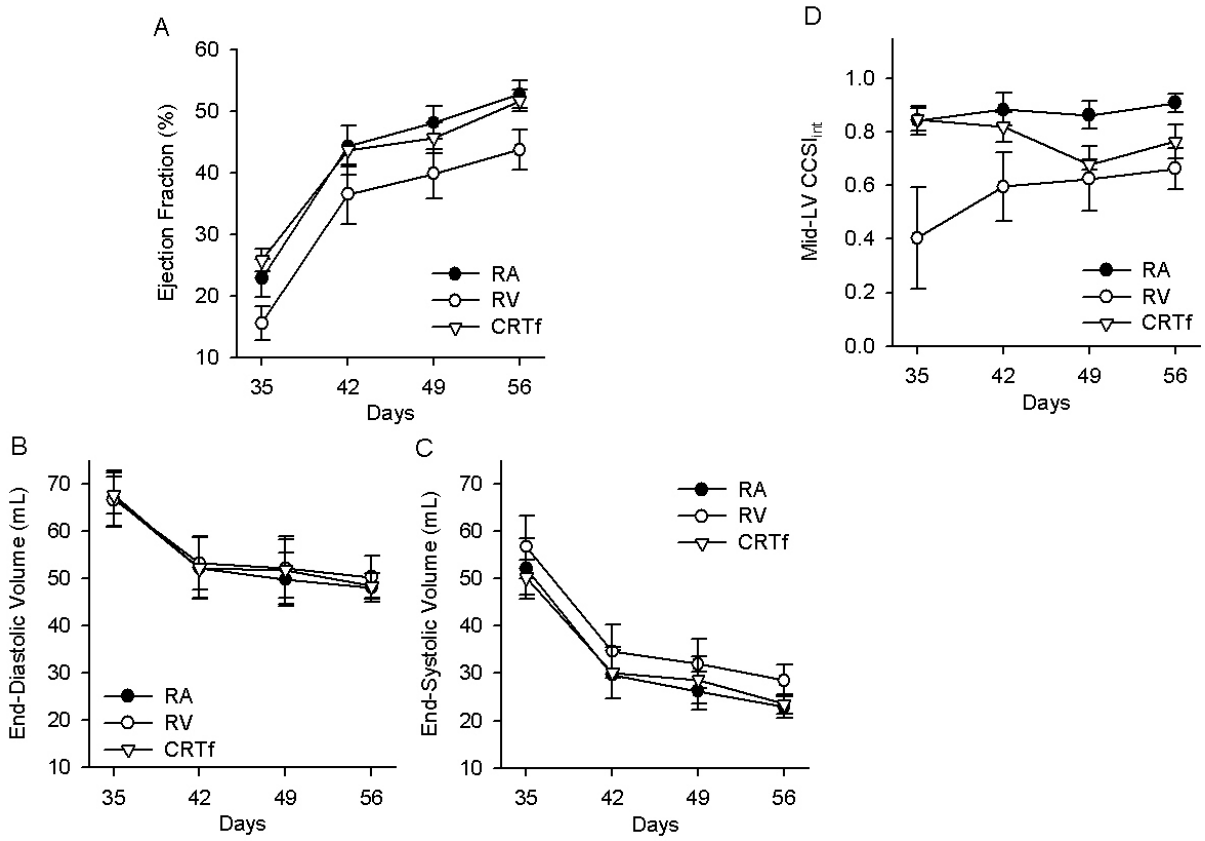

Figure 6-5. Trends in global and regional LV function with during HF recovery.

Effects dyssynchrony and resynchronization on **(A)** ejection fraction, **(B)** end-diastolic volume, **(C)** end-systolic volume, and **(D)** $CCSI_{int}$ at the mid-LV during recovery of heart failure. During recovery, patterns of synchrony and global LV function were mirror images of those observed during HF. Data: mean ± SEM, n = 5 for Day 0-28 and n = 4 for Day 35-56. Abbreviations as in **Figure 6-2**.

6.3.5 Simultaneous Comparisons of Pacing Sites

For simultaneous comparisons of all pacing modalities, we decided to focus on three discreet time points. A two-factor ANOVA structure (factor 1: pacing, factor 2: day) was used with data from baseline (i.e., Day 0), maximum degree of tachycardia pacing (i.e., Day 35), and maximum degree of recovery (i.e., Day 56). Focusing on RA pacing alone, as previously illustrated, induction of heart failure was clearly indicated as LV dilation and depression in EF due to an increase in end-systolic volumes (**Figure 6-6A-C**) at Day 35. The heart failure model was

relatively homogeneous with synchronous contraction at all three time points (**Figure 6-6D**). However, a heterogeneous pattern of regional function was observed with RV pacing. Although RV pacing was associated with greater dyssynchrony compared to RA pacing at all three time points, the effect of RV pacing on mid-LV $CCSI_{int}$ was exaggerated at Day 35 indicating that heart failure is associated with increased sensitivity to RV pacing-induced dyssynchrony. Interestingly, synchrony was improved with CRTf compared to RV pacing at baseline (Day 0) and maximum heart failure (Day 35); however, mid-LV $CCSI_{int}$ at maximum recovery (Day 56) was not different than that during RV pacing (P=NS, CRTf vs. RV pacing). With respect to global LV function, end-diastolic volumes were similar across all pacing modalities. However, RV pacing was associated with significantly higher end-systolic volumes compared to RA pacing that resulted in markedly lower EF at both Day 35 and Day 56. In contrast, resynchronization with CRTf improved global LV function compared to RV pacing such that end-systolic volumes were lower resulting in an increase in EF at both Day 35 and 56 that reached levels associated with RA pacing.

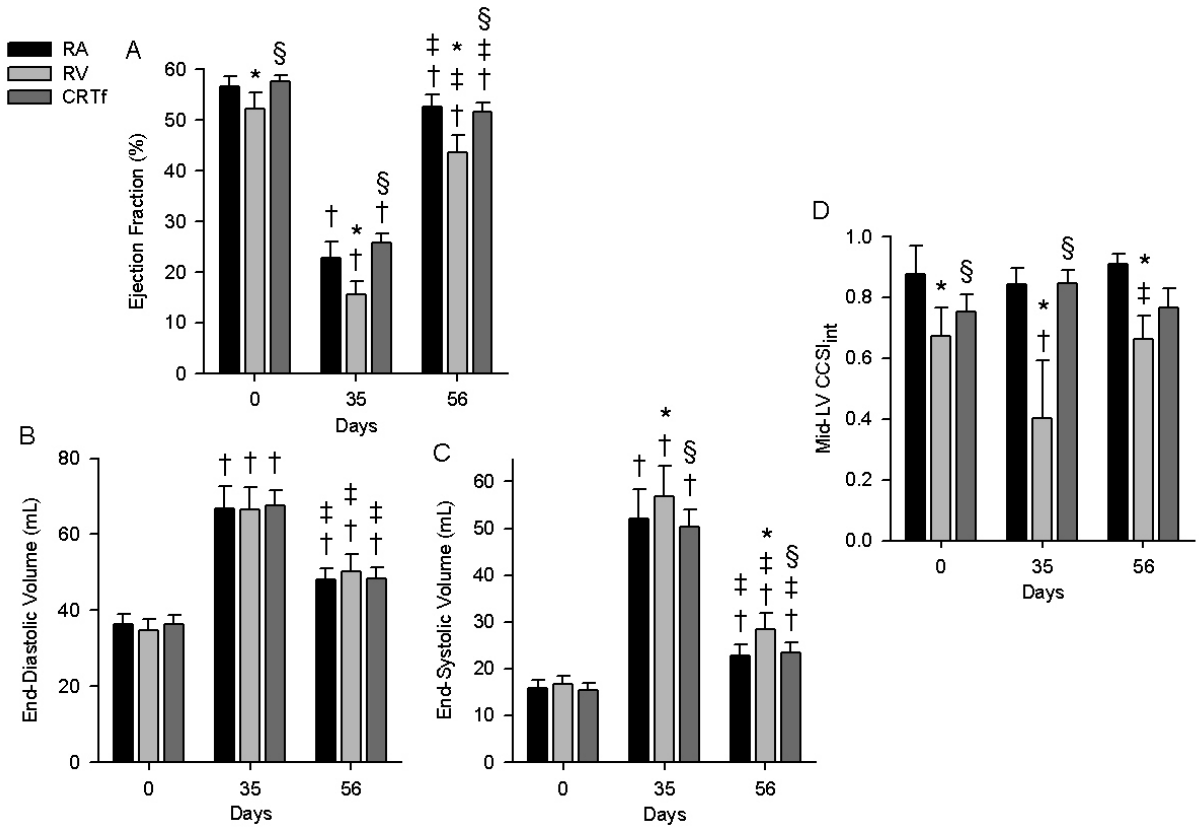

Figure 6-6. Global and regional LV function for all pacing modes at baseline, maximum HF, and maximum HF recovery.

Effects of RA and RV pacing and CRTf on **(A)** ejection fraction, **(B)** end-diastolic volume, **(C)** end-systolic volume, and **(D)** mid-LV $CCSI_{int}$ at baseline, maximum induction of heart failure, and maximum level of recovery. RV pacing was the only pacing modality to show marked differences in global LV function and synchrony compared to RA pacing. Compared to baseline, global LV function was depressed at Day 35, and improved at Day 56, but did not normalize to baseline values for all pacing modes. Data: mean ± SEM, n = 5 for Day 0 and n = 4 for Day 35 and Day 56. **P*<0.05 *vs.* RA pacing, §*P*<0.05 *vs.* RV pacing, † *P*<0.05 *vs.* Day 0, ‡ *P*<0.05 *vs.* Day 35. Abbreviations as in **Figure 6-2**.

6.3.6 Segmental Synchrony Analysis

In order to investigate if a certain segment was responsible for the exaggeration in dyssynchrony and functional depression associated with RV pacing as heart failure progressed, we performed segmental cross-correlation analysis as described in **Section 5.2.4.1**. At Day 0, mid-LV $CCSI_{seg}$ for all segments appeared to be relatively homogeneous (**Figure 6-7B**), although all values were low as reflected by the low integrated measure of synchrony (**Figure 6-7A**). Interestingly, as the

integrated measure of synchrony decreased at Day 35, the anterior (A) and antero-septal (AS) segments were both associated with significantly lower mid-LV $CCSI_{seg}$ values than the other segments during maximum HF. The dyssynchrony at A and AS segments were not observed at Day 56 and all segments were associated with nearly homogeneous segmental synchrony measures. These data suggest that the A and AS segments were responsible for the exaggeration of dyssynchrony with RV pacing during maximum heart failure.

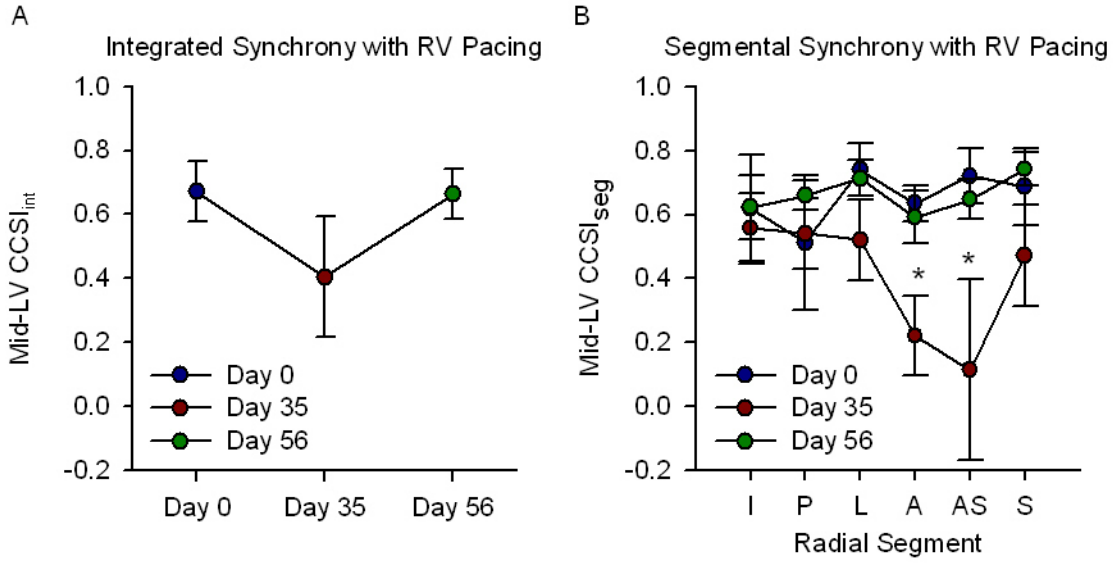

Figure 6-7. Segmental cross-correlation analysis with RV pacing induced dyssynchrony.

(A) Integrated cross-correlation index at baseline, maximum HF, and maximum recovery during RV pacing. **(B)** Segmental cross-correlation analysis indices for RV pacing at the same three discreet time points. Data: mean ± SEM, n = 5 for Day 0 and n = 4 for Day 35 and Day 56; **P*<0.05 *vs.* all other segments. Abbreviations as in **Figure 6-2**.

6.3.7 Standard Indices of Dyssynchrony

Since standard indices of dyssynchrony such as maximum time delay are subject to manual identification of peaks, we were interested to see if this analysis would yield the same result as observed using the integrated cross-correlation analysis to quantify synchrony. Since multiple

peak strains could occur during the cardiac cycle, especially with RV pacing-induced contraction dyssynchrony, the maximum delay between earliest an latest peak strain was chosen by two independent observers. The mid-LV time delay following RV pacing was similar between the two observers from Day 0 through Day 28, however, this was not the case from Day 35 through Day 56 (**Figure 6-8A**). Interestingly, one observer showed that RV pacing was associated with dyssynchrony during Day 35 through Day 56, but according to the other observer, dyssynchrony decreased during Day 35 and 42, then increased again during Day 49 and 56. Data derived from either of the observers did not follow trends that were observed for global LV function (i.e., EF; **Figure 6-8C**), however synchrony quantified using mid-LV $CCSI_{int}$ followed global LV functional trends (**Figure 6-8B**). Importantly, if two different observers performed cross-correlation analysis on the same data, the results would be exactly the same since there are not manual inputs into this analysis. The only potential input would be selection of end-systole, but this time point was automatically chosen by the program as the end of the T-wave from the ECG.

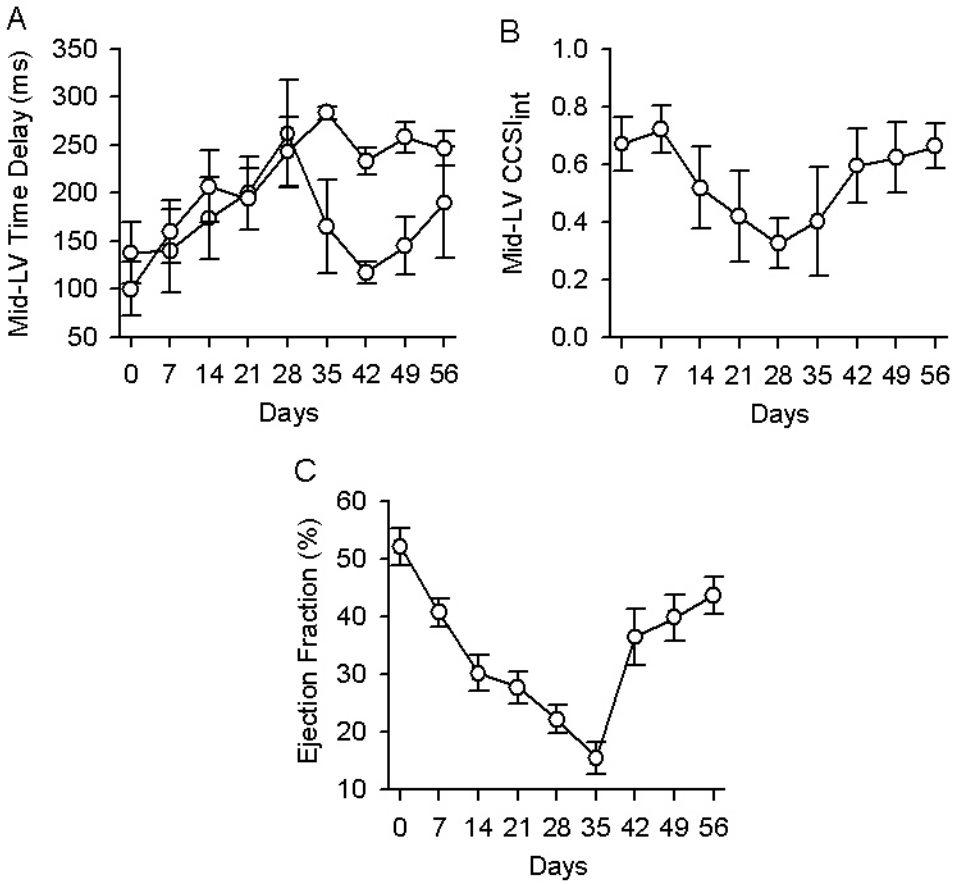

Figure 6-8. Indices of dyssynchrony with induction and recovery of heart failure.

(A) Dyssynchrony quantified by maximum time delay between earliest and latest peak strain calculated by two different observers. **(B)** Note that changes in regional function as quantified by $CCSI_{int}$ were qualitatively similar to changes in global LV function **(C)**. Data: mean ± SEM, n = 5 for Day 0 and n = 4 for Day 35 and Day 56. Abbreviations as in **Figure 6-2**.

6.4 DISCUSSION

In the current study, a consistent and reversible model of heart failure was established by chronic tachycardia pacing. Using this model, three primary findings were reported. (1) As global LV function progressively worsened with tachycardia pacing-induced heart failure, RV pacing-induced dyssynchrony and its adverse functional effects were exaggerated. (2) Resynchronization with CRTf was efficacious regardless of the degree of global LV depression.

(3) As global LV function improved during the recovery phase, RV pacing-induced dyssynchrony and its functional effects were less exaggerated and the efficacy of resynchronization with CRTf did not depend on the state of global LV function. These trends were mirror images of the observations during the heart failure phase. In addition, observations of dyssynchrony quantified using the standard time delay index were not consistent with trends in global LV function. However, changes in synchrony as quantified by mid-LV $CCSI_{int}$ seemed to qualitatively track the changes in global LV function. Before we address these findings in detail, we will discuss certain methodological concerns.

6.4.1 Methodological Considerations

First, similar to the previous canine studies, a short A-V delay was used with ventricular pacing modes. However, in the current study, end-diastolic volume was not different between RA and ventricular pacing modalities. Since atrio-ventricular coupling was not affected by the short A-V delay, direct comparisons of atrial and ventricular pacing modalities were performed. Second, although chronic rapid pacing has been shown to be an effective model of heart failure [103], this model may not extrapolate to traditional CRT patients (i.e., those with heart failure and conduction disturbances). Further studies with the induction of heart failure and structural abnormalities in the conduction system will address this issue.

The current study suffered from the methodological limitation of speckle tracking-derived radial strain. Echocardiographic data in the present study were collected during spontaneous breathing, whereas in the previous acute studies, data were collected during apneic states. Out-of-plane motion caused by breathing results in disappearance of speckles, however, this occurs over a few frames rather than within two consecutive frames [104]. Nonetheless, we

were still unable to derive reliable and reproducible strain waveforms from the LV basal or apical views. The papillary muscle level is less affected by rotation and out-of-plane movement [105], therefore, reliable images were obtained at the mid-LV and reproducible strain waveforms were derived at the mid-LV level.

6.4.2 Dyssynchrony and Resynchronization in Heart Failure

To our knowledge, this is the first longitudinal study to show that with increasing HF, RV pacing-induced dyssynchrony and its functional effects were exaggerated. Furthermore, we showed that the efficacy of CRTf did not depend on the level of heart failure. A recent study reported that speckle tracking-derived radial strain was more accurate than TDI velocity to detect cardiac dyssynchrony in a canine model [106]. Similar to the current study, HF was induced by rapid endocardial RV apical pacing in their study. They showed that following His-bundle ablation and 4 weeks of rapid RV apical pacing, EF effectively decreased and dyssynchrony as measured by the SD of time to peak radial strain was increased compared to baseline values during intrinsic sinus rhythm (comparative to RA pacing in the current study). The increase in dyssynchrony was most likely due to the His-bundle ablation, whereas in the current study, we did not observe dyssynchrony with heart failure under control RA pacing potentially due to an intact conduction system. Regardless, the strength of the current study was that trends in dyssynchrony patterns and global LV function were simultaneously studied during the evolution and de-evolution of heart failure. Importantly, we are the first to show in a comprehensive study that RV pacing-induced dyssynchrony became progressively worse as heart failure advanced and dyssynchrony became less exaggerated as heart failure was reversed. These results highlight the importance of treating dyssynchrony in heart failure patients.

Another study showed that biventricular (RV apical + LV lateral wall) pacing improved global and regional function [107]. They showed that, in canine hearts with structural abnormalities of the conduction system (i.e., chronic isolated LBBB via ablation), biventricular pacing improved global LV function and regional synchrony even in the absence of heart failure. These findings support and help extrapolate the results of the current study. Importantly, our model of dyssynchrony (i.e., RV pacing) was associated with an intact conduction system. However, since we too report similar efficacy with CRTf, we can cautiously extrapolate our results to cases where structural abnormalities, such as LBBB, are present.

6.4.3 Quantification of Dyssynchrony in Heart Failure

In the current study, quantification of dyssynchrony using standard time delay index did not result in trends that were consistent with changes in global LV function. This underscores a statement made in a recent review which noted that echocardiographic-derived parameters of mechanical dyssynchrony may not be useful in the selection of patients for CRT [101]. Ventricular mechanical motion is extremely intricate, and deformations become increasingly complex in dyssynchronous contraction. Simple parameters derived from time-to-peak data reflect only a "snap-shot" of the convoluted contraction pattern with dyssynchrony. It was recently suggested that a more comprehensive characterization of dyssynchrony may be achieved by indices that describe discoordination of contraction [108]. Cross-correlation algorithm accomplishes this goal in that it describes the overall differences in waveform morphology, as opposed to focusing on a single time point. Importantly, in the current study we showed that resynchronization as quantified by mid-LV $CCSI_{int}$ significantly correlated with changes in global LV function (**Figure 6-4E**). Although this supports the use of cross-correlation analysis

in the setting of a chronic canine model of heart failure, a more comprehensive study with human patients is required to support its use in the clinical realm.

6.5 CONCLUSIONS

As global LV function deteriorated with heart failure, RV pacing-induced dyssynchrony and its adverse functional effects were exaggerated. To correct for dyssynchrony, we used LV free-wall pacing (i.e., CRTf) and showed that resynchronization with CRTf was equally efficacious regardless of the degree of global LV depression. Furthermore, as global LV function improved during the recovery phase when tachycardia pacing was permanently discontinued, RV pacing-induced dyssynchrony was less exaggerated and the efficacy of resynchronization with CRTf did not depend on the state of global LV function. These trends were mirror images of the observations during the heart failure phase. In addition, we showed that changes in synchrony as quantified by mid-LV $CCSI_{int}$ qualitatively tracked the changes in global LV function, whereas the traditional dyssynchrony index (i.e., time delay) did not. Although we demonstrated the advantage of cross-correlation analysis in the setting of heart failure in an animal model, its utility in the clinical realm still needs to be assessed.

7.0 STUDY 5: UTILITY OF THE CROSS-CORRELATION ALGORITHM IN THE CLINICAL REALM

Specific Aim 6. To extend our analyses into the *clinical realm* by *assessing the efficacy of cross-correlation analysis* in a select cohort of human patients.

7.1 INTRODUCTION

All studies described so far were conducted using animal models. However, since CRT is ultimately practiced in the clinical realm, it is important to assess the efficacy of the developed tools to quantify dyssynchrony in a subset of human data (**Specific Aim 6**). Furthermore, in the animal models, we used RV outflow tract pacing to induce a LBBB-like pattern of dyssynchrony. However, RV apical (RVa) pacing, which has been implicated in dyssynchrony and heart failure exacerbation is more relevant than RVOT pacing in the human setting. Increasing evidence has shown that RVa pacing is detrimental to ventricular function, and several studies are currently examining other options (e.g., single LV pacing) for these patients [109-111]. Therefore, the goals of the current study were to (1) investigate the utility of cross-correlation analysis of speckle-derived radial strain at the mid-LV level and longitudinal motion (i.e., displacement) at the LV septal and lateral walls, and (2) link echocardiographic regional

information (i.e., radial strain or longitudinal displacement) with global LV performance using different clinically accepted pacing sites in patients with atrial fibrillation without heart failure.

7.2 METHODS

7.2.1 Patient Population

The study was approved by the Institutional Review Boards of University of Pittsburgh Medical Center and St. Paul Heart Clinic. The study cohort was comprised of 26 patients (18 men; 53±13 years) referred for invasive electrophysiologic evaluation, primarily for ablation of paroxysmal atrial fibrillation. All patients had normal LV dimensions (end-diastolic and end-systolic volumes 98±38 and 48±25 mL, respectively), ejection fraction of 54±8%, normal aortic and mitral valve function, QRS duration of 81±15 msec, and normal atrioventricular conduction. In addition, patients underwent pre-operative stress-nuclear imaging, which revealed healthy myocardial tissue (i.e., no LV scar).

7.2.2 Pacing Protocol

Pacing electrodes were placed transvenously into the right atrial appendage (RA), right ventricular apical septum (RVa), and left ventricular lateral base (LVf). The following pacing modalities were evaluated, in random order, at the same rate for each patient (10 beats•min^{-1} above intrinsic sinus rate): (1) RA pacing for control; (2) simultaneous RA and RVa pacing, referred to as RVa pacing; (3) simultaneous RA and LVf pacing, referred to as LVf pacing; and

(4) simultaneous RA, RVa, and LVf pacing, referred to as BiVf pacing. For ventricular pacing modes, an atrioventricular delay of 20 milliseconds was used to eliminate the possibility of fusion between paced (i.e., RVa, LVf, and BiVf pacing) and intrinsic ventricular activation wavefronts.

7.2.3 Echocardiographic Imaging

For each pacing modality, images were obtained using commercially available echocardiographic equipment (Vivid 7™, General Electric Vingmed Ultrasound Inc., Milwaukee, WI, USA) during end-expiratory apnea to minimize translational motion and cardiopulmonary interactions. A 3.5 MHz transducer was used at depths between 12 and 20 cm and via the following windows: parasternal long-axis, and apical 2, 3 and 4-chamber views. Tissue Doppler Imaging was performed at maximal frame rates (80-135 frames per second; velocity range ±16 centimeters/second). Gray-scale 2-dimensional and cine loops from 3 consecutive beats were obtained. Digitized images were analyzed off-line with commercially available software (Echopac™, version 6, General Electric Vingmed Ultrasound) Waveforms were extracted and further analyzed off-line using a custom written Matlab code (see **Appendix B.2**).

Longitudinal regional displacement data was derived using 2-dimensional tissue tracking technique. Tissue Doppler velocity was integrated over time at 5 longitudinally arrayed myocardial segments (8 millimeter sample volumes) along the septal and LV lateral walls (**Figure 7-1A**). Displacement onset was measured relative to mitral valve closure and end-systole was determined by aortic valve closure. Movement towards the transducer is represented by positive displacement. In addition, radial strain was derived from standard 2D

echocardiographic images taken from parasternal short axis views at the LV base, mid-LV, and LV apex using speckle-tracking algorithm similar to that described in **Section 5.2.3**. Radial strain was derived from 6 circumferentially arrayed segments each at the LV base and mid-LV, and 4 segments were assessed at the LV apex (**Figure 7-1B**).

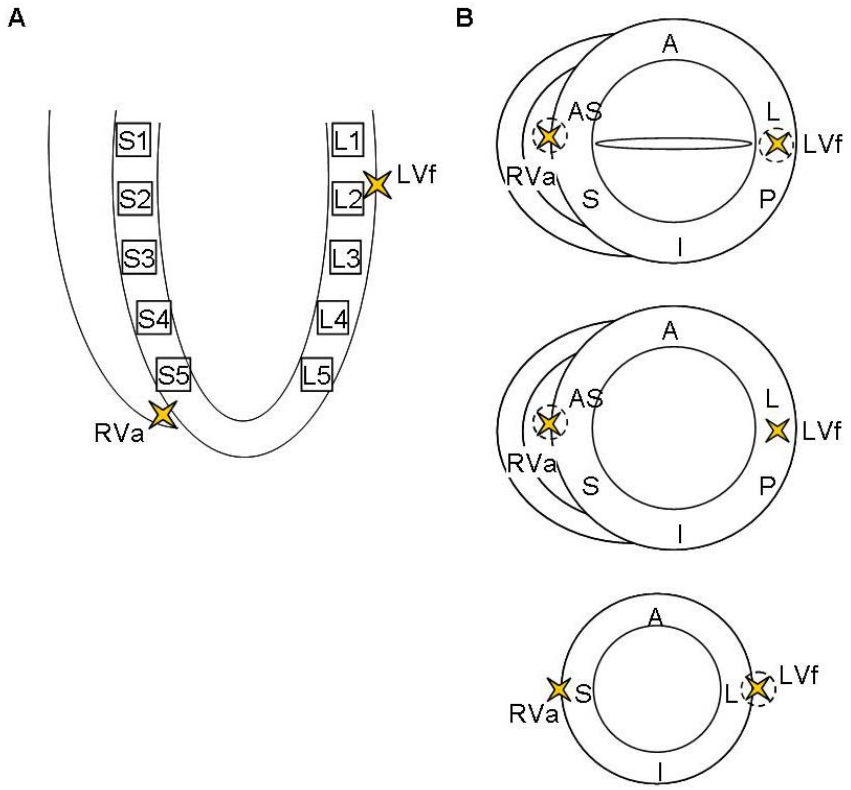

Figure 7-1. Segmentation for longitudinal and radial synchrony analyses.

Star symbols show location of ventricular pacing leads. **(A)** Segments assayed for longitudinal displacement along the septum (S1-S5) and LV lateral wall (L1-L5). Note that RVa and LVf pacing leads abut S5 and L2, respectively. **(B)** Short-axis schematics of the LV base, mid-LV, and LV apex showing segmentation for speckle-derived radial strain. Abbreviations: RVa = right ventricular apex; S1-S5 = septal segments 1-5; L1-L5 = lateral wall segments 1-5; I = inferior; P = posterior; L = lateral; A = anterior; AS = antero-septal; S = septal.

7.2.4 Synchrony Analyses

Regional LV systolic function was assessed using cross-correlation analysis and standard dyssynchrony indices (i.e., maximum time delay between earliest and latest peaks and standard

deviation of time to peak values for various segments). These analyses were applied to (1) longitudinal displacement data at the septal and LV lateral walls, and (2) speckle-tracking-derived radial strain data at the LV base, mid-LV, and LV apex.

7.2.4.1 Longitudinal Synchrony Analysis

Similar to the cross-correlation methods described in Section 4.2.4, longitudinal $CCSI_{int}$ indices were calculated for the septum and LV wall and longitudinal $CCSI_{seg}$ indices were calculated for each of the 10 longitudinal segments (Figure 7-1A). Each LV wall was treated as one entity (i.e., cross-correlation analysis was not performed with pairs between the two walls). For example, $CCSI_{int}$ for the septum was constructed from 10 pair-wise comparisons (S1 vs. S2, S1 vs. S3, S1 vs. S4, S1 vs. S5, S2 vs. S3, S2 vs. S4, S2 vs. S5, S3 vs. S4, S3 vs. S5, and S4 vs. S5); it did not contain data from any lateral wall segments (i.e., L1-L5). Similarly longitudinal $CCSI_{int}$ for the lateral free-wall was constructed from the following 10 pair-wise comparisons: L1 vs. L2, L1 vs. L3, L1 vs. L4, L1 vs. L5, L2 vs. L3, L2 vs. L4, L2 vs. L5, L3 vs. L4, L3 vs. L5, and L4 vs. L5.

7.2.4.2 Radial Synchrony Analysis

An analysis identical to that described in Section 4.2.4 was performed for the dataset in the current study. Radial $CCSI_{int}$ indices were calculated for the LV base, mid-LV, and LV apex; and radial $CCSI_{seg}$ indices were calculated for each of the 16 radial segments.

7.2.5 Global LV Performance Analysis

Indices of global LV performance were derived using P-V analysis from a conductance catheter placed into the LV as described in **Section 4.2.5**.

7.2.6 Statistical Analysis

Data are expressed as mean ± SEM. One-way analysis of variance (ANOVA) with repeated measures was used to evaluate the effects of different pacing modalities on regional LV synchrony and indices of global LV performance. If significant interactions were observed, comparisons between groups were performed using Fisher's least squared difference (LSD) or Tukey-Kramer test. Significance was determined as $P<0.05$.

7.3 RESULTS

7.3.1 Longitudinal Synchrony Analysis

Due to poor image quality in some patients, longitudinal synchrony was evaluated in only 18 of 26 patients. Compared to RA pacing, RVa pacing was associated with dyssynchronous longitudinal motion along the septum reflected as a decrease in septal $CCSI_{int}$ from 0.99 ± 0.003 to 0.74 ±0.07 (**Figure 7-2A**; $P<0.05$, RA *vs.* RV pacing). Compared to RA pacing, RVa pacing significantly decreased septal $CCSI_{seg}$ for all 5 septal segments (**Figure 7-2B-F**; septal $CCSI_{seg\ 1\text{-}5}$: $P<0.05$, RA *vs.* RV pacing).

When LVf pacing was used in conjunction with RVa pacing (i.e., BiVf pacing), resynchronization was not as effective as when LVf pacing was used alone. Compared to RA pacing, BiVf pacing was associated with dyssynchronous septal motion, which was similar to the septal dyssynchrony observed with RVa pacing (**Figure 7-2A**; septal $CCSI_{int}$: $P<0.05$, RA *vs.* BiVf pacing; P=NS, RVa *vs.* BiVf pacing;). Interestingly, the quantity of dyssynchrony during BiVf pacing was almost half the difference of dyssynchrony during RVa and LVf pacing. Furthermore, evaluation of synchrony patterns with BiVf pacing for individual segments revealed a significant decrease in septal $CCSI_{seg}$ for segments 3 and 5; this was similar to the level of segmental dyssynchrony observed with RVa pacing (**Figure 7-2D, F**; septal $CCSI_{seg\ 3,\ 5}$: $P<0.05$, RA *vs.* BiVf pacing; P=NS, RV *vs.* BiVf pacing).

Interestingly, single site LVf pacing was associated with septal motion similar to RA pacing and markedly more synchronous contraction than RVa pacing (**Figure 7-2A**; septal $CCSI_{int}$: P=NS, RA *vs.* LVf pacing; $P<0.05$, RVa *vs.* LVf pacing). Reflecting the synchronous integrated motion pattern observed with LVf pacing, septal $CCSI_{seg}$ for all segments were not different than that for RA pacing and markedly more synchronous than with RVa pacing (**Figure 7-2B-F**; septal CCSIseg 1-5: P=NS RA *vs.* LVf pacing; $P<0.05$ RVa *vs.* LVf pacing).

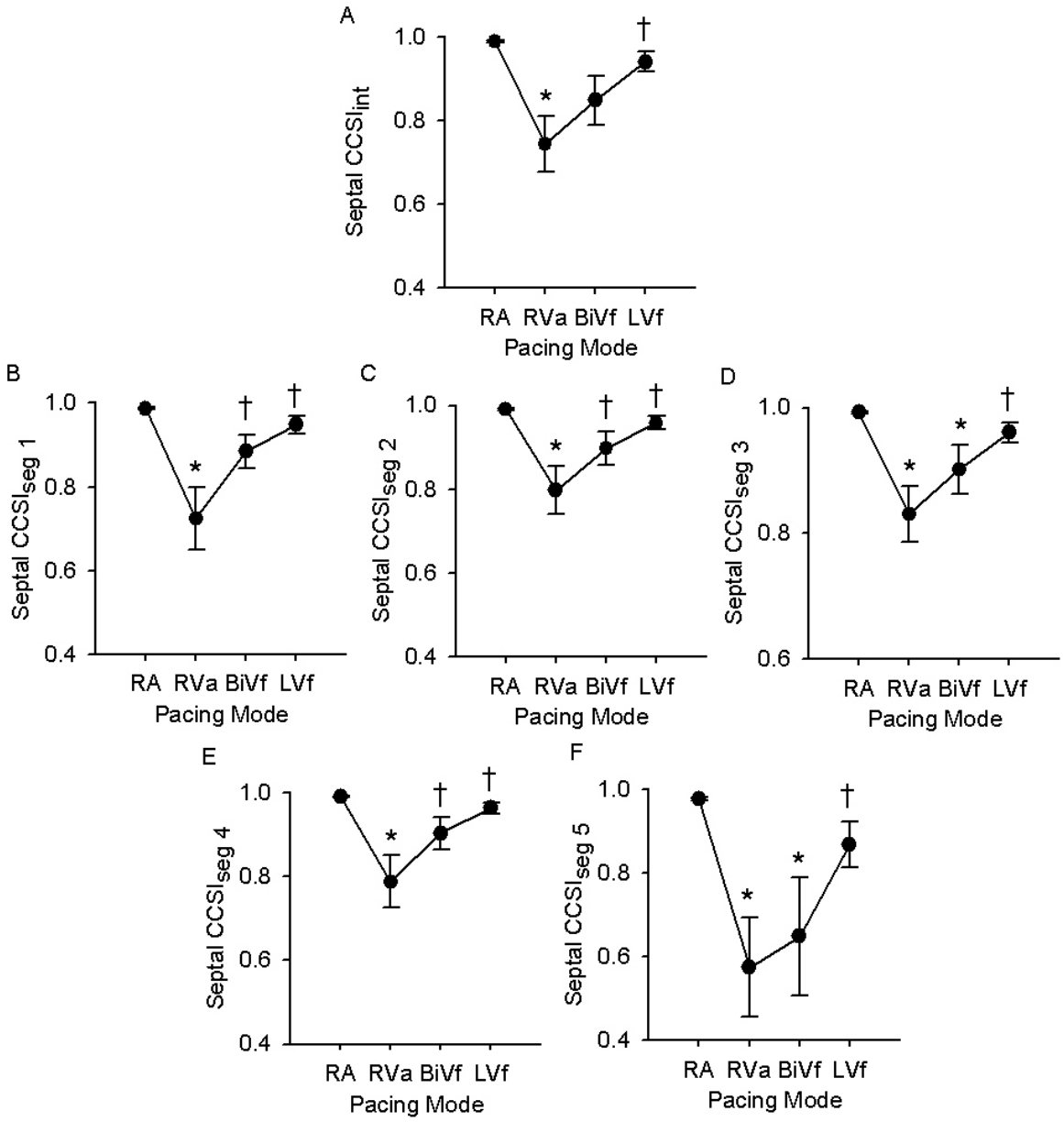

Figure 7-2. Synchrony analysis using longitudinal displacement data at the LV septum.

(A) Integrated measure of synchrony for longitudinal septal wall motion. **(B-F)** Segmental measures of synchrony for longitudinal wall motion for 5 septal wall segments. Data: mean ± SEM, n = 18; **P*<0.05 vs. RA pacing; †*P*<0.05 vs. RVa pacing. Abbreviations: $CCSI_{int}$ = integrated cross-correlation synchrony index; $CCSI_{seg\ 1\text{-}5}$ = segmental cross-correlation synchrony index for segments 1-5; RA = right atrial; RVa = right ventricular apical; LVf = left ventricular free-wall; BiVf = biventricular (RVa+LVf).

Some of the longitudinal synchrony responses at the lateral wall were similar to those observed at the septum. Specifically, RVa pacing was associated with dyssynchronous longitudinal motion at the lateral wall compared to RA pacing (**Figure 7-3A**; lateral $CCSI_{int}$:

P<0.05, RA *vs.* RVa pacing). Also, we observed synchronous longitudinal motion at the LV lateral wall with LVf pacing, which was significantly better than that observed with RVa pacing (**Figure 7-3A**). However, unlike the pattern observed at the septum, BiVf pacing was not associated with dyssynchronous motion at the LV lateral wall compared to RA pacing (**Figure 7-3A**). Interestingly, synchrony at the LV lateral wall was reflected by the synchronous motion for all $CCSI_{seg}$ compared to RA pacing (**Figure 7-3B-F**).

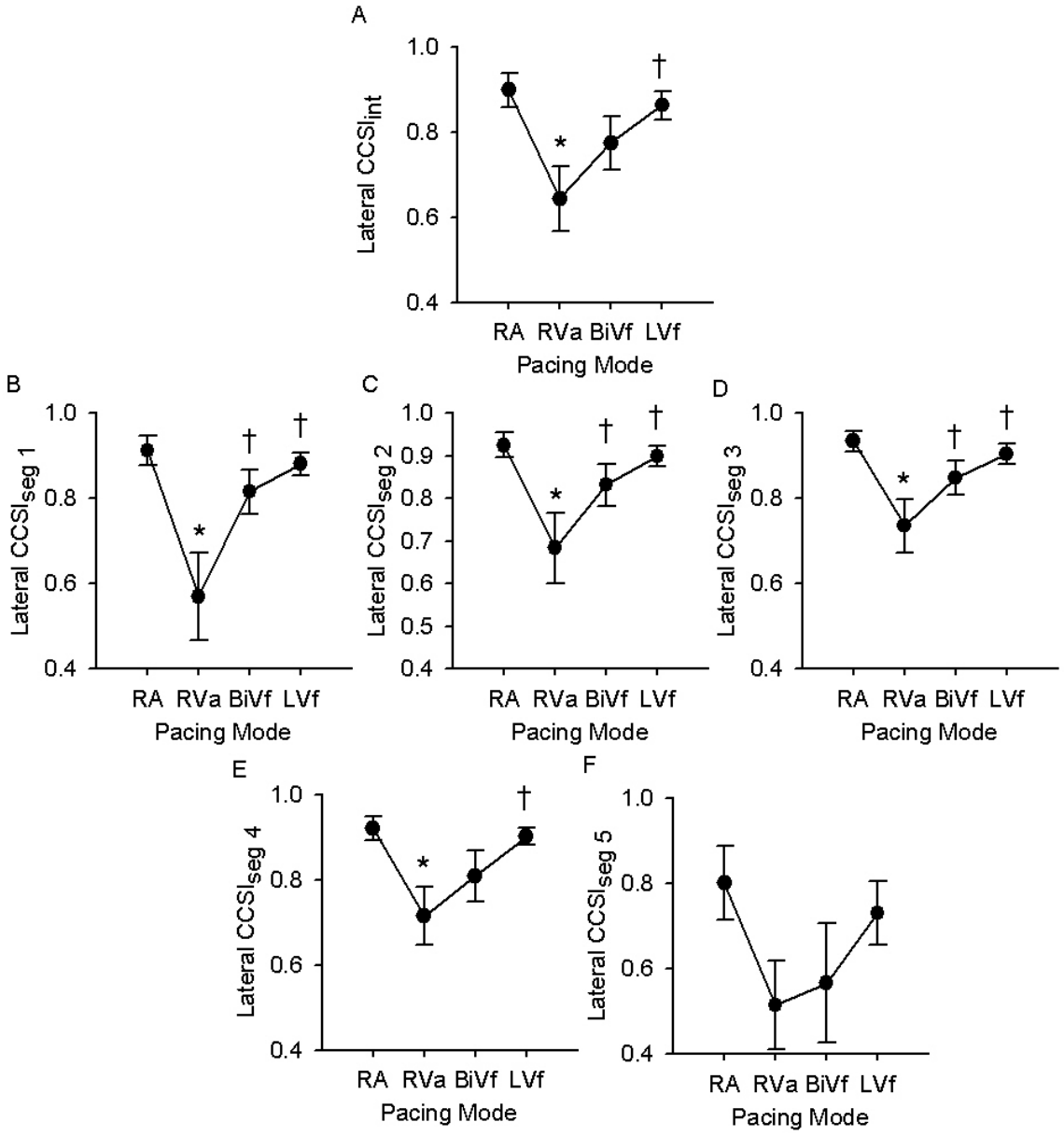

Figure 7-3. Synchrony analysis using longitudinal displacement data at the LV lateral wall.

(A) Integrated measure of synchrony for longitudinal lateral wall motion. **(B-F)** Segmental measures of synchrony for longitudinal wall motion for 5 lateral wall segments. Data: mean ± SEM, n = 18; **P*<0.05 vs. RA pacing; †*P*<0.05 vs. RV pacing. Abbreviations as in **Figure 7-2**.

Standard dyssynchrony indices such as maximum time delay between earliest and latest peak displacement (i.e., TD) and standard deviation of time-to-peak displacement (i.e., SD) at the septal or lateral walls, did not show any significant differences across pacing modalities (**Table 7-1**). However, compared to RA pacing, RVa pacing generally tended to be associated

with greater dyssynchrony with the highest indices at the septal wall. In addition, BiVf and LVf pacing also tended induce dyssynchrony as indicated by greater indices compared to RA pacing. Unlike the tendencies observed with RVa pacing, standard dyssynchrony indices appeared to be similar for the septal and lateral LV walls with either BiVf or LVf pacing.

Table 7-1. Standard dyssynchrony measures for longitudinal displacement data.

	RA Pacing	RVa Pacing	BiVf Pacing	LVf Pacing	*P*-value
Septal TD (ms)	100 ± 27	176 ± 49	245 ± 90	296 ± 118	*0.28*
Lateral TD (ms)	207 ± 91	333 ± 106	273 ± 115	348 ± 132	*0.73*
Septal SD (ms)	43 ± 11	86 ± 26	106 ± 39	132 ± 52	*0.29*
Lateral SD (ms)	92 ± 41	151 ± 47	117 ± 50	152 ± 59	*0.72*

Data: mean ± SEM, n=18. Abbreviations: TD = time delay; SD = standard deviation; RA = right atrial; RVa = right ventricular apical; LVf = left ventricular free-wall; BiVf = biventricular (RVa+LVf).

7.3.2 Radial Synchrony Analysis

Speckle-derived radial strain data was available in a limited number of patients due to poor image quality. Therefore, only 10 of 26 datasets were used for radial synchrony analysis. No significant changes were observed with radial synchrony quantified by $CCSI_{int}$ or standard dyssynchrony indices at the basal LV, mid-LV, or LV apex (**Table 7-2**). Although it appeared that basal $CCSI_{int}$ under RVa pacing was trending toward greater dyssynchrony compared to RA pacing, it did not reach statistical significance. In addition, $CCSI_{int}$ appeared to be similar at the mid-LV and LV apex across all pacing modes and standard indices of dyssynchrony appeared comparable across all pacing modes at all 3 LV levels. Furthermore, segmental cross-correlation analysis of radial strain data did not show any statistical differences for any pacing modality (data not shown).

Table 7-2. Standard dyssynchrony measures for longitudinal displacement.

	RA Pacing	RVa Pacing	BiVf Pacing	LVf Pacing	*P*-value
LV Basal $CCSI_{int}$	0.93 ± 0.03	0.76 ± 0.11	0.90 ± 0.24	0.89 ± 0.02	*0.24*
Mid-LV $CCSI_{int}$	0.96 ± 0.01	0.92 ± 0.03	0.96 ± 0.01	0.95 ± 0.02	*0.36*
LV Apical $CCSI_{int}$	0.97 ± 0.01	0.97 ± 0.01	0.93 ± 0.04	0.98 ± 0.005	*0.38*
LV Basal TD	134 ± 38	130 ± 31	95 ± 39	129 ± 26	*0.80*
Mid-LV TD	81 ± 15	84 ± 25	99 ± 28	112 ± 24	*0.73*
LV Apical TD	69 ± 23	91 ± 22	77 ± 42	26 ± 11	*0.36*
LV Basal SD	64 ± 19	57 ± 13	39 ± 15	55 ± 11	*0.62*
Mid-LV SD	34 ± 5	34 ±10	43 ± 13	50 ± 12	*0.61*
LV Apical SD	28 ± 8	40 ± 10	31 ± 16	11 ± 5	*0.27*

Data: mean ± SEM, n=10. $CCSI_{int}$ = integrated cross-correlation synchrony index. Abbreviations as in **Table 7-1**.

7.3.3 Global LV Performance Analysis

The short A-V delay of 20 ms used for ventricular pacing modes was expected to affect LV diastolic filling, so statistical comparisons were performed between ventricular pacing modes only. However, global LV performance values during RA pacing are listed as a reference state. As shown in **Table 7-1,** global LV performance with BiVf pacing was similar to that during RVa pacing. However, pacing at the LV free-wall alone (i.e., LVf pacing) appeared to be least detrimental to global LV function with values that tended to be greatest among ventricular pacing modes. Specifically, compared to RVa pacing, LVf pacing resulted in significantly greater LV CO, primarily due to increased end-systolic pressures and dP/dt_{max}.

Table 7-3. Global LV performance values for different pacing modalities.

	RA Pacing	RVa Pacing	LVf	BiVf	*P*-value
HR (beats•min^{-1})	*63 ± 1*	64 ±1	64 ±1	64 ±1	*0.39*
LV ESP (mmHg)	*125 ± 7*	97 ±6	113 ± 6†	99 ± 6	*0.004*
LV EDP (mmHg)	*15 ± 2*	13 ± 1	14 ± 1†	13 ± 1	*<0.001*
EDV (mL)	*116 ± 11*	93 ± 9	118 ± 14†	107 ± 14	*0.006*
ESV (mL)	*58 ±8*	38 ± 4	52 ±6	50 ± 5	*0.10*
SV (mL)	*58 ± 3*	38 ± 4	52 ±6†	50 ± 5	*0.04*
CO (L•min^{-1})	*3.7 ± 0.2*	2.5 ± 0.3	3.3 ± 0.4†	3.2 ± 0.3	*0.03*
dP/dt$_{max}$(mmHg•s^{-1})	*1285 ± 77*	1083 ± 92	1227 ± 101†	1154 ± 94	*0.18*
dP/dt$_{min}$ (mmHg•s^{-1})	*-1569 ± 99*	-1157 ± 144	-1200 ± 107	-1266 ± 116	*0.048*
SW (mJ)	*5929 ± 438*	3139 ± 377	4876 ± 624†	4243 ± 466	*0.61*

Data: mean ± SEM, n=11; †P<0.05 vs. RVa pacing. Abbreviations: HR = heart rate; LV = left ventricular; ESP = end-systolic pressure; EDP = end-diastolic pressure; EDV = end-diastolic volume; ESV = end-systolic volume; SV = stroke volume; CO = cardiac output; dP/dt$_{max}$ = maximum rate of pressure rise; dP/dt$_{min}$ = minimum rate of pressure rise; SW = stroke work; RA = right atrial; RVa = right ventricular apical; LVf = left ventricular free-wall; BiVf = biventricular (RVa+LVf).

7.4 DISCUSSION

The current study reports four primary findings: (1) Global LV depression following RVa and BiVf pacing was associated with longitudinal septal wall dyssynchrony. (2) Although longitudinal dyssynchrony was observed with RVa and BiVf pacing, radial contraction synchrony was preserved. Therefore, synchrony measures derived from a single plane of motion or contraction may not comprehensively describe regional function. (3) Synchrony indices derived from cross-correlation analysis ($CCSI_{int}$ and $CCSI_{seg}$) were the only measures that captured dyssynchronous longitudinal regional activity; standard dyssynchrony indices such as time delay and standard deviation of time to peak displacement failed to reveal longitudinal dyssynchrony. (4) LVf pacing was least detrimental to global LV performance and synchrony

compared to RVa and BiVf pacing. Therefore, BiVf pacing may not be the preferred pacing modality in patients with preserved EF. Before we discuss these findings in detail, we will consider some methodological limitations encountered in the current study.

7.4.1 Methodological Limitations

First, as with the animal studies, we used a short A-V delay during ventricular pacing, which restricts diastolic LV filling. Therefore, a direct functional comparison of intrinsic activation (i.e., RA pacing) and ventricular pacing (i.e., RVa, LVf, and BiVf pacing) could not be performed. Second, the patient cohort in the current study consisted of healthy hearts with normal ejection fractions. Although the results contribute valuable knowledge to this subset of patients who might be recommended for ventricular pacing, these observations may not extrapolate to heart failure patients. However, since heart failure is a clinical syndrome characterized by the inability to perform activities of daily living to an adequate degree, these findings could extrapolate to patients that are symptomatic with heart failure symptoms without reduced ejection fraction. Third, tissue-Doppler-derived displacement can introduce significant errors due to tethering [112]. However, these patients did not have myocardial scar tissue as noted in **Section 7.2.1**, therefore, tethering was less likely to occur and displacement data should have reflected active motion.

7.4.2 Mechanism of Global LV Performance Depression with RVa Pacing

The observed detriment in global LV performance with RVa pacing in the current study was consistent with previous reports [109-111]. However, the current study extended this knowledge

by showing that the depression in global LV performance with RVa pacing was primarily due to regional longitudinal disparities in septal wall motion. With normal activation, the left ventricular base moves towards the apex. We suspect that RVa stimulation introduces an electrical wavefront that pre-excites the septum and elicits movement of septal apical segments towards the base, competing with basal segmental displacement towards the apex. This theory is supported by the displacement waveforms during RVa pacing shown in **Figure 7-4**. At the septum, $CCSI_{int}$ is low (0.31), due to the disparity in the most apical segment (segment 5). After a temporal displacement towards the apex (positive displacement), this segment begins to move away from the apex, while the rest of the segments have positive displacement. Then finally, segment 5 has post-systolic movement in the apical direction. The septal disparity is nicely illustrated by the color-coded plot in **Figure 7-4** showing that the $CCSI_{seg}$ for segment 5 has the darkest color reflecting the lowest synchrony index. Since the RVa pacing site abuts segment 5 (**Figure 7-1A**), it is not surprising that this segment was affected by the early stimulation. Therefore, we suspect that the intramural regional disorder at the septum was responsible for the detriment in global LV performance observed with RVa pacing.

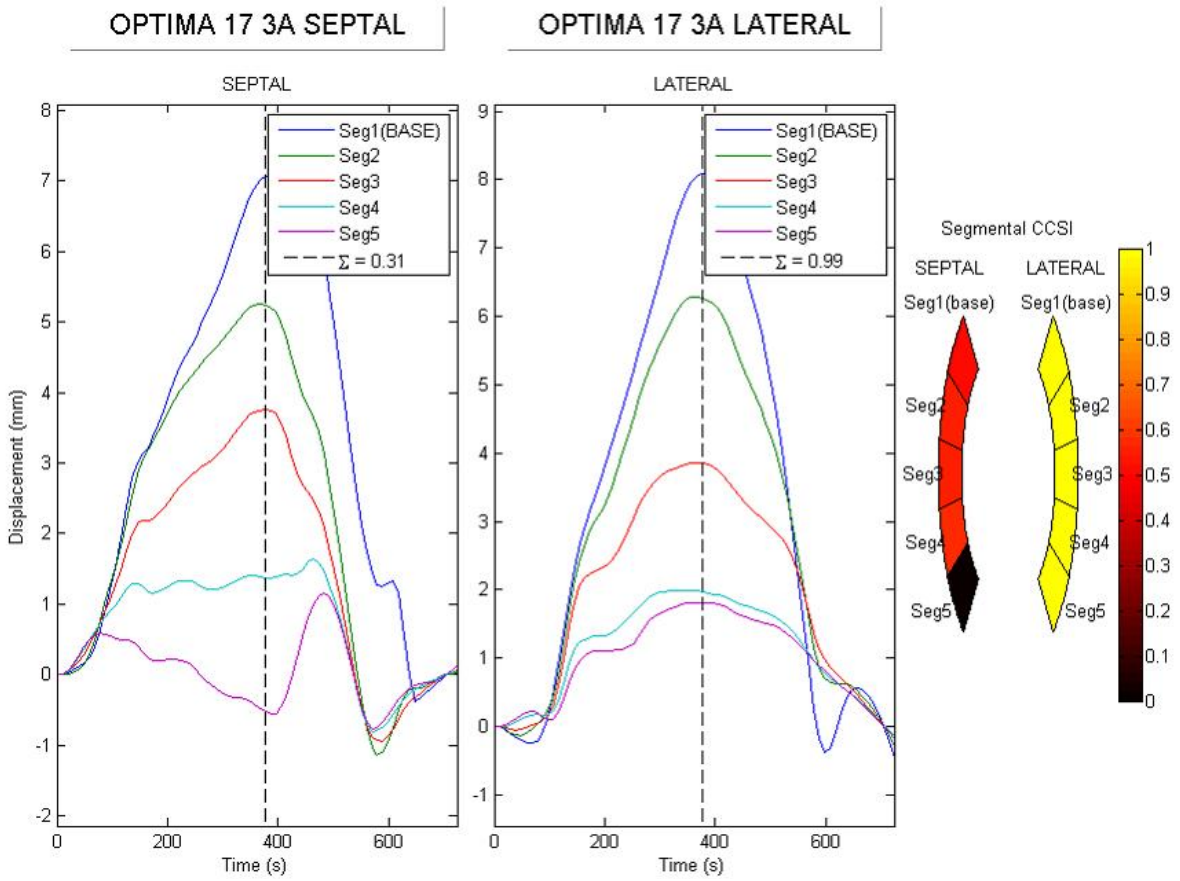

Figure 7-4. Cross-correlation program output for longitudinal displacement.

Septal and lateral time-displacement curves representing longitudinal myocardial motion during RVa pacing for one patient. The dashed line indicates end-systole determined by aortic valve closure from pulsed-Doppler information. The legend shows $CCSI_{int}$ calculated during systole and $CCSI_{seg}$ are color-coded and represented to the right of the displacement data with values ≤0.0 being black. Abbreviations: $CCSI_{int}$, $CCSI_{seg}$ = integrated and segmental cross-correlation synchrony index, respectively; Σ = $CCSI_{int}$.

7.4.3 Assessment of Synchrony

We assessed both longitudinal (based on displacement) and radial (based on strain) synchrony indices. Interestingly, radial synchrony indices derived from cross-correlation analysis as well as traditional indices were not different across pacing modalities. This was not surprising since LV dynamics are multi-dimensional and depending on the pattern of contraction, evaluation of

synchrony in a single plane may not completely characterize regional function. For example, although we did not observe radial contraction dyssynchrony in the current study with RVa pacing, we previously reported significant radial dyssynchrony (septal to free-wall) in canine studies due to RV outflow tract pacing [74]. Therefore, it appeared that although RV outflow tract pacing affected radial synchrony, longitudinal synchrony was mainly affected by RVa pacing. This emphasized the notion that not all dyssynchronous contraction patterns are created equal.

In the current study, we demonstrated the utility of cross-correlation analysis in the clinical realm. More importantly, synchrony indices derived using cross-correlation were the only measures able to demonstrate the regional disorder along the septum, which seems to explain the global detriment associated with RVa pacing. Currently, measures of dyssynchrony that incorporate time to peak values of displacement, strain, strain rate or velocity are the only indices being included in clinical studies. However, due to conflicting results using these indices to quantify dyssynchrony, it is not advisable to incorporate mechanical measures of dyssynchrony to the selection of candidates for CRT [101]. We suspect that these indices suffer from only describing dyssynchrony based on single points in time. With the discouraging results of echocardiographic-based parameters using time differences, it is becoming clear that a more comprehensive analysis of myocardial mechanics may be necessary to describe the regional discoordination observed with dyssynchrony [108]. Cross-correlation analysis uses the entire systolic portion of the waveform to more robustly describe synchrony patterns, and this analysis seems to have the ability to determine regional disorders among segments. Additional studies are needed to determine if synchrony measures derived from cross-correlation analysis can predict response to and identify patients for CRT.

7.4.4 Optimal Pacing Site

Compared to RVa pacing, we showed that BiVf pacing did not improve global LV performance in patients with normal ejection fraction. Although CRT is an established therapy to improve clinical status in heart failure patients, we suspect that CRT using simultaneous BiVf pacing may not benefit all patients with preserved ejection fraction. Other pacing modalities, such as single LV free-wall pacing may be superior to those patients. Previous studies have also reported superior global LV performance during LVf pacing relative to RVa pacing [113, 114]. Most of the data in these studies were from heart failure patients. However, a subset of patients with preserved ejection fraction was also studied, which showed the same superiority with LV free-wall pacing as reported in the current study [114]. Regardless, the optimal pacing site may be specific to the individual patient based on severity of heart failure, myocardial infarction area, and/or baseline dyssynchrony patterns. Thus, a procedure to determine the optimal pacing site(s) that offer the most benefit in global LV function and synchrony for individual patients may be necessary.

7.5 CONCLUSIONS

In the current study, we showed that in a cohort of patients with preserved ejection fraction, RVa pacing was associated with depression in global LV performance mainly caused by dyssynchronous longitudinal motion along the septal wall. Importantly, this dyssynchrony was not captured by standard indices using time-to-peak information. The cross-correlation analysis applied to longitudinal displacement data identified individual septal segments that were

responsible for the detriment in global LV performance associated with RVa pacing. In addition, we reported no significant changes in radial contraction across pacing modalities, indicating that multi-faceted dyssynchrony analysis may be necessary for a more complete evaluation of regional LV function. Finally, we observed a detriment in global LV performance with BiVf pacing, mostly due to the continued septal disparities in septal motion associated with RVa pacing. In patients with preserved ejection fraction, LV free-wall pacing appeared to be superior in the context of global LV performance and longitudinal synchrony. In summary, the utility of cross-correlation analysis in the clinical realm was established through characterization of longitudinal synchrony patterns. Although these results are promising, a more comprehensive study with a larger patient cohort is necessary to translate cross-correlation analysis into the clinical realm as a standard tool to quantify dyssynchrony and identify patients for CRT.

8.0 TAKE HOME MESSAGES

- In the presence of contraction dyssynchrony, global LV mechano-energetic function is adversely affected. A disconnect exists between regional (cellular) and global mechanical activities such that the observed mechanical energy at the global level underestimates internal work at the cellular level, which is likely to be the true determinant of myocardial oxygen consumption.
- Cross-correlation analysis is a robust tool to quantify contraction dyssynchrony, both at integrated and segmental levels. Specifically, cross-correlation analysis is fully automated and takes into account the entire systolic portion of the cardiac cycle. As a result, this methodology is associated with less intra-group variability compared to currently used indices of dyssynchrony that focus on manually chosen time points and are subject to user interpretability. Furthermore, segmental cross-correlation analysis provides insight into the integrated LV contraction pattern. The utility of this segmental approach is further emphasized by the finding that improvement in global LV contractility is dependent on the degree of resynchronization at the most dyssynchronous segment.
- Right ventricular pacing induces significant dyssynchrony that adversely affects global LV function. Left ventricular pacing appears superior, with preliminary data suggesting that pacing at the LV apex offers greater benefit in global and regional LV function than

at the LV free-wall. Importantly, in the clinical realm, it appears that single-site LV free-wall pacing is less detrimental than traditional RV apical or biventricular (RVa+LVf) pacing modalities. However, optimal pacing site(s) will clearly be specific to the individual patient.

- Changes in the integrated or segmental measures of radial synchrony at a single or multiple cross-sectional levels are unable to consistently predict the changes in global LV function. These results indicate that multi-faceted dyssynchrony analysis (perhaps, one that includes measures of longitudinal dyssynchrony) is necessary for establishing a better link between contraction dyssynchrony and global LV function.
- RV pacing-induced contraction dyssynchrony and its adverse functional effects are exaggerated as heart failure progresses and the reverse is true during the recovery from heart failure. In contrast, resynchronization using LV free wall pacing is equally efficacious regardless of the degree of heart failure.
- Cross-correlation analysis is applicable in the clinical realm. Dyssynchrony is better characterized using cross-correlation analysis compared to standard indices that focus on manually chosen individual points in the cardiac cycle. Although these results are promising, a more comprehensive study with a larger patient cohort is necessary to translate cross-correlation analysis into the clinical realm as a standard tool to quantify dyssynchrony and identify patients for CRT.

APPENDIX A

DETAILED ISOLATED HEART PREPARATION PROTOCOLS

A.1 PREPARATION OF ERYTHROCYTE SUSPENDED PERFUSION MEDIUM

The isolated rabbit hearts were perfused with washed bovine erythrocytes suspended in a modified Krebs-Hanseleit (KH) solution. The following is a detailed description of the preparation of this perfusion medium beginning with the bovine blood collection protocol to the final resuspension.

A.1.1 Bovine Blood Collection Protocol

First prepare two 2 L plastic containers with secure lids by rinsing with saline. Then add 10 $U \bullet mL^{-1}$ of heparin [1000 $U \bullet mL^{-1}$ concentration] with anticipation of filling each container with 2 L of blood (therefore, add 20mL of 1000 $U \bullet mL^{-1}$ heparin to each container). After blood is collected from the slaughterhouse (Thoma Meat Market, 748 Dinnerbell Road, Saxonburg, PA 16056), transport the containers on ice in a cooler. Once returning to the lab, add an antibiotic [250 $mg \bullet L^{-1}$ of Gentomyosin] to the blood and filter blood through a 40 μm filter to remove

gross particles (e.g., hair, skin). The blood should be filtered into a 4L plastic container pre-rinsed with saline.

A.1.2 Krebs-Hanseleit Solution Preparation

Fill three 3L glass containers with de-ionized water. Table A-1 shows the ingredients to add in each of the containers. Note that calcium chloride is not added in this step because this solution is used to wash the bovine blood; we experienced significant clotting inside the cell saver machine when calcium chloride was added to this solution. After the KH solutions are well mixed and brought to a pH of 7.5, the solution is then filtered through a 5 μm filter. Note that the solution should be prepared before the blood is returned from the slaughterhouse to prevent any delays with the blood processing.

Table A-1. Components of Modified Krebs-Hanseleit Solution

Components	Concentration ($mM \cdot L^{-1}$)	Formula Weight ($g \cdot M^{-1}$)	Concentration ($g \cdot L^{-1}$)	Add to 3L (g)
NaCl	124	58.44	7.25	**21.7397**
KCl	4.96	74.56	0.37	**1.1095**
$NaHCO_3$	24	84.01	2.02	**6.0487**
NaH_2PO4	0.362	137.99	0.05	**0.1499**
$MgCl_2 \cdot 6H_2O$	1.08	203.31	0.22	**0.6587**
Glucose	11.1	180.16	1.20	**5.9993**

A.1.3 Bovine Blood Processing Protocol

The following procedures will be necessary to process the bovine blood with the cell saver machine: *Fill, Wash, and Empty*. Before blood is started through the machine, the lines and bowl must be rinsed with the KH solution. This may be achieved by running through the *Fill, Wash,* and *Empty* procedures with the KH solution. Now the blood processing can begin. First, press the *Fill* button and wait about 10 seconds for the centrifuge to steadily spin the bowl. Then

increase the pump speed to 300 mL•min^{-1}. The bowl will begin to fill with blood with the RBCs being centrifuged to the bottom of the bowl and the plasma rising to the top. Once all plasma is eliminated from the bowl, press the *Wash* button. When the waste tube is clear the press *Stop*. Once the centrifuge ceases to spin, press *Empty* and increase the pump speed to 225 mL•min^{-1}. Note that it was easiest to empty the isolated RBCs into a plastic container pre-rinsed with KH solution and containing ~3mL of 1000 U•mL^{-1} concentration of heparin. Press *Stop* at the first signs of bubbles out of the bowl. Repeat this procedure until all 4L of whole blood is processed. Then repeat this entire procedure again with the "isolated RBCs" in the plastic container now at the *Fill* end. We found that washing the blood once did not efficiently isolate the RBCs; centrifuging a small sample revealed that plasma remained after a single wash. After all blood is processed through the cell saver machine twice, take a small sample and centrifuge to ensure that all plasma is eliminated; the RBCs should sediment to the bottom with the clear KH solution at the top.

A.1.4 Erythrocyte Suspended Perfusion Medium Protocol

The desired hematocrit for the final resuspension was 30-35%. However, the volume of washed RBCs was not known at this step of the process. Therefore, the following procedure allowed us to determine the initial volume of KH in the washed RBCs and subsequently the amount of KH needed to achieve a final hematocrit of 30-35%. Using an OSM3 Hemoximeter (Radiometer), determine the initial hemoglobin (Hgb) of the washed suspension. Hematocrit can be estimated by multiplying Hgb by three. Add 300 mL of KH solution to the blood, measure the Hgb with the OSM3 machine, and calculate the new hematocrit by multiplying by 3. The amount of KH to be added (V_A) to achieve the desired hematocrit of 30-35% can then be calculated by:

$$V_A = \frac{V_{300} \times H_1}{H_1 - H_2} \times \frac{H_2 - H_D}{H_D}$$

Where V_{300} is the volume added to initially change the hematocrit, H_1 is the initial hematocrit of the washed suspension, H_2 is the hematocrit after the 300 mL is added, and H_D is the desired hematocrit (our target was 33%). The final volume of the entire suspension can then be calculated by the initial volume of the washed suspension plus the volume added by:

$$V_f = \frac{V_A \times H_2}{H_1 - H_2} + V_{300} + V_A$$

Importantly, before V_A is added to the washed suspension, calcium chloride [1.8mM], heparin [10U•mL^{-1}], albumin [0.1%], and sodium bicarbonate [0.8M] should be mixed within V_A. However, the amount of these should be based on the final volume expected (V_f), not V_A.

A.2 MATLAB PROGRAM FOR QUANTIFICATION OF LV MECHANO-ENERGETIC FUNCTION

The data collection system for the isolated rabbit heart study used a file format that could only be read by the National Instrument Lab View program "Analyze Frank-Starling Experiment w/Trelax.VI" (this program has existed in the Cardiovascular Systems Laboratory for many years). Using this program, *read* the data then *write* the data making sure to export the raw data. The resulting text file can then opened and saved in an Excel format. From this file, time, pressures and volumes were saved and two more columns were added for manually entering AVO_2 and Q_{cor} collected at each volume step during the experiment. The file must be in this format for the following Matlab code to read the raw data. The program fitted ESPVR, EDPVR,

and MVO_2-PVA relationship (see equations in **Section 2.6**) and derived parameters for these relationships. The parameters and raw data were output into a text file for data compilation. In addition, a graphical output was also saved (**Figure A-1**); this output was helpful in determining the reliability of the data. The program as written in Matlab is as follows:

```
clear
CD = cd;

%Loads File
[datafile,directory] = uigetfile('*.xls','Choose Data File');
cd(directory)
[data,txt] = xlsread(datafile);
cd(CD);

%Input dialog: (1) volume steps to identify columns (2) pacing interval to calculate HR (3) balloon volume
prompstr = {'Enter number of volume steps'};
   titlestr = 'Volume Steps';
   initstr = {'4'};
   numstp = inputdlg(prompstr,titlestr,1,initstr);
   numstp=numstp{1};
   ns=str2double(numstp);
   int=460; %HR interval ms
   bal_vol=1.4; %
HR=(60/int)*1000;

%Assign variables
t=data(:,1);
for j=1:ns
   P(:,j)=data(:,j+1);
   V(:,j)=data(:,j+ns+1);
end
V=V+bal_vol;
AVO2temp=data(:,1+ns+ns+1);

%Finds text to eliminate header
i = find(~isnan(AVO2temp));
AVO2=AVO2temp(i);
Qcor=data(i,1+ns+ns+2);

%Find EDP and ESP
for k=1:ns
   Ped(1,k)=min(P(:,k));
   Pes(1,k)=max(P(:,k));
   Vst(1,k)=V(1,k);
end

%Fit raw data for ESPVR and EDPVR
%ESPVR --> Pes=Ees(Ves-Vd) %NO CONSTRAINTS
[y,S]=polyfit(Vst,Pes,1);
Pes_fit = y(1)*Vst + y(2);
```

```
%EDPVR --> Ped=alpha*(exp(beta(Ved-Vo))-1) %NO CONSTRAINTS
Xo = [0.1 0.1 0.1];
[x,RESNORM,RESIDUAL] = lsqcurvefit(@EDPVR,Xo,Vst,Ped);
Ped_fit = x(1)*(exp(x(2)*(Vst-x(3)))-1);

%Coefficients from ESPVR and EDPVR
Ees=y(1);
Vd=-y(2)/y(1);
alpha=x(1);
beta=x(2);
Vo=x(3);

%PVA Calculations
for i=1:ns
   vol(i,:)=linspace(Vd,Vst(i));
   ESP(i,:)=y(1)*vol(i,:)+y(2);
   EDP(i,:)=  x(1)*(exp(x(2)*(vol(i,:)-x(3)))-1);
   space=vol(i,2)-vol(i,1);
   pva(i,:) = trapz(ESP(i,:)-EDP(i,:));
   PVA(i,:)=pva(i,:)*space;
end
PVA_beat = PVA; % already [mL*mmHg/beat] so do NOT normalize to HR
MVO2_beat = (Qcor.*AVO2)/HR; %[mL O2 per beat] normalize to HR
r = polyfit(PVA_beat,MVO2_beat,1);
a=r(1); b=r(2);
fit = a*PVA_beat + b;
name = datafile(1:end-4);

%PLOT RAW DATA*******************
Hf_figure=figure('Name','Isolated Rabbit Heart Mechano-Energetic Analysis','Position',[4 39 1274
710],'Resize','on');
subplot(subplot('Position',[0.1 0.6 0.25 0.3]))
   plot(t,P)
   plttitle=sprintf('%s \n %s','Frank Starling Data',name);
   title(plttitle,'FontSize',16);
   ylabel('Pressure (mmHg)')
   xlabel('Time (s)')
subplot('Position',[0.1 0.1 0.25 0.3])
   plot(t,V)
   ylabel('Volume (mL)')
   xlabel('Time (s)')

%PLOT MECHANICAL DATA********
subplot(subplot('Position',[0.6 0.6 0.25 0.3]))
   plot(vol(ns,:),ESP(ns,:),'b--');
   hold on
   plot(vol(ns,:),EDP(ns,:),'b:');
   plot(V,P)
   title('Mechanics')
   xlabel('Volume (mL)')
   ylabel('Pressure (mmHg)')
   PVR1 = sprintf('%s \n %s %6.2f %s \n %s %6.2f %s','ESPVR','E_e_s =',Ees,'mmHg\bulletmL^-^1','V_d =',Vd,'
mL');
   PVR2 = sprintf('%s \n %s %6.2f %s \n %s %6.2f %s \n %s %6.2f %s','EDPVR','\alpha =',alpha,'mmHg','\beta
=',beta,'mL^-^1','Vo =',Vo,'mL');
   h1=legend(PVR1,PVR2,'Location','NorthWest');
```

```
    set(h1, 'Box', 'off')
    set(h1,'Interpreter','tex','FontSize',8)

%PLOT ENERGETIC DATA*******
subplot('Position',[0.6 0.1 0.25 0.3])
plot(PVA_beat,fit)
hold on
plot(PVA_beat,MVO2_beat,'*')
plttitle=sprintf('%s \n %s %s %s','Energetics','HR =',num2str(HR,'%3.0f'),'bpm');
    title(plttitle);
xlabel('PVA (mmHg\bulletmL\bulletbeat^-^1)')
ylabel('MVO_2 (mL O_2\bulletbeat^-^1)')
ener = sprintf('%s %6.3e %s \n%s %6.3e %s','a=',r(1),'mL O_2\bulletmmHg^-^1\bulletmL^-^1','b=',r(2),'mL
O_2\bulletbeat^-1');
    [h2] = legend(ener,'Location','NorthWest');
    set(h2,'Interpreter','tex','FontSize',8)
    set(h2, 'Box', 'off')
filesave=datafile(1:end-4);
filesave(end+1:end+4)='.fig';
saveas(gcf,filesave);
cd(CD)

%SAVE DATA TO FILE
fid=fopen('MechanoEnergetic Parameters.txt','a');
    fprintf(fid,'%s %06.4f %6.4f %6.4f %6.4f %6.4f %6.4f %6.4f\n',datafile(1:end-4),Ees,Vd,alpha,beta,Vo,a,b);
    fprintf(fid,'%s %s %s %s %s','- - - - -');
    fprintf(fid,'%s\n','');
fclose(fid);
fid1=fopen('Mechano-Energetics.txt','a');
    fprintf(fid1,'%s\n','');
    fprintf(fid1,'%s %s %s %s %s %s %s','---- ---- ---- ---- ---- ---- ----');
    fprintf(fid1,'%s\n','');
    fprintf(fid1,'%s',datafile(1:end-4));
    fprintf(fid1,'%s\n','');
    fprintf(fid1,'%s %s %s %s %s %s %s %s %s %s %s %s %s %s %s %s
%s','Vst','EDP','ESP','MVO2','PVA','AVO2','Qcor');
    fprintf(fid1,'%s\n','');
    fprintf(fid1,'%09.3f %9.3f %9.3f %9.3f %9.3f %9.3f %9.3f
%9.3f\n',[Vst;Ped;Pes;MVO2_beat';PVA_beat';AVO2';Qcor']);
fclose(fid1);
```

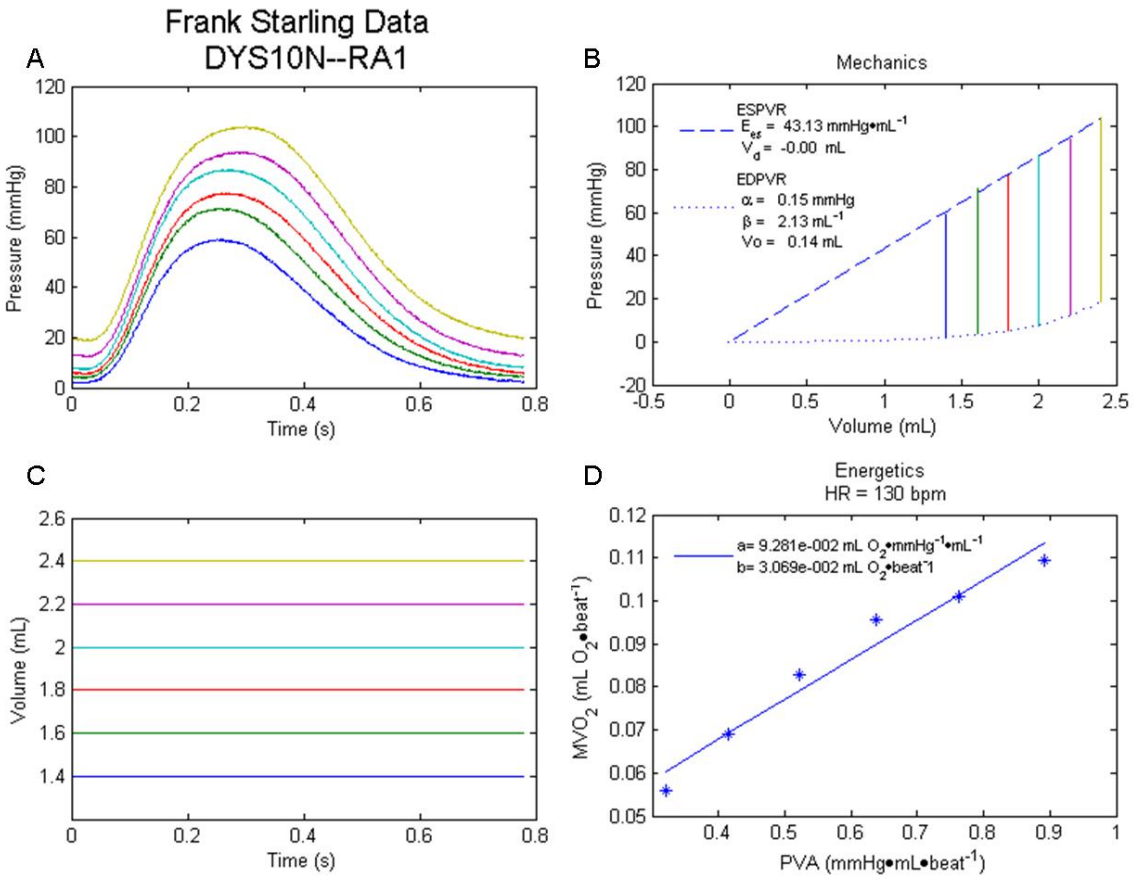

Figure A-1. Graphical output of Matlab program for mechano-energetic function.

(A) LV pressure waveforms collected at incremental end-diastolic volumes. **(B)** P-V relationships and isovolumic pressure trajectories for each volume step. **(C)** End-diastolic volumes for each isovolumic contraction. **(D)** MVO_2-PVA data points and derived relationship.

A.3 MIXED MODEL STATISTICS PROGRAM CODE

As stated in **Section 3.2.1.6**, relationships between RA and RVOT pacing were compared using a mixed model approach to account for both fixed and random effects. The "MIXED" process was used in the statistical software package, SAS (SAS Institute Inc., Cary, NC). The model solved for simultaneous changes in the slope and intercept of linear relationships for both ESPVR and

MVO_2-PVA relationship. Statistical analysis of ESPVR required two separate analyses. The program first solved for Y = mx + b. However, the intercept, b, is actually the Y-intercept. A separate program was executed to solve for the statistical properties of the X-axis intercept of ESPVR (i.e., V_d). This program simply set ESP as the independent variable and EDV as the dependent variable, thus solving for X = 1/m*Y – b/m. The mean slope values obtained from this program was validated against the intercept/slope obtained from the original program. The SAS code is as follows:

Reads in data and assigns variables:

```
libname file1 'C:\Documents and Settings\Lauren\My Documents\RABBIT';
PROC FORMAT;
VALUE PACINGF 1='RA' 2='RV';
data one;
        set file1.mvo2_pva_raw_new;
 IF PACING='RA' THEN PACINGN=1;
  ELSE IF PACING='RV' THEN PACINGN=2;
 label
  esp="ESP"
  mvo2="MVO2"
  pacing="PACING"
  pva="PVA"
  vst="EDV";
 FORMAT PACINGN PACINGF.;
 options NODATE NONUMBER;
 run;
```

Calculates mean values for Vst, ESP, PVA, and MVO2:

```
 PROC MEANS DATA=one MEAN;
 CLASS VST PACINGN;
 VAR ESP;
 VAR PVA;
 VAR MVO2;
 PROC FREQ;
 TABLES RABBIT PACINGN;
 RUN;
```

Random Effects Modeling for ESPVR (note: only use results for slope here):

```
**ESP AND VST**;
PROC MIXED DATA=ONE;
CLASS RABBIT PACINGN;
MODEL ESP=PACINGN VST PACINGN*VST/DDFM=SATTERTH SOLUTION;
RANDOM INT VST/SUBJECT=RABBIT TYPE=UN; *RANDOM COEFFICIENT MODEL;
ESTIMATE 'RA,VST SLOPE' VST 1 PACINGN*VST 1 0;
ESTIMATE 'RV,VST SLOPE' VST 1 PACINGN*VST 0 1;
ESTIMATE 'RA SLOPE - RV SLOPE' PACINGN*VST 1 -1;
ESTIMATE 'RA,INT' INT 1 PACINGN 1 0;
```

```
ESTIMATE 'RV,INT' INT 1 PACINGN 0 1;
ESTIMATE 'RA INT - RV INT' PACINGN 1 -1;
options NODATE NONUMBER formdlim='-';
title;
RUN;
```

Random Effects Modeling for MVO_2-PVA relationship:

```
**MVO2 AND PVA**;
PROC MIXED DATA=ONE;
CLASS RABBIT PACINGN;
MODEL MVO2=PACINGN PVA PACINGN*PVA/DDFM=SATTERTH SOLUTION;
RANDOM INT PVA/SUBJECT=RABBIT TYPE=UN;*RANDOM COEFFICIENTS MODEL;
ESTIMATE 'RA,PVA SLOPE' PVA 1 PACINGN*PVA 1 0;
ESTIMATE 'RV,PVA SLOPE' PVA 1 PACINGN*PVA 0 1;
ESTIMATE 'RA SLOPE - RV SLOPE' PACINGN*PVA 1 -1;
ESTIMATE 'RA,INT' INT 1 PACINGN 1 0;
ESTIMATE 'RV,INT' INT 1 PACINGN 0 1;
ESTIMATE 'RA INT - RV INT' PACINGN 1 -1;
options NODATE NONUMBER formdlim='-';
title;
RUN;
```

Random Effects Modeling for ESPVR to obtain statistical values for intercept (V_d):

```
*NOTE: VST IS NOW DEPENDENT VARIABLE AND ESP IS INDEPENDENT
libname file1 'C:\Documents and Settings\Lauren\My Documents\RABBIT';
PROC FORMAT;
VALUE PACINGF 1='RA' 2='RV';
data one;
            set file1.espvrvd;
  IF PACING='RA' THEN PACINGN=1;
   ELSE IF PACING='RV' THEN PACINGN=2;
    label
   esp="VOLUME STEP (NOW DEPENDENT)"
   pacing="CONDITION"
   vst="ESP/SLOPE (NOW INDEPENDENT)";
  FORMAT PACINGN PACINGF.;
  options NODATE NONUMBER;
  run;
****RANDOM EFFECTS MODELING****;**ESP AND VST**;
PROC MIXED DATA=ONE;
CLASS RABBIT PACINGN;
MODEL ESP=PACINGN VST PACINGN*VST/DDFM=SATTERTH SOLUTION;
RANDOM INT VST/SUBJECT=RABBIT TYPE=UN;
ESTIMATE 'RA,VST SLOPE' VST 1 PACINGN*VST 1 0;
ESTIMATE 'RV,VST SLOPE' VST 1 PACINGN*VST 0 1;
ESTIMATE 'RA SLOPE - RV SLOPE' PACINGN*VST 1 -1;
ESTIMATE 'RA,INT' INT 1 PACINGN 1 0;
ESTIMATE 'RV,INT' INT 1 PACINGN 0 1;
ESTIMATE 'RA INT - RV INT' PACINGN 1 -1;
options NODATE NONUMBER formdlim='-';
title;
RUN;
```

The output of the code is as follows:

The Mixed Procedure

Model Information

Data Set	WORK.ONE
Dependent Variable	ESP
Covariance Structure	Unstructured
Subject Effect	Rabbit
Estimation Method	REML
Residual Variance Method	Profile
Fixed Effects SE Method	Model-Based
Degrees of Freedom Method	Satterthwaite

Solution for Fixed Effects

Label	Estimate	StdError	DF	t Value	Pr > |t|
RA,VST SLOPE	56.0602	5.0657	11	11.07	<.0001
RV,VST SLOPE	58.5351	5.0465	10.8	11.60	<.0001
RA SLOPE - RV SLOPE	-2.4750	1.9063	93.5	-1.30	0.1974
RA,INT	-33.5617	8.9559	11.3	-3.75	0.0031
RV,INT	-42.1248	8.8925	11	-4.74	0.0006
RA INT - RV INT	8.5631	3.6968	93.6	2.32	0.0227

The Mixed Procedure

Model Information

Data Set	WORK.ONE
Dependent Variable	MVO2
Covariance Structure	Unstructured
Subject Effect	Rabbit
Estimation Method	REML
Residual Variance Method	Profile
Fixed Effects SE Method	Model-Based
Degrees of Freedom Method	Satterthwaite

Solution for Fixed Effects

Label	Estimate	StdError	DF	t Value	Pr > |t|
RA,PVA SLOPE	0.1492	0.01689	9.2	8.83	<.0001
RV,PVA SLOPE	0.1682	0.01695	9.4	9.92	<.0001
RA SLOPE - RV SLOPE	-0.01900	0.009777	94.8	-1.94	0.0549
RA,INT	0.02536	0.003459	11.2	7.33	<.0001
RV,INT	0.02864	0.003411	10.6	8.40	<.0001
RA INT - RV INT	-0.00328	0.001446	94.8	-2.27	0.0256

The Mixed Procedure

Model Information

Data Set	WORK.ONE
Dependent Variable	EDV
Covariance Structure	Unstructured
Subject Effect	Rabbit
Estimation Method	REML
Residual Variance Method	Profile
Fixed Effects SE Method	Model-Based
Degrees of Freedom Method	Satterthwaite

Solution for Fixed Effects

Label	Estimate	StdError	DF	t Value	Pr > |t|
RA,VST SLOPE	0.01833	0.001500	10.7	12.22	<.0001
RV,VST SLOPE	0.01800	0.001493	10.5	12.06	<.0001
RA SLOPE - RV SLOPE	0.000335	0.000454	93.2	0.74	0.4622
RA,INT	0.5846	0.1024	10.9	5.71	0.0001
RV,INT	0.6659	0.1013	10.5	6.57	<.0001
RA INT - RV INT	-0.08128	0.03398	93.3	-2.39	0.0188

A.4 MECHANO-ENERGETIC FUNCTION DURING BIVENTRICULAR PACING

In addition to assessing mechano-energetic function between RA and RVOT pacing, we also measured mechanical and energetic function during simultaneous RA, RVOT, and LV pacing at either the apex (BiVa) or free-wall (BiVf). These pacing modalities were investigated to assess the effects of counter-pacing (or resynchronization) RVOT pacing on mechano-energetic function. The ESPVR and MVO_2-PVA relationships under BiVa and BiVf pacing are superimposed on the data obtained for RA and RVOT pacing in **Figure A-2**. Although a statistical analysis was not performed for the BiVa and BiVf dataset, it appears that the ESPVR under BiVa pacing is similar to that of RVOT pacing. However, the MVO_2-PVA relationship under BiVa pacing is elevated compared to RVOT pacing, indicating lower mechano-energetic efficiency. In contrast, as the ESPVR for BiVf pacing seems slightly lower than that for RVOT pacing, the MVO_2-PVA relationship appears similar to that of RVOT pacing. However, we were not convinced of the stability of the data collected at the time of these pacing modalities. These data were collected approximately 1.5-2 hours after the preparation began. This was mainly due to repetition of RA pacing between each ventricular pacing modality. Future studies without repeated RA pacing conditions may allow one to collect data under all 4 conditions before deterioration of the preparation. We therefore focused on reporting mechano-energetic function during RA and RVOT pacing conditions only, which were collected <1 hour of the initiation of the experiment.

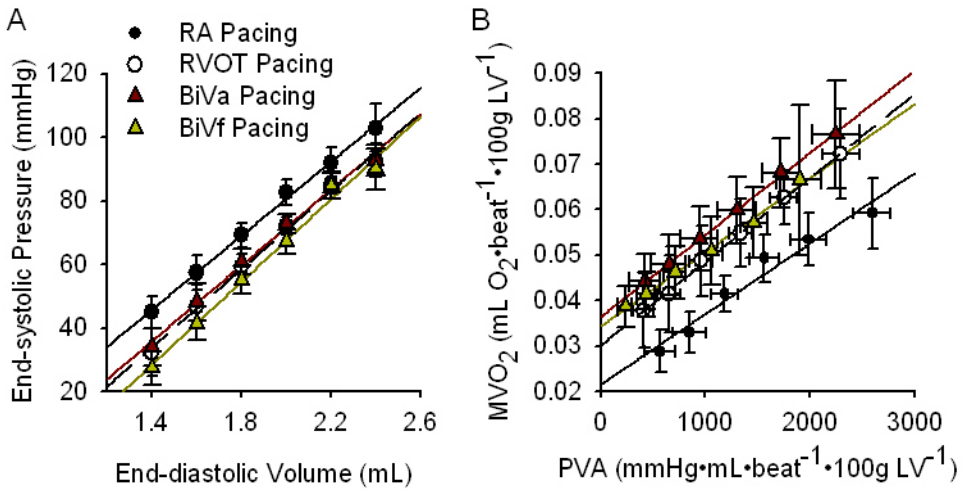

Figure A-2. Mechano-energetic function for several pacing modalities.

(A) Compared to RA pacing, the ESPVR was depressed with RVOT, BiVa, and BiVf pacing. **(B)** Despite the depression in mechanics, all ventricular pacing modes adversely affected global LV energetics manifested as an increase in the MVO_2-PVA intercept with BiVa pacing having the most elevated MVO_2-PVA relationship. Data: *n*=8 for RA and RVOT pacing, n=7 for BiVa pacing, n=6 for BiVf pacing.

APPENDIX B

MATLAB PROGRAMS FOR CROSS-CORRELATION ANALYSES

B.1 CROSS-CORRELATION ANALYSIS FOR TISSUE DOPPLER-DERIVED RADIAL STRAIN AT THE MID-LEFT VENTRICLE

For **Study 2** (**Section 4.0**), we used tissue-Doppler derived radial strain waveforms to quantify dyssynchrony using cross-correlation analysis. Six circumferentially arrayed segments at the mid-LV were assessed by deriving time-strain waveforms describing radial strain (thickening/thinning) at each of these segments. The cross-correlation analysis including derivation of cross-correlation spectrum is performed by using the Matlab statistics toolbox function *regress*. This function performs multiple linear regression where a response (strain for one segment in a pair) is modeled as a linear combination of functions (not necessarily linear) of a predictor (strain of second segment in the pair). From this function, several outputs relevant to statistical analysis of the regression can be derived. Specifically, the direction of the effects (signs of β term) and R^2 term was calculated to obtain the cross-correlation coefficient which indicated how well the two signals "lined up". In order to calculate a spectrum of cross-correlation coefficients, one segment in a pair was held constant, while the other segment was

shifted in time, and for each time shift, a cross-correlation coefficient was calculated. To accomplish this, a *for* loop is used in the code. An example of derivation of the cross-correlation spectra for 5 sine waves with varying amplitude and phase shifts is illustrated in **Figure B-1**. Correlation of the first two waveforms (which are both equally sin(x)) results in perfect synchrony at zero time shift (i.e., cross-correlation coefficient of 1.0 at zero time shift. The cross-correlation coefficient then decreases as the second waveform is shifted with respect to the first giving the lowest correlation of -1.0 when they are completely out of phase with each other at a shift of $\pm\pi$ units (**Figure B-1B**). Note that although the third waveform is twice the amplitude of the first sine wave, the same spectrum just described (i.e., comparing the first two sine waves) is obtain when correlating the first and third waveforms because cross-correlation analysis cannot distinguish between differing amplitudes. In contrast, since the fourth waveform is already out of phase from the first waveform by π units, then it is not surprising that the cross-correlation spectrum reveals the lowest correlation (-1.0) at zero time shift and highest correlation (+1.0) at $\pm\pi$ units. Similarly, the fifth waveform is out of phase with the first by $\pi/2$ units, therefore the lowest correlation is at $+ \pi/2$ and the highest correlation is at $- \pi/2$. As shown in **Figure B-1C**, the same spectra as in **Figure B-1B** are obtained when the second waveform is correlated with the rest since they are both sin(x). Similarly, the spectra are repeated in **Figure B-1D** since the waveforms 2•sin(x) and sin(x) do not result in different cross-correlation spectra when combined with other waveforms because amplitude does not affect derivation of cross-correlation coefficients. Finally, when combining the last two segments, it is now clear that since they are shifted by $\pi/2$, this is where the maximum correlation occurs (**Figure B-1E**).

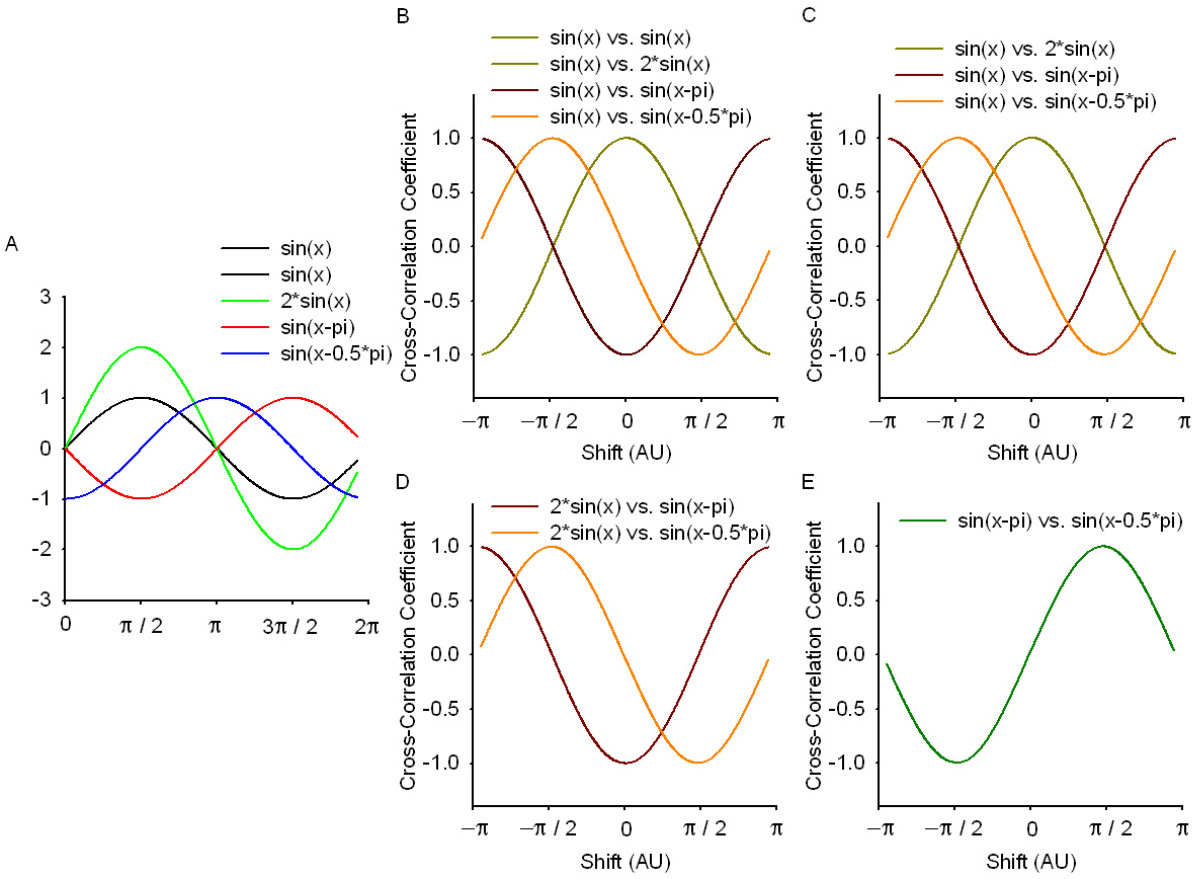

Figure B-1. Example of cross-correlation spectrum derivation.

(A) Five sine waves with varying amplitude and phase shifts. Note that the first two waveforms are the same. **(B)** Cross-correlation spectra obtained for correlations of the first waveform [i.e., sin(x)] and the other 4. **(C)** Cross-correlation spectra obtained for correlations of the second waveform [i.e., sin(x)] and the other 3. **(D)** Cross-correlation spectra obtained for correlations of the third waveform [i.e., 2*sin(x)] and the other 2. **(E)** Cross-correlation spectra obtained for correlations of the fourth waveform [i.e., sin(x-pi)] and the fourth.

The Matlab code allows one to load a dataset containing a column of time and 6 columns of strain. The data is interpolated to yield 10 ms sampling interval for easier calculation of the cross-correlation spectrum. Outputs from this analysis are saved into a text file for offline data compilation. In addition, a graphical output is also saved as shown in **Figure B-2**. The actual code is protected under copyright by the University of Pittsburgh and therefore is not displayed in the current thesis.

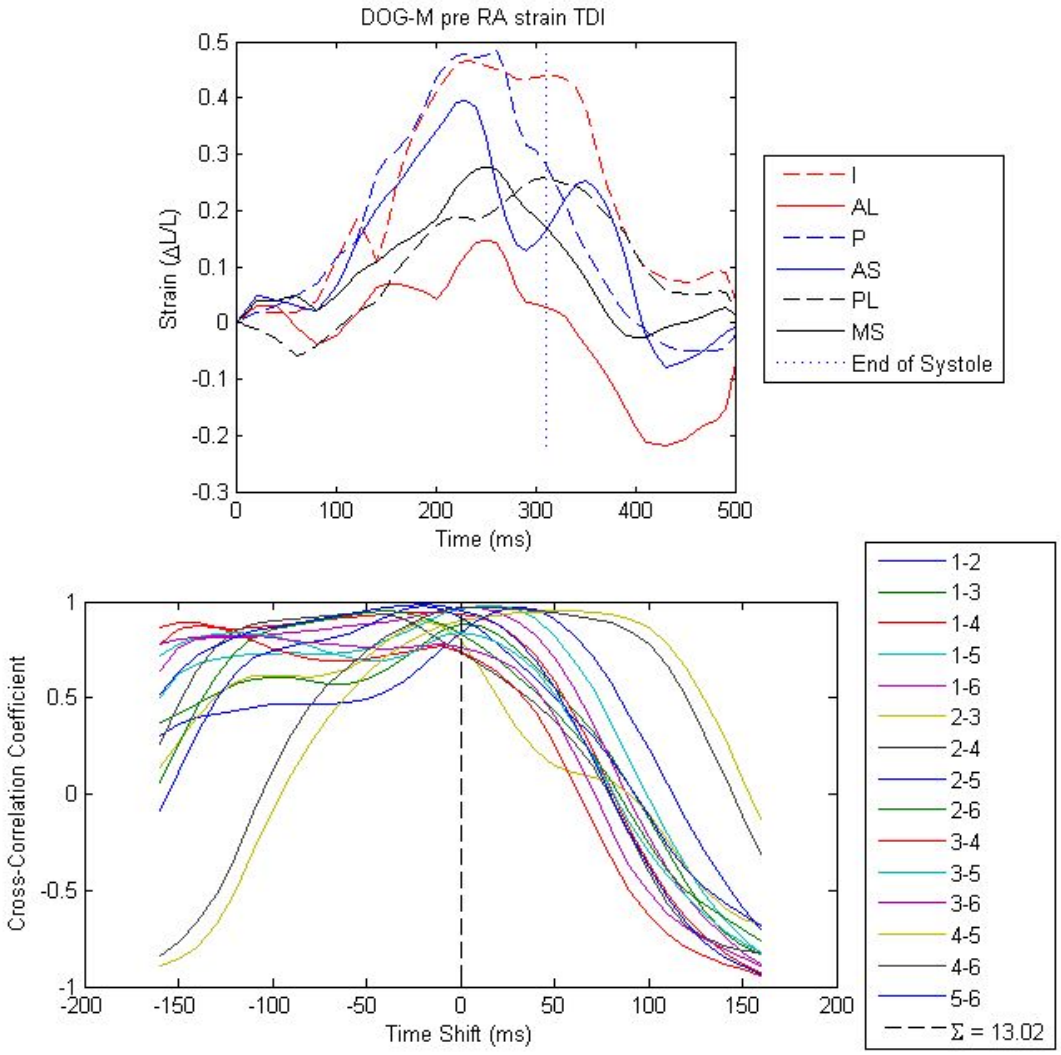

Figure B-2. Graphical output for TD-strain and corresponding cross-correlation analysis.

The top plot shows TD derived radial strain from the mid-LV. End of systole is also marked on the plot to emphasize that cross-correlation analysis was only performed during systole. The bottom plot contains cross-correlations spectra derived for the 15 pair-wise correlations.

B.2 CROSS-CORRELATION ANALYSIS FOR SPECKLE-DERIVED STRAIN AT MULIPLE LV CROSS-SECTIONS

The previous analysis was extended for a multi-dimensional approach to quantify dyssynchrony in **Study 3** (**Section 5.0**). Here, radial strain was derived using speckle tracking algorithm on standard gray scale 2D echocardiographic images at three short-axis LV levels (i.e., LV base, mid-LV, and LV apex). In addition, the speckle tracking software derived circumferential strain of each of the segments in addition to deriving radial strain. Therefore, the cross-correlation analyses for radial strain were repeated for circumferential strain. In addition to applying cross-correlation analysis within each short-axis level, we also assessed "longitudinal" disparities by correlating segments I, L, A, and S across LV levels. However, we did not report indices derived from this analysis since it did not actually represent longitudinal dyssynchrony because the strain was radially derived. Furthermore, we were also able to assess torsion since the speckle tracking software derived rotation of segments at the LV base and LV apex. However, we did not report circumferential or torsion indices in our results. Essential to this study, we developed a new method to quantify segmental contributions to the integrated measure of synchrony (**Section 5.2.4.2**). With this information, Bull's Eye plots were constructed which color-coded synchrony indices in order to easily interpret the results.

The developed Matlab code contains several imbedded files for an extensive software suite to quantify dyssynchrony using cross-correlation analysis. The code is self-automated such that the user loads 3 files containing time, radial and circumferential strain, and rotation at the LV base, mid-LV, and LV apex and the program performs the analysis automatically. In addition, several more files were written to save graphical outputs and data derived from this analysis. The code to perform the cross-correlation analysis is now protected under copyright

("Cross-Correlation Analysis: A Novel Bedside Tool to Quantify Left Ventricular Contraction Dyssynchrony" ©2008 University of Pittsburgh) and therefore will not be shown in the current thesis. Graphical outputs are as follows:

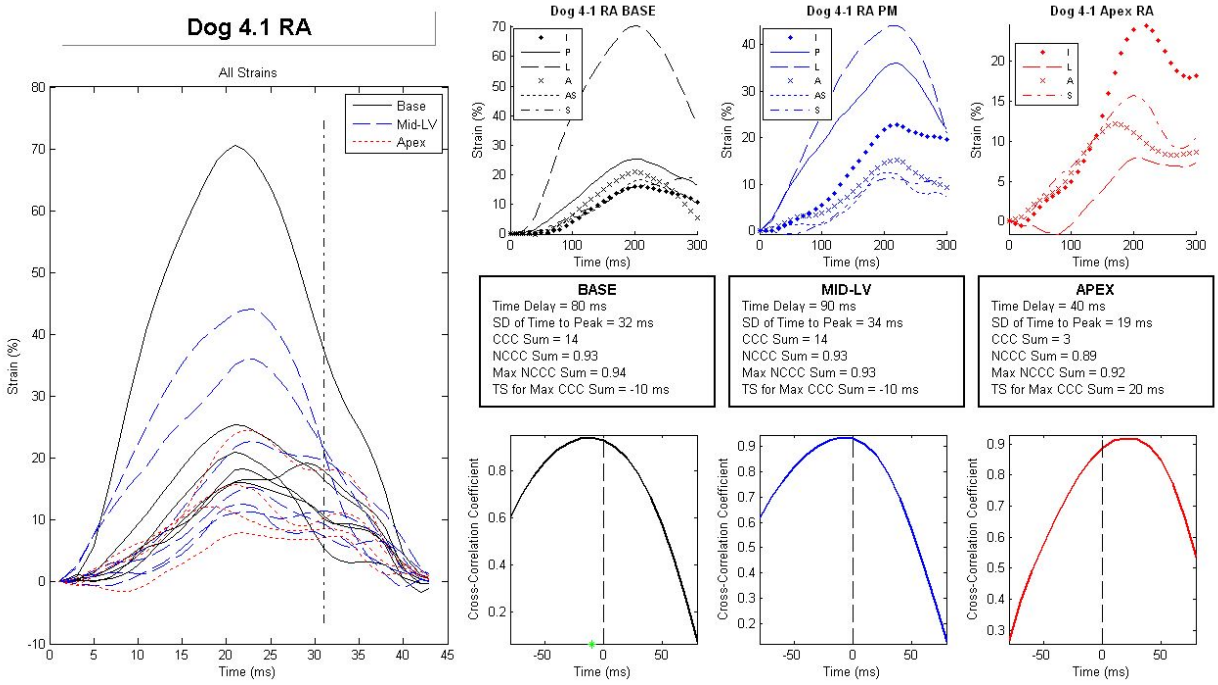

Figure B-3. User interface for multi-dimensional cross-correlation analysis.

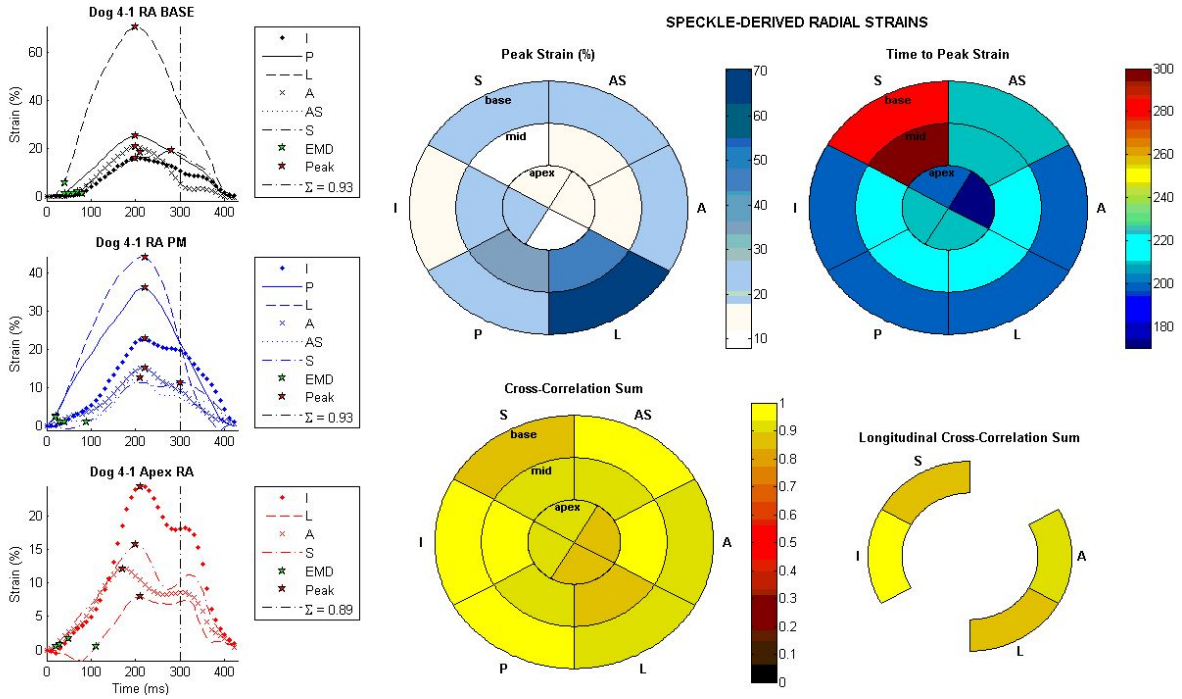

Figure B-4. Radial strain Bull's Eye plots from cross-correlation analysis.

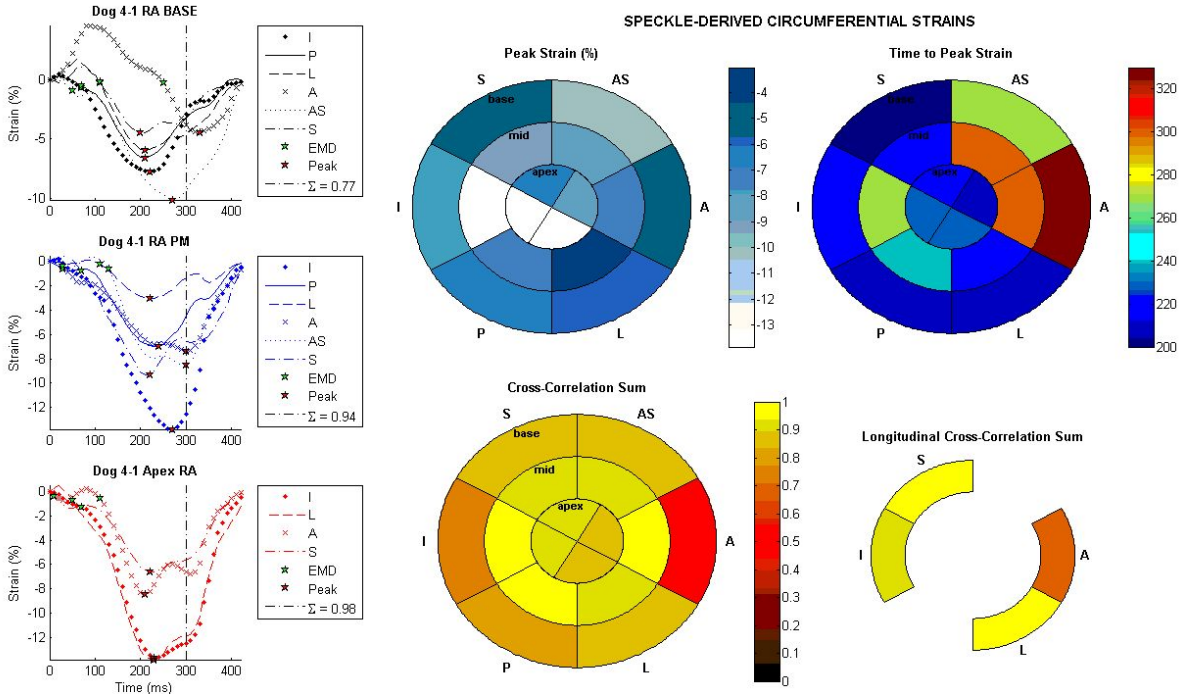

Figure B-5. Circumferential strain Bull's Eye plots from cross-correlation analysis.

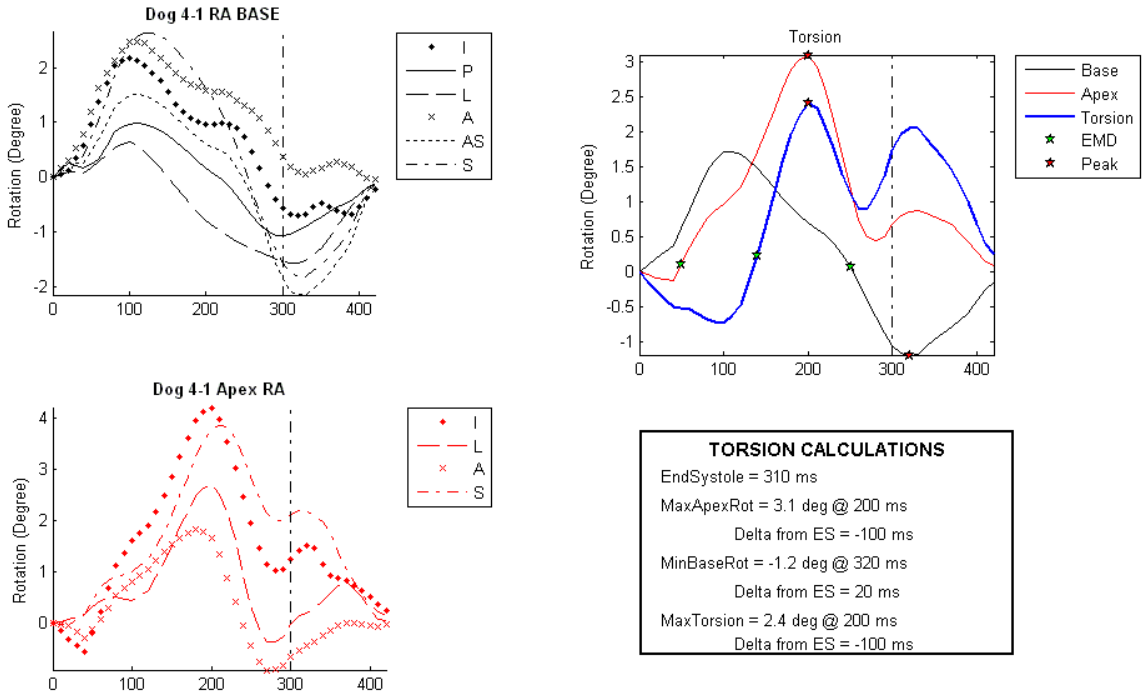

Figure B-6. Basal and apical rotation and corresponding torsion plots.

B.3 CROSS-CORRELATION ANALYSIS IN THE HUMAN REALM: RADIAL AND LONGIDUDINAL SYNCHRONY ANALYSES

The cross-correlation analysis suite from **Study 3** (see **Appendix B.2**) was slightly modified to handle the strain data obtained in the human study. Specifically, the "Loading" file needed to be adjusted since the raw data files were extracted using different speckle tracking software providers. In addition, the human data contained 6 apical segments. However, the radial strain at the base and apex were not reliable due to image quality. Therefore, only results derived from radial strain were reported.

The cross-correlation analysis was extended to handle longitudinal displacement data. As described above (see **Section 7.2.4**), the septal and LV lateral walls were each segmented into 5 regions which were tracked by the software and time-displacement curves were derived. Each patient had a file with time and displacement data for the septum and another file for the LV lateral wall. For each wall, an integrated cross-correlation synchrony index was derived in addition to segmental indices for each of the 5 regions. An example of the graphical output from this code is shown in **Figure 7-4**. Again, the code is not displayed because of copyright issues.

APPENDIX C

MATLAB PROGRAM FOR PRESSURE-VOLUME LOOP ANALYSIS

Indices of global LV performance were derived using P-V analysis from a conductance catheter placed into the LV. Electrical conductance of blood in the LV was converted into volume using the following equation:

$$V_{LV} = \frac{1}{\alpha}(\rho \times L^2 - V_c) \quad \textbf{(C-1)}$$

where α is a dimensionless constant, ρ is blood resistivity, L is electrode spacing, and V_c is an offset, or corrective volume, that represents parallel conductance (i.e., conductance of myocardial tissue and/or surrounding electrical conductance) [55]. Unfortunately, when LV volumes were collected, proper calibration factors (i.e., α, ρ, L, and V_c) were not applied to the calculation of total LV volume. Therefore, volumes had to be calibrated during post-processing of the data. A custom-written Matlab code was used to calibrate and select the desired segmental volumes to be included in the analysis (see below). First, conductance (G) for each segment was back-calculated using the preset calibration values of α = 1.0, V_c = 0 mL, ρ = 146.91 Ω•cm, and L = 0.6 cm and the equation:

$$G_i = \frac{V}{\rho \times L^2} \quad \textbf{(C-2)}$$

where i is for each segment along the conductance catheter. Then blood resistivity, ρ, was calculated from hematocrit data using an equation derived by Geddes and Sadler [115] given by:

$$\rho = 0.537e^{0.025\times\text{Hematocrit}} \quad \textbf{(C-3)}$$

where hematocrit is in %. Next, α and V_c were derived from echocardiographic measures of LV volumes. Under baseline conditions (i.e. RA pacing), α was calculated by the stroke volume derived from the conductance catheter divided by echocardiographic-derived stroke volume. Under the same conditions, V_c was calculated as the end-diastolic volume derived from the conductance catheter minus the product of α and echocardiographic-derived end-diastolic volume. Since echocardiographic volume data was not available for other pacing modalities, we assumed that the calibration factors α and V_c derived under baseline were the same throughout the pacing protocols. After α, ρ, and V_c were derived for each patient, LV volume was calculated using **Equation C-1** above for the other pacing modalities. Conductance (or volume) was measured for 7 segments, however, we assumed that segments 2, 3, and 4 were most likely the segments that were consistently within the LV cavity (i.e., away from apical tissue and the mitral valve). Therefore, total LV volume was calculated by the sum of only segments 2-4.This program code was written because it was unclear which volume segments to include into the calculation of total LV volume. In addition, the volumes (or conductance) needed to be scaled since appropriate calibration coefficients were not applied during data collection (see **Section 7.2.5**).

The program written to calibrate and analyze P-V data consists of several files and callbacks. The first file loads the user interface so that patient data may be loaded (**Figure C-1**). Once the data is loaded, a graphical user interface asks the user to select the range of data to be analyzed; this was incorporated because some datasets contained several minutes of data. Once

loaded, several check boxes are displayed for the user to select which segments to be included (**Figure C-1**). Each time a box is checked, total LV volume is calculated and a P-V loop is displayed. This was necessary because the loops become distorted if the segmental volume is not accurate (e.g., outside of the ventricle). Once the user is satisfied with the morphology of the P-V loop, the "finished" button is pressed and indices of global LV performance are calculated for each of the cardiac cycles contained in the dataset; the indices are averaged and displayed on the plot (**Figure C-1**).

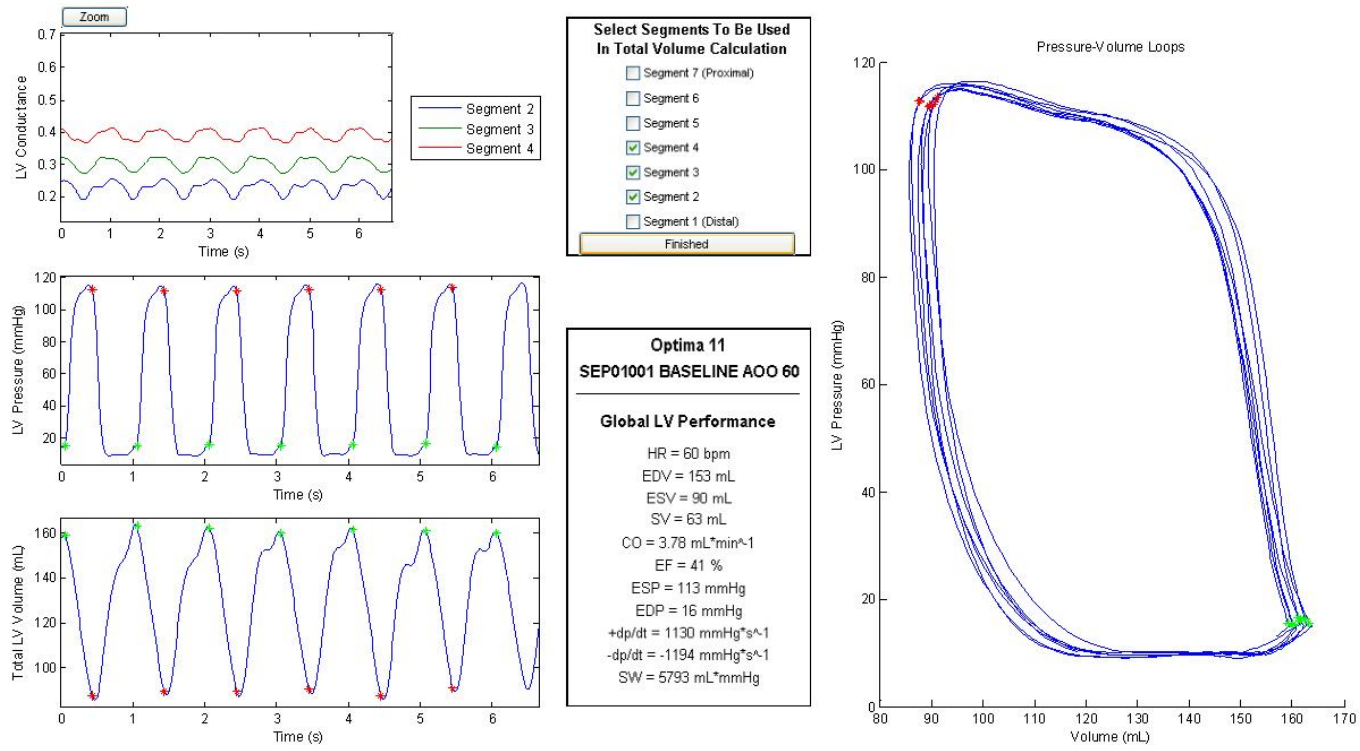

Figure C-1. User interface and graphical output for P-V loop analysis.

The Matlab code for P-V loop analysis is as follows:

User Interface:

```
close all; clear all; clc;

Hf_figure=figure('Name','P-V Analysis','Position',[4 39 1274 710],'Resize','off');
set(Hf_figure,'Menubar','none')
   Hm_File = uimenu(Hf_figure,'Label','File','Position',1);
      Hm_PatientNew = uimenu(Hm_File,'Label','Open New Patient','Callback','Another=0;Loading;');
```

```
    Hm_Another = uimenu(Hm_File,'Label','Open Another File','Enable','on','Callback',...

'Another=1;set(cbh1,"value",0);set(cbh2,"value",0);set(cbh3,"value",0);set(cbh4,"value",0);set(cbh5,"value",0);set(cb
h6,"value",0);set(cbh7,"value",0);Loading');
    Hm_FilePrint = uimenu(Hm_File,'Label','Print Figure','Enable','on','Callback','orient landscape;printdlg');
    Hm_FilePrintReport = uimenu(Hm_File,'Label','Print Report','Enable','on','Callback','PrintReport');
  Hm_window = uimenu(Hf_figure,'Label','Window','Position',2,'Enable','on');
    Hm_PV = uimenu(Hm_window,'Label','PV Loops','Enable','off');
    Hm_CCA = uimenu(Hm_window,'Label','Cross-Correlation Analysis','Enable','on','Callback','Plot_CCA;');
  Hm_save = uimenu(Hf_figure,'Label','Save Analysis','Enable','on');
    Hm_saveGP = uimenu(Hm_save,'Label','Save Global and CC Analysis','Callback','SaveData');
    Hm_saveCCA = uimenu(Hm_save,'Label','Save Cross-Correlation Analysis','Enable','off');
    Hm_saveAll = uimenu(Hm_save,'Label','Save All
Analyses','Enable','off','Callback','SaveData;Plot_CCA;SaveCCA');
%------------------------------------------------------------
hp = uipanel('BorderType','line','BorderWidth',2,'HighlightColor','black','BackgroundColor','White','Position',[0.42
0.06 0.18 0.5]);
hc_title=uicontrol(hp,'style','text','FontSize',11,'string','Global LV
Performance','Units','normalized','FontWeight','bold','Position',[0.0328 0.74 0.93 0.05],'BackgroundColor','White');
hc_und1=uicontrol(hp,'style','text','FontSize',11,'string','_____','Units','norma
lized','FontWeight','bold','Position',[0.0328 0.83 0.93 0.0487],'BackgroundColor','White');
hc_patientname=uicontrol(hp,'style','text','FontSize',11,'string','Patient
Name','Units','normalized','FontWeight','bold','Position',[0.0285 0.94 0.96 0.05],'BackgroundColor','White');
hc_filename=uicontrol(hp,'style','text','FontSize',11,'string','Pacing
Mode','Units','normalized','FontWeight','bold','Position',[0.0285 0.8709 0.96 0.05],'BackgroundColor','White');

  hc_hr= uicontrol(hp,'style','text','FontSize',10,'string','HR =      bpm','Units','normalized','Position',[0.05 0.64 0.9
0.06],'BackgroundColor','White');
  hc_edv= uicontrol(hp,'style','text','FontSize',10,'string','EDV =      mL','Units','normalized','Position',[0.05 0.58 0.9
0.06],'BackgroundColor','White');
  hc_esv= uicontrol(hp,'style','text','FontSize',10,'string','ESV =     mL','Units','normalized','Position',[0.05 0.52 0.9
0.06],'BackgroundColor','White');
  hc_sv= uicontrol(hp,'style','text','FontSize',10,'string','SV =     mL','Units','normalized','Position',[0.05 0.46 0.9
0.06],'BackgroundColor','White');
  hc_co= uicontrol(hp,'style','text','FontSize',10,'string','CO =     mL*min^-1','Units','normalized','Position',[0.05 0.4
0.9 0.06],'BackgroundColor','White');
  hc_ef= uicontrol(hp,'style','text','FontSize',10,'string','EF =     %','Units','normalized','Position',[0.05 0.34 0.9
0.06],'BackgroundColor','White');
  hc_esp= uicontrol(hp,'style','text','FontSize',10,'string','ESP =     mmHg','Units','normalized','Position',[0.05 0.28
0.9 0.06],'BackgroundColor','White');
  hc_edp= uicontrol(hp,'style','text','FontSize',10,'string','EDP =     mmHg','Units','normalized','Position',[0.05 0.22
0.9 0.06],'BackgroundColor','White');
  hc_pdpdt= uicontrol(hp,'style','text','FontSize',10,'string','+dp/dt =     mmHg*s^-
1','Units','normalized','Position',[0.05 0.16 0.9 0.06],'BackgroundColor','White');
  hc_ndpdt= uicontrol(hp,'style','text','FontSize',10,'string','-dp/dt =     mmHg*s^-
1','Units','normalized','Position',[0.05 0.10 0.9 0.06],'BackgroundColor','White');
  hc_sw= uicontrol(hp,'style','text','FontSize',10,'string','SW =     mL*mmHg','Units','normalized','Position',[0.05
0.04 0.9 0.06],'BackgroundColor','White');

  hp2 = uipanel('BorderType','line','BorderWidth',2,'HighlightColor','black','BackgroundColor','White',
'Position',[0.42 0.655 0.18 0.3154]);
  hp1_title=uicontrol(hp2,'style','text','FontSize',10,'string','Select Segments To Be
Used','Units','normalized','BackgroundColor','White','FontWeight','bold','Position',[0.05 0.92 0.93 0.08]);
  hp2_title=uicontrol(hp2,'style','text','FontSize',10,'string','In Total Volume
Calculation','Units','normalized','BackgroundColor','White','FontWeight','bold','Position',[0.05 0.84 0.93 0.08]);
```

```
    cbh1 = uicontrol(hp2,'Style','checkbox','Tag','save option','String','Segment 1
(Distal)','Units','Normalized','BackgroundColor','White','Position',[0.2397 0.0860 0.7
0.1145],'Value',0,'Callback','Plot_PV_loop');
    cbh2 = uicontrol(hp2,'Style','checkbox','Tag','save option','String','Segment
2','Units','Normalized','BackgroundColor','White','Position',[0.2397 0.191 0.4687
0.1145],'Value',0,'Callback','Plot_PV_loop');
    cbh3 = uicontrol(hp2,'Style','checkbox','Tag','save option','String','Segment
3','Units','Normalized','BackgroundColor','White','Position',[0.2397 0.296 0.4687
0.1145],'Value',0,'Callback','Plot_PV_loop');
    cbh4 = uicontrol(hp2,'Style','checkbox','Tag','save option','String','Segment
4','Units','Normalized','BackgroundColor','White','Position',[0.2397 0.401 0.4687
0.1145],'Value',0,'Callback','Plot_PV_loop');
    cbh5 = uicontrol(hp2,'Style','checkbox','Tag','save option','String','Segment
5','Units','Normalized','BackgroundColor','White','Position',[0.2397 0.506 0.4687
0.1145],'Value',0,'Callback','Plot_PV_loop');
    cbh6 = uicontrol(hp2,'Style','checkbox','Tag','save option','String','Segment
6','Units','Normalized','BackgroundColor','White','Position',[0.2397 0.611 0.4687
0.1145],'Value',0,'Callback','Plot_PV_loop');
    cbh7 = uicontrol(hp2,'Style','checkbox','Tag','save option','String','Segment 7
(Proximal)','Units','Normalized','BackgroundColor','White','Position',[0.2397 0.716 0.7
0.1145],'Value',0,'Callback','Plot_PV_loop');
    h_push_done=uicontrol(hp2,'style','pushbutton','String', 'Finished','Units','normalized','Position',[0.05 0.001
0.8954 0.10],'Callback','Finished=1;Global_Analysis');
    hp3p=uipanel('BorderType','line','HighlightColor','black','BackgroundColor','White','Position',[0.05 0.955 0.05
0.03]);
    hp3 = uicontrol(hp3p,'style','pushbutton','string','Zoom','Units','Normalized','Position',[0 0 1 1],'Callback','Zoom');
    Finished=0;
%-----------------------------------------------------------
subplot('Position',[0.05 0.7 0.35 0.25])
    cla
    ylabel('LV Volume (mL)')

subplot('Position',[0.05 0.38 0.35 0.25])
    cla
    ylabel('LV Pressure (mmHg)')

subplot('Position',[0.05 0.06 0.35 0.25])
    cla
    xlabel('Time (s)')
    ylabel('Total LV Volume (mL)')
subplot('Position',[0.65 0.06 0.34 0.85])
    cla
    xlabel('Volume (mL)')
    ylabel('Pressure (mmHg)')
    title('Pressure-Volume Loops');
```

This file is used to load the file and calibrate conductance signals:

```
if Another==0
    directory='C:\Documents and Settings\Lauren\My Documents\HUMAN DATA\OPTIMA P-V Files\OPTIMA
Code';
    cd(directory);
else
    cd(directory)
```

```
end

%-------------------------------------------------------------
subplot('Position',[0.05 0.7 0.35 0.25])
   cla
   ylabel('LV Volume (mL)')

subplot('Position',[0.05 0.38 0.35 0.25])
   cla
   ylabel('LV Pressure (mmHg)')

subplot('Position',[0.05 0.06 0.35 0.25])
   cla
   xlabel('Time (s)')
   ylabel('Total LV Volume (mL)')
subplot('Position',[0.65 0.06 0.34 0.85])
   cla
   xlabel('Volume (mL)')
   ylabel('Pressure (mmHg)')
   title('Pressure-Volume Loops');

   hc_hr= uicontrol(hp,'style','text','FontSize',10,'string','HR =       bpm','Units','normalized','Position',[0.05 0.64 0.9
0.06],'BackgroundColor','White');
   hc_edv= uicontrol(hp,'style','text','FontSize',10,'string','EDV =       mL','Units','normalized','Position',[0.05 0.58 0.9
0.06],'BackgroundColor','White');
   hc_esv= uicontrol(hp,'style','text','FontSize',10,'string','ESV =      mL','Units','normalized','Position',[0.05 0.52 0.9
0.06],'BackgroundColor','White');
   hc_sv= uicontrol(hp,'style','text','FontSize',10,'string','SV =      mL','Units','normalized','Position',[0.05 0.46 0.9
0.06],'BackgroundColor','White');
   hc_co= uicontrol(hp,'style','text','FontSize',10,'string','CO =      mL*min^-1','Units','normalized','Position',[0.05 0.4
0.9 0.06],'BackgroundColor','White');
   hc_ef= uicontrol(hp,'style','text','FontSize',10,'string','EF =      %','Units','normalized','Position',[0.05 0.34 0.9
0.06],'BackgroundColor','White');
   hc_esp= uicontrol(hp,'style','text','FontSize',10,'string','ESP =      mmHg','Units','normalized','Position',[0.05 0.28
0.9 0.06],'BackgroundColor','White');
   hc_edp= uicontrol(hp,'style','text','FontSize',10,'string','EDP =      mmHg','Units','normalized','Position',[0.05 0.22
0.9 0.06],'BackgroundColor','White');
   hc_pdpdt= uicontrol(hp,'style','text','FontSize',10,'string','+dp/dt =      mmHg*s^-
1','Units','normalized','Position',[0.05 0.16 0.9 0.06],'BackgroundColor','White');
   hc_ndpdt= uicontrol(hp,'style','text','FontSize',10,'string','-dp/dt =      mmHg*s^-
1','Units','normalized','Position',[0.05 0.10 0.9 0.06],'BackgroundColor','White');
   hc_sw= uicontrol(hp,'style','text','FontSize',10,'string','SW =      mL*mmHg','Units','normalized','Position',[0.05
0.04 0.9 0.06],'BackgroundColor','White');

   hp2 =
uipanel('BorderType','line','BorderWidth',2,'HighlightColor','black','BackgroundColor','White','Position',[0.42 0.655
0.18 0.3154]);
   hp1_title=uicontrol(hp2,'style','text','FontSize',10,'string','Select Segments To Be
Used','Units','normalized','BackgroundColor','White','FontWeight','bold','Position',[0.05 0.92 0.93 0.08]);
   hp2_title=uicontrol(hp2,'style','text','FontSize',10,'string','In Total Volume
Calculation','Units','normalized','BackgroundColor','White','FontWeight','bold','Position',[0.05 0.84 0.93 0.08]);
   cbh1 = uicontrol(hp2,'Style','checkbox','Tag','save option','String','Segment 1
(Distal)','Units','Normalized','BackgroundColor','White','Position',[0.2397 0.0860 0.7
0.1145],'Value',0,'Callback','Plot_PV_loop');
```

```
    cbh2 = uicontrol(hp2,'Style','checkbox','Tag','save option','String','Segment
2','Units','Normalized','BackgroundColor','White','Position',[0.2397 0.191 0.4687
0.1145],'Value',0,'Callback','Plot_PV_loop');
    cbh3 = uicontrol(hp2,'Style','checkbox','Tag','save option','String','Segment
3','Units','Normalized','BackgroundColor','White','Position',[0.2397 0.296 0.4687
0.1145],'Value',0,'Callback','Plot_PV_loop');
    cbh4 = uicontrol(hp2,'Style','checkbox','Tag','save option','String','Segment
4','Units','Normalized','BackgroundColor','White','Position',[0.2397 0.401 0.4687
0.1145],'Value',0,'Callback','Plot_PV_loop');
    cbh5 = uicontrol(hp2,'Style','checkbox','Tag','save option','String','Segment
5','Units','Normalized','BackgroundColor','White','Position',[0.2397 0.506 0.4687
0.1145],'Value',0,'Callback','Plot_PV_loop');
    cbh6 = uicontrol(hp2,'Style','checkbox','Tag','save option','String','Segment
6','Units','Normalized','BackgroundColor','White','Position',[0.2397 0.611 0.4687
0.1145],'Value',0,'Callback','Plot_PV_loop');
    cbh7 = uicontrol(hp2,'Style','checkbox','Tag','save option','String','Segment 7
(Proximal)','Units','Normalized','BackgroundColor','White','Position',[0.2397 0.716 0.7
0.1145],'Value',0,'Callback','Plot_PV_loop');
    h_push_done=uicontrol(hp2,'style','pushbutton','String', 'Finished','Units','normalized','Position',[0.05 0.001
0.8954 0.10],'Callback','Global_Analysis');

    hp3p=uipanel('BorderType','line','HighlightColor','black','BackgroundColor','White','Position',[0.05 0.955 0.05
0.03]);
    hp3 = uicontrol(hp3p,'style','pushbutton','string','Zoom','Units','Normalized','Position',[0 0 1 1],'Callback','Zoom');
    Finished=0;
%-------------------------------------------------------------
clc
clear all
WD=('C:\Documents and Settings\Lauren\My Documents\HUMAN DATA\OPTIMA P-V Files\OPTIMA Code');

[datafile,directory] = uigetfile('*.csv;*.xls','Choose Data File');
cd(directory)  %allows to choose file from another directory
[data,txt] = xlsread(datafile);
filename=datafile(1:end-4);
patientname=directory(75:84); %Will need to change this if directory changes!

cd(WD)

beat=data(:,1);
time=data(:,2);
Volumes_unsc=data(:,3:9);
ECG=data(:,10);
LVP=data(:,11);
    %Smooth LVP
%     LVP=csaps(time,LVP,0.9999,time);
x=1:length(time);

%Need to convert "volumes" back to conductance
%[know that alpha=1;Vc=0;rho=146.91;L=0.6cm (except #17:1.0cm)]

patient_number=str2double(patientname(8:9));
pacing_site=str2double(filename(end-1));

if patient_number == 17
```

```
   l=1.0;
else
   l=0.6;
end

G=Volumes_unsc/(146.91*(l^2));

%Now convert conductance to volume each case refers to each patient (only 2 are displayed to save space)
switch patient_number
   case 11
      rho=142.37;
      EDVecho=153;
      ESVecho=90;
      alpha=0.2899;
      Vc=93.5765;
   case 12
       rho=139.9;
      EDVecho=74;
      ESVecho=31;
      alpha=0.5634;
      Vc=84.8776;
end
L=1.0;
%Volumes_o=(rho*L^2*G - 0); %Let alpha = 1.0 for now
Volumes_o = G; %Let individual segments just be conductance for now
G_sum = sum(G,2);

PV_loops
Finished=0;
%FILTERING SCRIPT**********************
      blackmanNum = [0.0 0.0023325 -0.017436 -0.032217 0.26477 0.5651 0.26477 -0.032217 -0.017436
0.0023325];
      blackmanDen = [ 1 ];

      Volumes_o = filtfilt(blackmanNum,blackmanDen,Volumes_o);
      LVP = filtfilt(blackmanNum,blackmanDen,LVP);
%**************************************
%Smoothing volumes
for i=1:7
   ys(:,i)=csaps(time,Volumes_o(:,i),0.999,time);
end
Volumes_o=ys;
%**************************************
subplot('Position',[0.05 0.7 0.35 0.25])
   cla
   plot(x,Volumes_o)
   ylabel('LV Conductance')
   axis([0 length(x) min(min(G)) max(max(G))])
subplot('Position',[0.05 0.38 0.35 0.25])
   cla
   plot(x,LVP)
   ylabel('LV Pressure (mmHg)')
   axis([0 length(x) 0 max(max(LVP)+5)])
subplot('Position',[0.05 0.06 0.35 0.25])
   cla
```

```
    xlabel('Time (s)')
    ylabel('Total LV Volume (mL)')
subplot('Position',[0.65 0.06 0.34 0.85])
    cla
    hold on
    xlabel('Volume (mL)')
    ylabel('Pressure (mmHg)')
    title('Pressure-Volume Loops');

hp = uipanel('BorderType','line','BorderWidth',2,'HighlightColor','black','Position',[0.42 0.06 0.18
0.5],'BackgroundColor','White');
hc_title=uicontrol(hp,'style','text','FontSize',11,'string','Global LV
Performance','Units','normalized','FontWeight','bold','Position',[0.0328 0.74 0.93 0.05],'BackgroundColor','White');
hc_und1=uicontrol(hp,'style','text','FontSize',11,'string','_____','Units','norma
lized','FontWeight','bold','Position',[0.0328 0.83 0.93 0.0487],'BackgroundColor','White');
hc_patientname=uicontrol(hp,'style','text','FontSize',11,'string',patientname,'Units','normalized','FontWeight','bold','P
osition',[0.0285 0.94 0.96 0.05],'BackgroundColor','White');
hc_filename=uicontrol(hp,'style','text','FontSize',11,'string',filename,'Units','normalized','FontWeight','bold','Position'
,[0.0285 0.8709 0.96 0.05],'BackgroundColor','White');
%Selects window to analyze
h=helpdlg('Select the first and last points of the beats you want to analyze','User Input');
uiwait(h);

[x_sel,y_sel]=ginput(2);
x1=round(x_sel(1));
x2=round(x_sel(2));

x_new=x1:x2;

%Assign only selected region to variables
beat=beat(x_new);
time=time(x_new)-min(time(x_new)); %starts from zero again
Volumes_o=Volumes_o(x_new,:);
ECG=ECG(x_new);
LVP=LVP(x_new);
%V_tot_unsc=sum(Volumes_o,2);
V_tot_unsc = rho*(L^2)*G_sum;
x=1:length(time);

S1=0; S2=0; S3=0; S4=0; S5=0; S6=0; S7=0;
subplot('Position',[0.05 0.7 0.35 0.25])
    cla
    plot(time,Volumes_o)
    xlabel('Time (s)')
    ylabel('LV Conductance')
    axis([0 max(time) min(min(G)) max(max(G))])
    legend('Distal (Seg1)','Seg2','Seg3','Seg4','Seg5','Seg6','Proximal (Seg7)','Location','NorthEastOutside')
subplot('Position',[0.05 0.38 0.35 0.25])
    cla
    plot(time,LVP)
    xlabel('Time (s)')
    ylabel('LV Pressure (mmHg)')
    axis([0 max(time) 0 max(max(LVP)+5)])
subplot('Position',[0.65 0.06 0.34 0.85])
    cla
```

```
    hold on
    xlabel('Volume (mL)')
    ylabel('Pressure (mmHg)')


    hp2 =
uipanel('BorderType','line','BorderWidth',2,'HighlightColor','black','BackgroundColor','White','Position',[0.42 0.655
0.18 0.3154]);
    hp1_title=uicontrol(hp2,'style','text','FontSize',10,'string','Select Segments To Be
Used','Units','normalized','BackgroundColor','White','FontWeight','bold','Position',[0.05 0.92 0.93 0.08]);
    hp2_title=uicontrol(hp2,'style','text','FontSize',10,'string','In Total Volume
Calculation','Units','normalized','BackgroundColor','White','FontWeight','bold','Position',[0.05 0.84 0.93 0.08]);
    cbh1 = uicontrol(hp2,'Style','checkbox','Tag','save option','String','Segment 1
(Distal)','Units','Normalized','BackgroundColor','White','Position',[0.2397 0.0860 0.7
0.1145],'Value',0,'Callback','Plot_PV_loop');
    cbh2 = uicontrol(hp2,'Style','checkbox','Tag','save option','String','Segment
2','Units','Normalized','BackgroundColor','White','Position',[0.2397 0.191 0.4687
0.1145],'Value',0,'Callback','Plot_PV_loop');
    cbh3 = uicontrol(hp2,'Style','checkbox','Tag','save option','String','Segment
3','Units','Normalized','BackgroundColor','White','Position',[0.2397 0.296 0.4687
0.1145],'Value',0,'Callback','Plot_PV_loop');
    cbh4 = uicontrol(hp2,'Style','checkbox','Tag','save option','String','Segment
4','Units','Normalized','BackgroundColor','White','Position',[0.2397 0.401 0.4687
0.1145],'Value',0,'Callback','Plot_PV_loop');
    cbh5 = uicontrol(hp2,'Style','checkbox','Tag','save option','String','Segment
5','Units','Normalized','BackgroundColor','White','Position',[0.2397 0.506 0.4687
0.1145],'Value',0,'Callback','Plot_PV_loop');
    cbh6 = uicontrol(hp2,'Style','checkbox','Tag','save option','String','Segment
6','Units','Normalized','BackgroundColor','White','Position',[0.2397 0.611 0.4687
0.1145],'Value',0,'Callback','Plot_PV_loop');
    cbh7 = uicontrol(hp2,'Style','checkbox','Tag','save option','String','Segment 7
(Proximal)','Units','Normalized','BackgroundColor','White','Position',[0.2397 0.716 0.7
0.1145],'Value',0,'Callback','Plot_PV_loop');
    h_push_done=uicontrol(hp2,'style','pushbutton','String', 'Finished','Units','normalized','Position',[0.05 0.001
0.8954 0.10],'Callback','Global_Analysis');
```

Global LV Performance Calculations:

```
%Calculate # of combo's n!/(k!(n-k)! where n=segments k=#in combo
nc = factorial(ns)/(factorial(2)*factorial(ns-2));

%DETERMINES LEGEND BASED ON SELECTED SEGMENTS
for i=1:7
    if s(i)>0
        SegLeg(i,:)=sprintf('%s %1.0f','Segment',s(i));
    end
end
SegLeg=SegLeg(S,:);

%Identify cycles by finding end diastole (before isovolumic contraction)
    edvx=[];
    minitemp=[];
    pp=spline(x,LVP); %spline is a curve fitting tool
```

```
    ppd=mmspder(pp); %mmspder takes derivative; smooths curve
    slope=ppval(ppd,x); %ppval gets slope
    mark=0;
    for i=1:length(slope)  %for loop goes through slope curve and looks for 0's on the curves --> peaks of fx! b/c
derivative
        if slope(i)<0.55 && slope(i)>-.50 %& LVpressure(i)<lim
            mark=1; %just a counter
            Minimumtemp=i; %remembers iteration
        end
        if mark==1
            if slope(i)>= 2.2  %(1.2=>2.1)Adjust the sensitivity, up is less sensitive (tells you have a major peak b/c big
jump in slope)
                edvx(i)=Minimumtemp;
                mark=0; %if slope not >=2.2, mark still is 1 so continues in this loop
                %only when slope >=2.2 does mark=0 and edvx is chosen!
            end
        end
    end
    edvx=nonzeros(edvx)'; %gets rid of all zeros so now have only edvx

%*END SYSTOLE DETERMINED FROM MAX Ees******************
for i=1:length(edvx)-1
    [PPdPdt(i),PPdPdt_x(i)]=max(slope(edvx(i):edvx(i+1)));
    [PNdPdt(i),PNdPdt_x(i)]=min(slope(edvx(i):edvx(i+1)));
    dpdt_x(i)=edvx(i)+PPdPdt_x(i);
    dpdt_x2(i)=edvx(i)+PNdPdt_x(i);
end
%CONITNUED BELOW***************%NEED TO DETERMINE ALPHA VIA SVcc/SVdop
ESVtemp=[];EDVtemp=[];SVcc=[];
for i=1:(length(edvx)-1)
    ESVtemp(i)       = V_tot_unsc(dpdt_x2(i));  %V_tot(ES(i));
    EDVtemp(i)       = V_tot_unsc(dpdt_x(i)); %V_tot(edvx(i));
    SVcc(i)      = EDVtemp(i)-ESVtemp(i);
end
%THIS IS USED INITIALLY TO SOLVE FOR ALPHA AND VC FOR BASELINE CONDITIONS
% alpha = mean(SVcc)/(EDVecho-ESVecho);
% Vc = mean(EDVtemp) - alpha*EDVecho;

% %Now need to convert into real volume
V_tot = (1/alpha)*(V_tot_unsc-Vc); %alpha and Vc derived from AAI (in Loading.m)

%Find end systole
Ees = LVP./(V_tot);
    for i=1:length(dpdt_x)
        [Emax(i),ind2(i)] = max(Ees(dpdt_x(i):dpdt_x2(i)));
         ES(i)=dpdt_x(i)+ind2(i);
    end

%GLOBAL LV PERFORMANCE************************
%Averages total volume waveform to find global end systole (min vol)
V=[];Mean_Seg=[];vtot=[];Mean_V_tot=[];Mean_LVP=[];GES=[];
cycle=min(diff(edvx));
for j=1:length(edvx)-1
    vtot(:,j)=V_tot(edvx(j):edvx(j)+cycle);
    LVp(:,j)=LVP(edvx(j):edvx(j)+cycle);
```

```
end
Mean_V_tot=mean(vtot,2);
Mean_LVP=mean(LVp,2);
GES=find(Mean_V_tot==min(Mean_V_tot)); %Global End Systole

%Averages segmental volume waveforms
for i=1:ns;
   for j=1:(length(edvx)-1)
   V(:,j)=Volumes(edvx(j):edvx(j)+cycle,i);
   end
   Mean_Seg(:,i)=mean(V,2);
end

freq=250;
pp=spline(time,V_tot);
pp2=spline(time(1:length(LVP)),LVP);
ppd=mmspder(pp);
ppd2=mmspder(pp2);
Pressureslope=ppval(ppd2,time);
%%
HR=[]; Vmin=[]; Vmax=[];ESV=[];EDV=[];SV_minmax=[];SV=[];EF=[];
ESP=[];EDP=[];dPdt_max=[];dPdt_min=[];EA=[];SW=[];CO=[];
for i=1:(length(edvx)-1)
   HR(i)      = 60/((edvx(i+1)-edvx(i))/freq);              % Cycle Time of Beat in seconds
   Vmin(i)    = min(V_tot(edvx(i):edvx(i+1)));              % Minimum Area [cm^2]
   [Vmax(i),VmaxX(i)]    = max(V_tot(edvx(i):edvx(i+1)));   % Maximum Area [cm^2]
   ESV(i)       = V_tot(dpdt_x2(i));  %V_tot(ES(i));
   EDV(i)       = V_tot(dpdt_x(i)); %V_tot(edvx(i));
   SV_minmax(i)  = Vmax(i)-Vmin(i);
   SV(i)      = EDV(i)-ESV(i);                           % Stroke Area [cm^2]
   EF(i)      = (SV(i)/EDV(i))*100;                      % Ejection Fraction
   ESP(i)     = LVP(ES(i));                              % End Systolic Pressure [mmHg]
   EDP(i)     = LVP(edvx(i));                            % End Diastolic Pressure [mmHg]
   dPdt_max(i)  = max(Pressureslope(edvx(i):edvx(i+1)));       % Peak Positive dPdt [mmHg/s]
   dPdt_min(i)  = min(Pressureslope(edvx(i):edvx(i+1)));       % Peak Negative dPdt [mmHg/s]
   EA(i)      = ESP(i)/SV(i);                            % Arterial Elastance [mmHg/cc]
   SW(i)      = -1*trapz(V_tot(edvx(i):edvx(i+1)),LVP(edvx(i):edvx(i+1))); %Stroke Work mmHg*cm^3
   %SW_mJ(i)=SF(i)*0.133;                                % SW in mJ
   CO(i)      = HR(i)*SV(i)/1000;
   %CO(i)      = HR(i)*SV_minmax(i)/1000; %Cardiac output
end
%%
HRm=mean(HR);Vminm=mean(Vmin);Vmaxm=mean(Vmax);ESVm=mean(ESV);EDVm=mean(EDV);SV_minm
axm=mean(SV_minmax);SVm=mean(SV);EFm=mean(EF);
ESPm=mean(ESP);EDPm=mean(EDP);dPdt_maxm=mean(dPdt_max);dPdt_minm=mean(dPdt_min);EAm=mean(E
A);SWm=mean(SW);COm=mean(CO);

HRsd=std(HR);Vminsd=std(Vmin);Vmaxsd=std(Vmax);ESVsd=std(ESV);EDVsd=std(EDV);SV_minmaxsd=std(S
V_minmax);SVsd=std(SV);EFsd=std(EF);
ESPsd=std(ESP);EDPsd=std(EDP);dPdt_maxsd=std(dPdt_max);dPdt_minsd=std(dPdt_min);EAsd=std(EA);SWsd=
std(SW);COsd=std(CO);

subplot('Position',[0.05 0.7 0.35 0.25])
      cla
      plot(time,Volumes)
```

```
        hold on
        axis([min(time) max(time) min(min(G)) max(max(G))])
        xlabel('Time (s)')
        ylabel('LV Conductance')
        legend(SegLeg,'Location','EastOutside')
subplot('Position',[0.05 0.38 0.35 0.25])
        cla
        plot(time,LVP)
        hold on
        plot(time(edvx),LVP(edvx),'g*')
        plot(time(ES),LVP(ES),'r*')
        axis([min(time) max(time) min(min(LVP))-5 max(max(LVP))+5])
        xlabel('Time (s)')
        ylabel('LV Pressure (mmHg)')
subplot('Position',[0.05 0.06 0.35 0.25])
        cla
        plot(time,V_tot)
        hold on
        plot(time(edvx),V_tot(edvx),'g*')
        plot(time(ES),V_tot(ES),'r*')
        axis([min(time) max(time) min(min(V_tot))-3 max(max(V_tot))+3])
        xlabel('Time (s)')
        ylabel('Total LV Volume (mL)')
subplot('Position',[0.65 0.06 0.34 0.85])
    cla
    plot(V_tot,LVP)
    hold on
    plot(V_tot(edvx),LVP(edvx),'g*')
    plot(V_tot(ES),LVP(ES),'r*')
    xlabel('Volume (mL)')
    ylabel('LV Pressure (mmHg)')

%hp defined in PV_loops
    hc_hr= uicontrol(hp,'style','text','FontSize',10,'string',['HR = ' num2str(HRm,'%6.0f') '
bpm'],'Units','normalized','Position',[0.05 0.64 0.9 0.06],'BackgroundColor','White');
    hc_edv= uicontrol(hp,'style','text','FontSize',10,'string',['EDV = ' num2str(EDVm,'%6.0f') '
mL'],'Units','normalized','Position',[0.05 0.58 0.9 0.06],'BackgroundColor','White');
    hc_esv= uicontrol(hp,'style','text','FontSize',10,'string',['ESV = ' num2str(ESVm,'%6.0f') '
mL'],'Units','normalized','Position',[0.05 0.52 0.9 0.06],'BackgroundColor','White');
    hc_sv= uicontrol(hp,'style','text','FontSize',10,'string',['SV = ' num2str(SVm,'%6.0f') '
mL'],'Units','normalized','Position',[0.05 0.46 0.9 0.06],'BackgroundColor','White');
    hc_co= uicontrol(hp,'style','text','FontSize',10,'string',['CO = ' num2str(COm,'%6.2f') ' mL*min^-
1'],'Units','normalized','Position',[0.05 0.4 0.9 0.06],'BackgroundColor','White');
    hc_ef= uicontrol(hp,'style','text','FontSize',10,'string',['EF = ' num2str(EFm,'%6.0f') '
%'],'Units','normalized','Position',[0.05 0.34 0.9 0.06],'BackgroundColor','White');
    hc_esp= uicontrol(hp,'style','text','FontSize',10,'string',['ESP = ' num2str(ESPm,'%6.0f') '
mmHg'],'Units','normalized','Position',[0.05 0.28 0.9 0.06],'BackgroundColor','White');
    hc_edp= uicontrol(hp,'style','text','FontSize',10,'string',['EDP = ' num2str(EDPm,'%6.0f') '
mmHg'],'Units','normalized','Position',[0.05 0.22 0.9 0.06],'BackgroundColor','White');
    hc_pdpdt= uicontrol(hp,'style','text','FontSize',10,'string',['+dp/dt = ' num2str(dPdt_maxm,'%6.0f') ' mmHg*s^-
1'],'Units','normalized','Position',[0.05 0.16 0.9 0.06],'BackgroundColor','White');
    hc_ndpdt= uicontrol(hp,'style','text','FontSize',10,'string',['-dp/dt = ' num2str(dPdt_minm,'%6.0f') ' mmHg*s^-
1'],'Units','normalized','Position',[0.05 0.10 0.9 0.06],'BackgroundColor','White');
    hc_sw= uicontrol(hp,'style','text','FontSize',10,'string',['SW = ' num2str(SWm,'%6.0f') '
mL*mmHg'],'Units','normalized','Position',[0.05 0.04 0.9 0.06],'BackgroundColor','White');
```

```
Hf_figure=gcf;
PlotCCA=0;
Finished=1;
```

APPENDIX D

ERROR PROPAGATION

Calculated variables are affected by the errors associated with the experimental measurements used to quantify them. For example, myocardial oxygen consumption (MVO_2) is calculated using several measured variables: coronary flow (Q_{cor}), arteriovenous oxygen content difference (AVO_2), heart rate (HR), and the mass of the left ventricle (LV). The specific equation is as follows:

$$MVO_2 = \frac{Q_{cor} \cdot AVO_2}{HR \cdot LV} \quad \textbf{(D-1)}$$

Uncertainties due to measurement limitations of these variables propagate through the calculation of MVO_2. Specifically, the total error in MVO_2 due to measurement inaccuracies in Q_{cor}, AVO_2, HR, and LV can be determined by the following equation:

$$\Delta MVO_2 = \left|\frac{\partial MVO_2}{\partial Q_{cor}}\right| \cdot \left|\Delta Q_{cor}\right| + \left|\frac{\partial MVO_2}{\partial AVO_2}\right| \cdot \left|\Delta AVO_2\right| + \left|\frac{\partial MVO_2}{\partial HR}\right| \cdot \left|\Delta HR\right| + \left|\frac{\partial MVO_2}{\partial LV}\right| \cdot \left|\Delta LV\right| \quad \textbf{(D-2)}$$

where the partial derivatives with respect to each of the measured variable are given by:

$$\frac{\partial MVO_2}{\partial Q_{cor}} = \frac{AVO_2}{HR \cdot LV}; \frac{\partial MVO_2}{\partial AVO_2} = \frac{Q_{cor}}{HR \cdot LV}; \frac{\partial MVO_2}{\partial HR} = -\frac{Q_{cor} \cdot AVO_2}{HR^2 \cdot LV}; \frac{\partial MVO_2}{\partial LV} = -\frac{Q_{cor} \cdot AVO_2}{HR \cdot LV^2} \quad \textbf{(D-3)}$$

Substituting Eq. (D-3) into Eq. (D-2), one gets:

$$\Delta MVO_2 = \frac{AVO_2}{HR \cdot LV} \cdot \Delta Q_{cor} + \frac{Q_{cor}}{HR \cdot LV} \cdot \Delta AVO_2 + \frac{Q_{cor} \cdot AVO_2}{HR^2 \cdot LV} \cdot \Delta HR + \frac{Q_{cor} \cdot AVO_2}{HR \cdot LV^2} \cdot \Delta LV \quad \textbf{(D-4)}$$

Note that the goal of error propagation is to determine the percentage error of the calculated variable, which in this case is the error associated with MVO_2 divided by some nominal value of MVO_2 (i.e., $\Delta MVO_2/MVO_2$). Therefore, equation D-4 can be simplified to:

$$\frac{\Delta MVO_2}{MVO_2} = \frac{\Delta Q_{cor}}{Q_{cor}} + \frac{\Delta AVO_2}{AVO_2} + \frac{\Delta HR}{HR} + \frac{\Delta LV}{LV} \quad \textbf{(D-5)}$$

Interestingly, in this case, Equation D-1 is simplified such that the total error in the calculation of MVO_2 can be determined by the simple addition of the errors associated with each measured variable. The percentage errors for each of the measured quantities was found by technical specification literature supplied by the company for each device (Q_{cor}=5%, AVO_2=4.4%, LV=0.02%, HR=0.001%). Therefore, a 9.4% error is propagated through the calculation of MVO_2 due to inaccuracies of measured variables used to calculate this quantity. Of note, this is a relatively large percent error, however, it should be kept in mind that this is an estimate based on a "worst case" scenario.

The determination of error propagation for cross-correlation analysis is much more difficult. For example, it is not possible to write explicit equations for cross correlation-based indices of LV regional synchrony in terms of measured quantities. However, one can theoretically speculate that the majority of error associated with the quantification of regional function would be due to the methodology used to derive the strain waveforms. In the current research, speckle tracking was shown to be superior to other methods in quantifying myocardial contraction. However, echocardiographic images must be of acceptable quality for the speckle tracking algorithm to yield reliable and reproducible results. The temporal resolution of strain

data can affect the results of the cross correlation analysis and therefore, the sampling rate of the imaging system should be maximized.

BIBLIOGRAPHY

1. **Bader H, Garrigue S, Lafitte S, Reuter S, Jais P, Haissaguerre M, Bonnet J, Clementy J, and Roudaut R**. Intra-left ventricular electromechanical asynchrony: A new independent predictor of severe cardiac events in heart failure patients. *J Am Coll Cardiol* 43(2): 248-256, 2004.

2. **Strickberger SA, Conti J, Daoud EG, Havranek E, Mehra MR, Pina IL, and Young J**. Patient selection for cardiac resynchronization therapy: from the Council on Clinical Cardiology Subcommittee on Electrocardiography and Arrhythmias and the Quality of Care and Outcomes Research Interdisciplinary Working Group, in collaboration with the Heart Rhythm Society. *Circulation* 111(16): 2146-50, 2005.

3. Medtronic I. *Treating ventricular dyssynchrony with CRT*. [JPEG] 2008 [cited 2008 February 25]; http://www.medtronic.com/physician/hf/illustrations/slide19.jpg.

4. **Abraham WT, Fisher WG, Smith AL, Delurgio DB, Leon AR, Loh E, Kocovic DZ, Packer M, Clavell AL, Hayes DL, Ellestad M, Trupp RJ, Underwood J, Pickering F, Truex C, McAtee P, and Messenger J**. Cardiac resynchronization in chronic heart failure. *N Engl J Med* 346(24): 1845-53, 2002.

5. **Auricchio A, Stellbrink C, Butter C, Sack S, Vogt J, Misier AR, Bocker D, Block M, Kirkels JH, Kramer A, and Huvelle E**. Clinical efficacy of cardiac resynchronization therapy using left ventricular pacing in heart failure patients stratified by severity of ventricular conduction delay. *J Am Coll Cardiol* 42(12): 2109-16, 2003.

6. **Auricchio A, Stellbrink C, Sack S, Block M, Vogt J, Bakker P, Huth C, Schondube F, Wolfhard U, Bocker D, Krahnefeld O, and Kirkels H**. Long-term clinical effect of hemodynamically optimized cardiac resynchronization therapy in patients with heart failure and ventricular conduction delay. *J Am Coll Cardiol* 39(12): 2026-33, 2002.

7. **Bristow MR, Saxon LA, Boehmer J, Krueger S, Kass DA, De Marco T, Carson P, DiCarlo L, DeMets D, White BG, DeVries DW, and Feldman AM**. Cardiac-resynchronization therapy with or without an implantable defibrillator in advanced chronic heart failure. *N Engl J Med* 350(21): 2140-50, 2004.

8. **Cazeau S, Leclercq C, Lavergne T, Walker S, Varma C, Linde C, Garrigue S, Kappenberger L, Haywood GA, Santini M, Bailleul C, and Daubert JC**. Effects of multisite biventricular pacing in patients with heart failure and intraventricular conduction delay. *N Engl J Med* 344(12): 873-80, 2001.

9. **Cleland JG, Daubert JC, Erdmann E, Freemantle N, Gras D, Kappenberger L, and Tavazzi L**. The effect of cardiac resynchronization on morbidity and mortality in heart failure. *N Engl J Med* 352(15): 1539-49, 2005.

10. **Reuter S, Garrigue S, Barold SS, Jais P, Hocini M, Haissaguerre M, and Clementy J**. Comparison of characteristics in responders versus nonresponders with biventricular pacing for drug-resistant congestive heart failure. *Am J Cardiol* 89(3): 346-50, 2002.

11. **Young JB, Abraham WT, Smith AL, Leon AR, Lieberman R, Wilkoff B, Canby RC, Schroeder JS, Liem LB, Hall S, and Wheelan K**. Combined cardiac resynchronization and implantable cardioversion defibrillation in advanced chronic heart failure: the MIRACLE ICD Trial. *Jama* 289(20): 2685-94, 2003.

12. **Bax JJ, Abraham T, Barold SS, Breithardt OA, Fung JWH, Garrigue S, Gorcsan III J, Hayes DL, Kass DA, and Knuuti J**. Cardiac Resynchronization Therapy: Part 1--Issues Before Device Implantation. *J Am Coll Cardiol* 46(12): 2153-2167, 2005.

13. Guyton AC and Hall JE. Textbook of medical physiology. 11th ed. 2006, Philadelphia: Elsevier Saunders. xxxv, 1116.

14. **Greenbaum RA, Ho SY, Gibson DG, Becker AE, and Anderson RH**. Left ventricular fibre architecture in man. *Br Heart J* 45(3): 248-63, 1981.

15. **Grines CL, Bashore TM, Boudoulas H, Olson S, Shafer P, and Wooley CF**. Functional abnormalities in isolated left bundle branch block. The effect of interventricular asynchrony. *Circulation* 79(4): 845-53, 1989.

16. **Bonow RO**. Regional left ventricular nonuniformity. Effects on left ventricular diastolic function in ischemic heart disease, hypertrophic cardiomyopathy, and the normal heart. *Circulation* 81(2 Suppl): III54-65, 1990.

17. **Xiao HB, Roy C, and Gibson DG**. Nature of ventricular activation in patients with dilated cardiomyopathy: evidence for bilateral bundle branch block. *Br Heart J* 72(2): 167-74, 1994.

18. **Prinzen FW and Peschar M**. Relation between the pacing induced sequence of activation and left ventricular pump function in animals. *Pacing Clin Electrophysiol* 25(4 Pt 1): 484-98, 2002.

19. **Kingma I, Tyberg JV, and Smith ER**. Effects of diastolic transseptal pressure gradient on ventricular septal position and motion. *Circulation* 68(6): 1304-14, 1983.

20. **Little WC, Reeves RC, Arciniegas J, Katholi RE, and Rogers EW**. Mechanism of abnormal interventricular septal motion during delayed left ventricular activation. *Circulation* 65(7): 1486-91, 1982.

21. **Leclercq C, Cazeau S, Ritter P, Alonso C, Gras D, Mabo P, Lazarus A, and Daubert JC**. A pilot experience with permanent biventricular pacing to treat advanced heart failure. *Am Heart J* 140(6): 862-70, 2000.

22. **Nelson GS, Berger RD, Fetics BJ, Talbot M, Spinelli JC, Hare JM, and Kass DA**. Left ventricular or biventricular pacing improves cardiac function at diminished energy cost in patients with dilated cardiomyopathy and left bundle-branch block. *Circulation* 102(25): 3053-9, 2000.

23. **Meisel E, Pfeiffer D, Engelmann L, Tebbenjohanns J, Schubert B, Hahn S, Fleck E, and Butter C**. Investigation of coronary venous anatomy by retrograde venography in patients with malignant ventricular tachycardia. *Circulation* 104(4): 442-7, 2001.

24. **Nelson GS, Curry CW, Wyman BT, Kramer A, Declerck J, Talbot M, Douglas MR, Berger RD, McVeigh ER, and Kass DA**. Predictors of systolic augmentation from left ventricular preexcitation in patients with dilated cardiomyopathy and intraventricular conduction delay. *Circulation* 101(23): 2703-9, 2000.

25. **Bleeker GB, Schalij MJ, Molhoek SG, Verwey HF, Holman ER, Boersma E, Steendijk P, Van Der Wall EE, and Bax JJ**. Relationship between QRS duration and left ventricular dyssynchrony in patients with end-stage heart failure. *J Cardiovasc Electrophysiol* 15(5): 544-9, 2004.

26. **Bax JJ, Bleeker GB, Marwick TH, Molhoek SG, Boersma E, Steendijk P, van der Wall EE, and Schalij MJ**. Left ventricular dyssynchrony predicts response and prognosis after cardiac resynchronization therapy. *J Am Coll Cardiol* 44(9): 1834-40, 2004.

27. **Penicka M, Bartunek J, De Bruyne B, Vanderheyden M, Goethals M, De Zutter M, Brugada P, and Geelen P**. Improvement of left ventricular function after cardiac resynchronization therapy is predicted by tissue Doppler imaging echocardiography. *Circulation* 109(8): 978-83, 2004.

28. **Sogaard P, Egeblad H, Kim WY, Jensen HK, Pedersen AK, Kristensen BO, and Mortensen PT**. Tissue Doppler imaging predicts improved systolic performance and reversed left ventricular remodeling during long-term cardiac resynchronization therapy. *J Am Coll Cardiol* 40(4): 723-30, 2002.

29. **Yu CM, Fung WH, Lin H, Zhang Q, Sanderson JE, and Lau CP**. Predictors of left ventricular reverse remodeling after cardiac resynchronization therapy for heart failure secondary to idiopathic dilated or ischemic cardiomyopathy. *Am J Cardiol* 91(6): 684-8, 2003.

30. **Axel L and Dougherty L**. MR imaging of motion with spatial modulation of magnetization. *Radiology* 171(3): 841-5, 1989.

31. **Zerhouni EA, Parish DM, Rogers WJ, Yang A, and Shapiro EP**. Human heart: tagging with MR imaging--a method for noninvasive assessment of myocardial motion. *Radiology* 169(1): 59-63, 1988.

32. **Abraham TP, Dimaano VL, and Liang HY**. Role of tissue Doppler and strain echocardiography in current clinical practice. *Circulation* 116(22): 2597-609, 2007.

33. **Marcus GM, Rose E, Viloria EM, Schafer J, De Marco T, Saxon LA, and Foster E**. Septal to posterior wall motion delay fails to predict reverse remodeling or clinical improvement in patients undergoing cardiac resynchronization therapy. *J Am Coll Cardiol* 46(12): 2208-14, 2005.

34. **Pitzalis MV, Iacoviello M, Romito R, Guida P, De Tommasi E, Luzzi G, Anaclerio M, Forleo C, and Rizzon P**. Ventricular asynchrony predicts a better outcome in patients with chronic heart failure receiving cardiac resynchronization therapy. *J Am Coll Cardiol* 45(1): 65-9, 2005.

35. **Pitzalis MV, Iacoviello M, Romito R, Massari F, Rizzon B, Luzzi G, Guida P, Andriani A, Mastropasqua F, and Rizzon P**. Cardiac resynchronization therapy tailored by echocardiographic evaluation of ventricular asynchrony. *J Am Coll Cardiol* 40(9): 1615-22, 2002.

36. **Notabartolo D, Merlino JD, Smith AL, DeLurgio DB, Vera FV, Easley KA, Martin RP, and Leon AR**. Usefulness of the peak velocity difference by tissue Doppler imaging technique as an effective predictor of response to cardiac resynchronization therapy. *Am J Cardiol* 94(6): 817-20, 2004.

37. **Sogaard P, Egeblad H, Pedersen AK, Kim WY, Kristensen BO, Hansen PS, and Mortensen PT**. Sequential versus simultaneous biventricular resynchronization for severe heart failure: evaluation by tissue Doppler imaging. *Circulation* 106(16): 2078-84, 2002.

38. **Yu CM, Chau E, Sanderson JE, Fan K, Tang MO, Fung WH, Lin H, Kong SL, Lam YM, Hill MR, and Lau CP**. Tissue Doppler echocardiographic evidence of reverse remodeling and improved synchronicity by simultaneously delaying regional contraction after biventricular pacing therapy in heart failure. *Circulation* 105(4): 438-45, 2002.

39. **Yu CM, Fung JW, Zhang Q, Chan CK, Chan YS, Lin H, Kum LC, Kong SL, Zhang Y, and Sanderson JE**. Tissue Doppler imaging is superior to strain rate imaging and postsystolic shortening on the prediction of reverse remodeling in both ischemic and nonischemic heart failure after cardiac resynchronization therapy. *Circulation* 110(1): 66-73, 2004.

40. **Bax JJ, Marwick TH, Molhoek SG, Bleeker GB, van Erven L, Boersma E, Steendijk P, van der Wall EE, and Schalij MJ**. Left ventricular dyssynchrony predicts benefit of cardiac resynchronization therapy in patients with end-stage heart failure before pacemaker implantation. *Am J Cardiol* 92(10): 1238-40, 2003.

41. **Gorcsan J, 3rd, Kanzaki H, Bazaz R, Dohi K, and Schwartzman D**. Usefulness of echocardiographic tissue synchronization imaging to predict acute response to cardiac resynchronization therapy. *Am J Cardiol* 93(9): 1178-81, 2004.

42. **Dohi K, Pinsky MR, Kanzaki H, Severyn D, and Gorcsan J, 3rd**. Effects of radial left ventricular dyssynchrony on cardiac performance using quantitative tissue Doppler radial strain imaging. *J Am Soc Echocardiogr* 19(5): 475-82, 2006.

43. **Dohi K, Suffoletto MS, Schwartzman D, Ganz L, Pinsky MR, and Gorcsan J, 3rd**. Utility of echocardiographic radial strain imaging to quantify left ventricular dyssynchrony and predict acute response to cardiac resynchronization therapy. *Am J Cardiol* 96(1): 112-6, 2005.

44. **Suffoletto MS, Dohi K, Cannesson M, Saba S, and Gorcsan J, 3rd**. Novel speckle-tracking radial strain from routine black-and-white echocardiographic images to quantify dyssynchrony and predict response to cardiac resynchronization therapy. *Circulation* 113(7): 960-8, 2006.

45. **Liu L, Tockman B, Girouard S, Pastore J, Walcott G, KenKnight B, and Spinelli J**. Left ventricular resynchronization therapy in a canine model of left bundle branch block. *Am J Physiol Heart Circ Physiol* 282(6): H2238-44, 2002.

46. **Verbeek XA, Vernooy K, Peschar M, Cornelussen RN, and Prinzen FW**. Intra-ventricular resynchronization for optimal left ventricular function during pacing in experimental left bundle branch block. *J Am Coll Cardiol* 42(3): 558-67, 2003.

47. **Verbeek XA, Vernooy K, Peschar M, Van Der Nagel T, Van Hunnik A, and Prinzen FW**. Quantification of interventricular asynchrony during LBBB and ventricular pacing. *Am J Physiol Heart Circ Physiol* 283(4): H1370-8, 2002.

48. **Vernooy K, Verbeek XA, Peschar M, and Prinzen FW**. Relation between abnormal ventricular impulse conduction and heart failure. *J Interv Cardiol* 16(6): 557-62, 2003.

49. **Vassallo JA, Cassidy DM, Marchlinski FE, Buxton AE, Waxman HL, Doherty JU, and Josephson ME**. Endocardial activation of left bundle branch block. *Circulation* 69(5): 914-23, 1984.

50. **Gilmore JP, Sarnoff SJ, Mitchell JH, and Linden RJ**. Synchronicity of ventricular contraction: observations comparing haemodynamic effects of atrial and ventricular pacing. *Br Heart J* 25: 299-307, 1963.

51. **Park RC, Little WC, and O'Rourke RA**. Effect of alteration of left ventricular activation sequence on the left ventricular end-systolic pressure-volume relation in closed-chest dogs. *Circ Res* 57(5): 706-17, 1985.

52. **Schreuder JJ, Castiglioni A, Maisano F, Steendijk P, Donelli A, Baan J, and Alfieri O**. Acute decrease of left ventricular mechanical dyssynchrony and improvement of contractile state and energy efficiency after left ventricular restoration. *J Thorac Cardiovasc Surg* 129(1): 138-45, 2005.

53. **Boerth RC and Covell JW**. Mechanical performance and efficiency of the left ventricle during ventricular stimulation. *Am J Physiol* 221(6): 1686-91, 1971.

54. **Owen CH, Esposito DJ, Davis JW, and Glower DD**. The effects of ventricular pacing on left ventricular geometry, function, myocardial oxygen consumption, and efficiency of contraction in conscious dogs. *Pacing Clin Electrophysiol* 21(7): 1417-29, 1998.

55. **Baan J, van der Velde ET, de Bruin HG, Smeenk GJ, Koops J, van Dijk AD, Temmerman D, Senden J, and Buis B**. Continuous measurement of left ventricular volume in animals and humans by conductance catheter. *Circulation* 70(5): 812-23, 1984.

56. **Suga H and Sagawa K**. Instantaneous pressure-volume relationships and their ratio in the excised, supported canine left ventricle. *Circ Res* 35(1): 117-26, 1974.

57. **Glower DD, Spratt JA, Snow ND, Kabas JS, Davis JW, Olsen CO, Tyson GS, Sabiston DC, Jr., and Rankin JS**. Linearity of the Frank-Starling relationship in the intact heart: the concept of preload recruitable stroke work. *Circulation* 71(5): 994-1009, 1985.

58. **Mirsky I**. Assessment of passive elastic stiffness of cardiac muscle: mathematical concepts, physiologic and clinical considerations, directions of future research. *Prog Cardiovasc Dis* 18(4): 277-308, 1976.

59. **Suga H**. Cardiac mechanics and energetics--from Emax to PVA. *Front Med Biol Eng* 2(1): 3-22, 1990.

60. **Suga H**. Cardiac energetics: from E(max) to pressure-volume area. *Clin Exp Pharmacol Physiol* 30(8): 580-5, 2003.

61. **Lozano I, Bocchiardo M, Achtelik M, Gaita F, Trappe HJ, Daoud E, Hummel J, Duby C, and Yong P**. Impact of biventricular pacing on mortality in a randomized crossover study of patients with heart failure and ventricular arrhythmias. *Pacing Clin Electrophysiol* 23(11 Pt 2): 1711-2, 2000.

62. **Yu CM, Bleeker GB, Fung JW, Schalij MJ, Zhang Q, van der Wall EE, Chan YS, Kong SL, and Bax JJ**. Left ventricular reverse remodeling but not clinical improvement predicts long-term survival after cardiac resynchronization therapy. *Circulation* 112(11): 1580-6, 2005.

63. **Chung ES, Leon AR, Tavazzi L, Sun JP, Nihoyannopoulos P, Merlino J, Abraham WT, Ghio S, Leclercq C, Bax JJ, Yu CM, Gorcsan J, 3rd, St John Sutton M, De Sutter J, and Murillo J**. Results of the Predictors of Response to CRT (PROSPECT) trial. *Circulation* 117(20): 2608-16, 2008.

64. Fozzard HA. The Heart and cardiovascular system : scientific foundations. 2nd ed. 1991, New York: Raven Press. 2 v. (xxi, 2193, 71).

65. **Khalafbeigui F, Suga H, and Sagawa K**. Left ventricular systolic pressure-volume area correlates with oxygen consumption. *Am J Physiol* 237(5): H566-9, 1979.

66. **Suga H, Hayashi T, and Shirahata M**. Ventricular systolic pressure-volume area as predictor of cardiac oxygen consumption. *Am J Physiol* 240(1): H39-44, 1981.

67. **Doring HJ**. The isolated perfused heart according to Langendorff technique--function--application. *Physiol Bohemoslov* 39(6): 481-504, 1990.

68. **Bergmann SR, Clark RE, and Sobel BE**. An improved isolated heart preparation for external assessment of myocardial metabolism. *Am J Physiol* 236(4): H644-61, 1979.

69. **Duvelleroy MA, Duruble M, Martin JL, Teisseire B, Droulez J, and Cain M**. Blood-perfused working isolated rat heart. *J Appl Physiol* 41(4): 603-7, 1976.

70. **Campbell KB, Shroff SG, and Kirkpatrick RD**. Short-time-scale left ventricular systolic dynamics. Evidence for a common mechanism in both left ventricular chamber and heart muscle mechanics. *Circ Res* 68(6): 1532-48, 1991.

71. **Shepherd AP and Burgar CG**. A solid-state arteriovenous oxygen difference analyzer for flowing whole blood. *Am J Physiol* 232(4): H437-40, 1977.

72. **Suga H, Futaki S, Ohgoshi Y, Yaku H, and Goto Y**. Arteriovenous oximeter for O2 content difference, O2 saturations, and hemoglobin content. *Am J Physiol* 257(5 Pt 2): H1712-6, 1989.

73. Brown H and Prescott R. Applied mixed models in medicine. 2nd ed. Statistics in practice. 2006, Chichester, England ; Hoboken, NJ: John Wiley. xviii, 455.

74. **Johnson L, Kim HK, Tanabe M, Gorcsan J, Schwartzman D, Shroff SG, and Pinsky MR**. Differential effects of left ventricular pacing sites in an acute canine model of contraction dyssynchrony. *Am J Physiol Heart Circ Physiol* 293(5): H3046-55, 2007.

75. **Yaku H, Slinker BK, Myhre ES, Watkins MW, and Lewinter MM**. Stability of myocardial O2 consumption-pressure-volume area relation in red cell-perfused rabbit heart. *Am J Physiol* 261(5 Pt 2): H1630-5, 1991.

76. **Grandis DJ, DelNido PJ, and Koretsky AP**. Functional and energetic effects of the inotropic agents EMD-57033 and BAPTA on the isolated rat heart. *Am J Physiol* 269(2 Pt 1): C472-9, 1995.

77. **Suga H**. Ventricular energetics. *Physiol Rev* 70(2): 247-77, 1990.

78. **Prinzen FW, Augustijn CH, Arts T, Allessie MA, and Reneman RS**. Redistribution of myocardial fiber strain and blood flow by asynchronous activation. *Am J Physiol* 259(2 Pt 2): H300-8, 1990.

79. **Burkhoff D, Oikawa RY, and Sagawa K**. Influence of pacing site on canine left ventricular contraction. *Am J Physiol* 251(2 Pt 2): H428-35, 1986.

80. **Wilkoff BL, Cook JR, Epstein AE, Greene HL, Hallstrom AP, Hsia H, Kutalek SP, and Sharma A**. Dual-chamber pacing or ventricular backup pacing in patients with an implantable defibrillator: the Dual Chamber and VVI Implantable Defibrillator (DAVID) Trial. *JAMA* 288(24): 3115-23, 2002.

81. **Leclercq C, Faris O, Tunin R, Johnson J, Kato R, Evans F, Spinelli J, Halperin H, McVeigh E, and Kass DA**. Systolic improvement and mechanical resynchronization does not require electrical synchrony in the dilated failing heart with left bundle-branch block. *Circulation* 106(14): 1760-3, 2002.

82. **Verbeek XA, Auricchio A, Yu Y, Ding J, Pochet T, Vernooy K, Kramer A, Spinelli J, and Prinzen FW**. Tailoring cardiac resynchronization therapy using interventricular asynchrony. Validation of a simple model. *Am J Physiol Heart Circ Physiol* 290(3): H968-77, 2006.

83. **Wyman BT, Hunter WC, Prinzen FW, Faris OP, and McVeigh ER**. Effects of single- and biventricular pacing on temporal and spatial dynamics of ventricular contraction. *Am J Physiol Heart Circ Physiol* 282(1): H372-9, 2002.

84. **Strum DP and Pinsky MR**. Modeling ischemia-induced dyssynchronous myocardial contraction. *Anesth Analg* 103(4): 846-53, 2006.

85. **Yu CM, Zhang Q, Fung JW, Chan HC, Chan YS, Yip GW, Kong SL, Lin H, Zhang Y, and Sanderson JE**. A novel tool to assess systolic asynchrony and identify responders of cardiac resynchronization therapy by tissue synchronization imaging. *J Am Coll Cardiol* 45(5): 677-84, 2005.

86. **Hettrick DA, Mittelstadt JR, Kehl F, Kress TT, Tessmer JP, Krolikowski JG, Kersten JR, Warltier DC, and Pagel PS**. Atrial pacing lead location alters the hemodynamic effects of atrial-ventricular delay in dogs with pacing induced cardiomyopathy. *Pacing Clin Electrophysiol* 26(4 Pt 1): 853-61, 2003.

87. **Mele D, Pasanisi G, Capasso F, De Simone A, Morales MA, Poggio D, Capucci A, Tabacchi G, Sallusti L, and Ferrari R**. Left intraventricular myocardial deformation dyssynchrony identifies responders to cardiac resynchronization therapy in patients with heart failure. *Eur Heart J* 27(9): 1070-8, 2006.

88. **Sade LE, Kanzaki H, Severyn D, Dohi K, and Gorcsan J, 3rd**. Quantification of radial mechanical dyssynchrony in patients with left bundle branch block and idiopathic dilated cardiomyopathy without conduction delay by tissue displacement imaging. *Am J Cardiol* 94(4): 514-8, 2004.

89. **Kass DA**. An epidemic of dyssynchrony: but what does it mean? *J Am Coll Cardiol* 51(1): 12-7, 2008.

90. **Helm RH, Byrne M, Helm PA, Daya SK, Osman NF, Tunin R, Halperin HR, Berger RD, Kass DA, and Lardo AC**. Three-dimensional mapping of optimal left ventricular pacing site for cardiac resynchronization. *Circulation* 115(8): 953-61, 2007.

91. **Peschar M, de Swart H, Michels KJ, Reneman RS, and Prinzen FW**. Left ventricular septal and apex pacing for optimal pump function in canine hearts. *J Am Coll Cardiol* 41(7): 1218-26, 2003.

92. **Prinzen FW, Van Oosterhout MF, Vanagt WY, Storm C, and Reneman RS**. Optimization of ventricular function by improving the activation sequence during ventricular pacing. *Pacing Clin Electrophysiol* 21(11 Pt 2): 2256-60, 1998.

93. **Vanagt WY, Verbeek XA, Delhaas T, Mertens L, Daenen WJ, and Prinzen FW**. The left ventricular apex is the optimal site for pediatric pacing: correlation with animal experience. *Pacing Clin Electrophysiol* 27(6 Pt 2): 837-43, 2004.

94. **Myerburg RJ, Nilsson K, and Gelband H**. Physiology of canine intraventricular conduction and endocardial excitation. *Circ Res* 30(2): 217-43, 1972.

95. **Simantirakis EN, Vardakis KE, Kochiadakis GE, Manios EG, Igoumenidis NE, Brignole M, and Vardas PE**. Left ventricular mechanics during right ventricular apical or left ventricular-based pacing in patients with chronic atrial fibrillation after atrioventricular junction ablation. *J Am Coll Cardiol* 43(6): 1013-8, 2004.

96. **Wallace AG, Skinner NS, Jr., and Mitchell JH**. Hemodynamic determinants of the maximal rate of rise of left ventricular pressure. *Am J Physiol* 205: 30-6, 1963.

97. **Helm RH, Leclercq C, Faris OP, Ozturk C, McVeigh E, Lardo AC, and Kass DA**. Cardiac dyssynchrony analysis using circumferential versus longitudinal strain: implications for assessing cardiac resynchronization. *Circulation* 111(21): 2760-7, 2005.

98. **Bohs LN, Friemel BH, and Trahey GE**. Experimental velocity profiles and volumetric flow via two-dimensional speckle tracking. *Ultrasound Med Biol* 21(7): 885-98, 1995.

99. **Cerqueira MD, Weissman NJ, Dilsizian V, Jacobs AK, Kaul S, Laskey WK, Pennell DJ, Rumberger JA, Ryan T, and Verani MS**. Standardized myocardial segmentation and nomenclature for tomographic imaging of the heart: a statement for healthcare professionals from the Cardiac Imaging Committee of the Council on Clinical Cardiology of the American Heart Association. *Circulation* 105(4): 539-42, 2002.

100. **Langeland S, D'Hooge J, Wouters PF, Leather HA, Claus P, Bijnens B, and Sutherland GR**. Experimental validation of a new ultrasound method for the simultaneous assessment of radial and longitudinal myocardial deformation independent of insonation angle. *Circulation* 112(14): 2157-62, 2005.

101. **Anderson LJ, Miyazaki C, Sutherland GR, and Oh JK**. Patient selection and echocardiographic assessment of dyssynchrony in cardiac resynchronization therapy. *Circulation* 117(15): 2009-23, 2008.

102. **Burkhoff D, Mirsky I, and Suga H**. Assessment of systolic and diastolic ventricular properties via pressure-volume analysis: a guide for clinical, translational, and basic researchers. *Am J Physiol Heart Circ Physiol* 289(2): H501-12, 2005.

103. **Recchia FA and Lionetti V**. Animal models of dilated cardiomyopathy for translational research. *Vet Res Commun* 31 Suppl 1: 35-41, 2007.

104. **Perk G, Tunick PA, and Kronzon I**. Non-Doppler two-dimensional strain imaging by echocardiography--from technical considerations to clinical applications. *J Am Soc Echocardiogr* 20(3): 234-43, 2007.

105. **Mirro MJ, Rogers EW, Weyman AE, and Feigenbaum H**. Angular displacement of the papillary muscles during the cardiac cycle. *Circulation* 60(2): 327-33, 1979.

106. **Arita T, Sorescu GP, Schuler BT, Schmarkey LS, Merlino JD, Vinten-Johansen J, Leon AR, Martin RP, and Sorescu D**. Speckle-tracking strain echocardiography for detecting cardiac dyssynchrony in a canine model of dyssynchrony and heart failure. *Am J Physiol Heart Circ Physiol* 293(1): H735-42, 2007.

107. **Vernooy K, Cornelussen RN, Verbeek XA, Vanagt WY, van Hunnik A, Kuiper M, Arts T, Crijns HJ, and Prinzen FW**. Cardiac resynchronization therapy cures dyssynchronopathy in canine left bundle-branch block hearts. *Eur Heart J* 28(17): 2148-55, 2007.

108. **Auricchio A and Prinzen FW**. Update on the pathophysiological basics of cardiac resynchronization therapy. *Europace* 10(7): 797-800, 2008.

109. **Lieberman R, Padeletti L, Schreuder J, Jackson K, Michelucci A, Colella A, Eastman W, Valsecchi S, and Hettrick DA**. Ventricular pacing lead location alters systemic hemodynamics and left ventricular function in patients with and without reduced ejection fraction. *J Am Coll Cardiol* 48(8): 1634-41, 2006.

110. **Nahlawi M, Waligora M, Spies SM, Bonow RO, Kadish AH, and Goldberger JJ**. Left ventricular function during and after right ventricular pacing. *J Am Coll Cardiol* 44(9): 1883-8, 2004.

111. **Vernooy K, Dijkman B, Cheriex EC, Prinzen FW, and Crijns HJ**. Ventricular remodeling during long-term right ventricular pacing following His bundle ablation. *Am J Cardiol* 97(8): 1223-7, 2006.

112. **Gorcsan J, 3rd**. Cardiac resynchronization in 2008: an echo approach. *Curr Cardiol Rep* 10(3): 211-7, 2008.

113. **Tomaske M, Breithardt OA, Balmer C, and Bauersfeld U**. Successful cardiac resynchronization with single-site left ventricular pacing in children. *Int J Cardiol*, 2008.

114. **Puggioni E, Brignole M, Gammage M, Soldati E, Bongiorni MG, Simantirakis EN, Vardas P, Gadler F, Bergfeldt L, Tomasi C, Musso G, Gasparini G, and Del Rosso A**. Acute comparative effect of right and left ventricular pacing in patients with permanent atrial fibrillation. *J Am Coll Cardiol* 43(2): 234-8, 2004.

115. **Geddes LA and Sadler C**. The specific resistance of blood at body temperature. *Med Biol Eng* 11(3): 336-9, 1973.